

2023-08-01

Inkjet-Printed Electrochemical Sensors For Lead Detection

Annatoma Arif
University of Texas at El Paso

Follow this and additional works at: https://scholarworks.utep.edu/open_etd



Part of the [Analytical Chemistry Commons](#), and the [Electrical and Electronics Commons](#)

Recommended Citation

Arif, Annatoma, "Inkjet-Printed Electrochemical Sensors For Lead Detection" (2023). *Open Access Theses & Dissertations*. 3895.

https://scholarworks.utep.edu/open_etd/3895

This is brought to you for free and open access by ScholarWorks@UTEP. It has been accepted for inclusion in Open Access Theses & Dissertations by an authorized administrator of ScholarWorks@UTEP. For more information, please contact lweber@utep.edu.

INKJET-PRINTED ELECTROCHEMICAL SENSORS
FOR LEAD DETECTION

ANNATOMA ARIF

Doctoral Program in Electrical and Computer Engineering

APPROVED:

Robert C. Roberts, Ph.D., Chair

David Zubia, Ph.D.

Raymond C. Rumpf, Ph.D.

Carlos R. Cabrera Martinez, Ph.D.

Christina Sobin, Ph.D.

Stephen L. Crites, Jr., Ph.D.
Dean of the Graduate School

Copyright 2023 Annatoma Arif

Dedication

I would like to dedicate this work to my family, friends, and most importantly my mentor Dr.

Robert Chris Roberts.

INKJET-PRINTED ELECTROCHEMICAL SENSORS
FOR LEAD DETECTION

by

ANNATOMA ARIF, M.S.

DISSERTATION

Presented to the Faculty of the Graduate School of
The University of Texas at El Paso
in Partial Fulfillment
of the Requirements
for the Degree of

DOCTOR OF PHILOSOPHY

Department of Electrical and Computer Engineering

THE UNIVERSITY OF TEXAS AT EL PASO

August 2023

Acknowledgements

I am deeply grateful to several people for the guidance, insights, time, and support in the development of this dissertation and my entire doctoral journey. My dissertation chair and mentor, Dr. Robert Chris Roberts provided countless hours of mentorship in the scholarly development of my life. I will be grateful for the time and effort Dr. Robert has invested on me for my personal and professional development. I am sincerely thankful to all my committee members. It was a great honor and privilege to work with all committee members who are exceptionally talented and gifted scholars in the field of engineering and science. I am thankful to my department chair Dr. Miguel Velez-Reyes, for his countless effort, meaningful encouragement, and professional support during my pursuit of this doctoral degree.

There are several other people I would like to acknowledge for their role and assistance in this dissertation project. Dr. Christina Sobin has provided such an amazing insight and positive direction in the development of cutting-edge device for lead sensing in aqueous solution. I would also like to thank Dr. Carlos R. Cabrera Martinez, department of Chemistry and Biochemistry and Dr. David A. Roberson, department of Metallurgical, Materials, and Biomedical Engineering. Their active support and resources at UTEP allowed me to be vigilant and become an independent researcher. I would also like to thank all the faculty members and staff in my department – Electrical and Computer Engineering including my peers at CML lab for their committed support to help me to follow my passion and grow as a researcher in the exact area I was striving for.

My family and friends helped me to be motivated and move along this challenging doctoral journey. I would not be at this point in my life without the amazing support, continuous encouragement, and unconditional love of my spouse, son, mother, sister, and all the family members.

Abstract

This PhD dissertation research has developed a simple, miniaturized, sensitive, selective, reproducible, and disposable 3D (inkjet printed – additive manufacturing technology) gold (Au) plated electrochemical sensor (ECS) on shape memory polymer (SMP) for aqueous lead detection. This technology has shown promising performance in the application of electrochemical sensing (lead (II) detection) due to increased effective electrode surface area ($7.25 \text{ mm}^2 \pm 0.15 \text{ mm}^2$) despite miniaturizing lateral surface area (4.19 mm^2). The design, fabrication processes, optimization including bismuth functionalization, evaluation, uncertainty analysis, and cost analysis of the novel SMP based inkjet printed Au plated sensor have been delineated in this manuscript in detail. Sensor characterization, optimization, and evaluation have been performed using electrochemical analysis i.e., cyclic voltammetry (CV), square wave anodic stripping voltammetry (SWASV), and electrochemical impedance spectroscopy (EIS). The fabricated ECS consists of Au working electrode (WE), Au counter electrode (CE), and silver chloride (AgCl) reference electrode (RE). Immersion Au plating (24K) has been applied on inkjet printed silver (Ag) electrodes to fabricate Au WE and CE. Chlorination using sodium hypochlorite solution has been utilized to fabricate AgCl reference electrode. Bismuth functionalization has been performed in two different ways i.e., ex situ - a full range of CV has been conducted to bismuth plate the Au electrode with the solution of $400 \text{ }\mu\text{g/L}$ bismuth salt and in situ – CV and SWASV have been performed with lead contaminated aqueous solution diluted with $200 \text{ }\mu\text{g/L}$ bismuth salt. The limit of detection of the fabricated inkjet printed ECSs are $0.76 \text{ }\mu\text{g/dL}$ – Au WE, $0.64 \text{ }\mu\text{g/dL}$ – bismuth plated WE, and $1.4 \text{ }\mu\text{g/dL}$ – Au WE with lead contaminated aqueous solution diluted with $200 \text{ }\mu\text{g/L}$ bismuth salt. EIS measurement for the fabricated ECSs ($64.07 \pm 7.19 \text{ }\Omega$) has also been

conducted using phosphate buffer saline (PBS; pH 7.4) to investigate the reproducibility of the fabricated ECSs.

Table of Contents

Acknowledgements.....	v
Abstract.....	vi
Table of Contents.....	viii
List of Tables.....	xii
List of Figures.....	xiii
List of Acronyms.....	xiix
List of Units.....	xiixiv
Chapter 1: Inkjet Printed Electrochemical Sensor for Lead Detection.....	1
Section 1.1. Introduction.....	2
Section 1.2. Why Inkjet Printed Electrochemical Sensor?.....	3
Section 1.3. Problem Statement.....	4
Section 1.4. Research Goals.....	6
Section 1.5. Scope and Objective.....	8
Section 1.6. Outline.....	8
Chapter 2: Background.....	11
Section 2.1. Inkjet Printing Basics.....	11
Section 2.2. Shape Memory Polymer.....	12
Section 2.3. Three Electrode System.....	14
Section 2.4. Electrochemical Analysis.....	14
Section 2.5. Uncertainty Analysis.....	20
Section 2.6. History and State of the Art.....	21
Section 2.7. Summary.....	32
Chapter 3: Fabrication of Inkjet Printed Electrochemical Sensor.....	33
Section 3.1. Materials and Methods.....	33

Section 3.1.1. Apparatus and Reagents.....	33
Section 3.1.2. Design of the Sensor.....	34
Section 3.2. Inkjet Printing Recipe Development.....	37
Section 3.2.1. Fluid Properties of Nanoparticle Ink.....	37
Section 3.2.2. Recipe Development for Inkjet Printheads.....	38
Section 3.3. Characterization of Shape Memory Polymer Substrate.....	41
Section 3.4. Fabrication Processes.....	43
Section 3.5. Summary.....	48
Chapter 4: Optimization and Characterization of the Inkjet Printed Electrochemical Sensor.....	50
Section 4.1. Resistivity.....	50
Section 4.2. Cleaning Cycle.....	52
Section 4.3. Electrochemical Analysis.....	53
Section 4.4. Summary.....	56
Chapter 5: Results - Gold Plated Inkjet Printed Silver based Electrode.....	57
Section 5.1. Effective Electrode Surface Area.....	57
Section 5.2. Gold Plated Inkjet Printed Electrochemical Sensor.....	63
Section 5.3. Bismuth Functionalization.....	68
Section 5.4. Reusability.....	76
Section 5.5. Simultaneous Detection of Other HMIs.....	79
Section 5.6. Compatibility with Real Sample.....	81
Section 5.7. Uncertainty Analysis.....	82
Section 5.8. Cost Analysis.....	85
Section 5.9. Summary.....	87
Chapter 6: Conclusion.....	88
Section 6.1. Summary.....	88

Section 6.2. Contributions of This Work.....	90
Section 6.2.1. Publication and Conference Proceeding Contributions.....	91
Section 6.3. Limitations.....	92
Section 6.4. Future Work.....	93
References.....	95
Appendix.....	112
Vita.....	120

List of Tables

Table 2.1: STATE OF THE ART POTENTIAL ELECTROCHEMICAL SENSORS (ECSs) FOR HEAVY METAL IONS (HMIs) DETECTION.....	23
Table 2.2: Inkjet Printed Electrochemical Sensors (ECSs) for Different Applications.....	25
Table 2.3: State of the Art Potential Bismuth Modified Electrochemical Sensors (ECSs) for Heavy metal ions (HMIs) Detection.....	28
Table 3.1: Inkjet Printing Recipes (Fujifilm Dimatix DMP 2850) of Silver Nanoparticle Conductive Ink.....	40
Table 3.2: SHRINKING CHARACTERISTICS OF INKJET PRINTED (SILVER NANOPARTICLE INK) SMP BASED ELECTROCHEMICAL SENSORS.....	43
Table 4.1: Resistivity of The Silver Patterns for Multiple Samples.....	51
Table 5.1: Type A and NIST TN 1297 Mean and Standard Deviation Data of Inkjet Printed Gold Plated Electrochemical Sensor.....	84
Table 5.2: Summary of Uncertainty Analysis for Inkjet Printed Gold Plated Electrochemical Sensor.....	85
Table 5.3: Time Analysis of Inkjet Printed Gold Plated Electrochemical Sensor.....	86
Table 5.4: Cost Analysis of Inkjet Printed Gold Plated Electrochemical Sensor.....	86
Table B.1: Peak Currents at Different Scan Rates.....	115
Table C.1: Peak Currents of Square Wave Anodic Stripping Voltammetry for Different Concentrations of Lead (II) Contaminated Optimized DI Water.....	116
Table C.2: Summary Output of Regression Statistics Analyzed using Excel.....	117

List of Figures

Figure 2.1: Inkjet printing (IP) - additive manufacturing (AM) processes for electrochemical sensor (ECS) fabrication.....	12
Figure 2.2: Shape memory polymer (SMP) cycle consists of three stages: programming, storing, and recovery stage.....	13
Figure 2.3: Three electrode system with working electrode – WE, counter electrode – CE, and reference electrode – RE.....	15
Figure 2.4: Step by step processes of cyclic voltammetry.....	16
Figure 2.5: Cyclic voltammogram for 5 mM of lead (II) contaminated optimized (0.1 M HCl) DI water.....	17
Figure 2.6: Square wave anodic stripping voltammetry for 5 mM of lead (II) contaminated optimized (0.1 M HCl) DI water.....	19
Figure 2.7: Impedance vs. Frequency response using electrochemical impedance spectroscopy measurement in case of phosphate buffer saline (PBS) with pH 7.42.....	20
Figure 2.8: Maximum allowable rate of HMIs in aqueous solution by USEPA (2023)	22
Figure 2.9: Percentage of various materials' contribution for electrochemical sensor (ECS) fabrication for HMIs detection.....	27
Figure 2.10: Cyclic voltammetry (CV) for inkjet printed gold plated electrochemical sensor (ECS) using 0.5 M sulfuric acid (H ₂ SO ₄). Scan rate is 100 mV/s.....	31
Figure 3.1: Inkjet printed shape memory polymer (SMP) incorporated gold plated electrochemical sensors (ECSs) for lead (II) detection: (a) square working electrode and (b) circular working electrode.....	35

Figure 3.2: Cyclic voltammogram (CV) for inkjet printed gold electrochemical sensor (square working electrode surface area) for 5 mM of lead (II) contaminated optimized (0.1 M HCl) deionized water for different scan rate (10, 20, 30, and 50 mV/s).....36

Figure 3.3: Cyclic voltammogram (CV) for inkjet printed gold electrochemical sensor (circular working electrode surface area) for 5 mM of lead (II) contaminated optimized (0.1 M HCl) deionized water for different scan rate (10, 20, 30, and 50 mV/s).....37

Figure 3.4: Waveform data for the silver nanoparticle conductive ink (a) DMC-11610 (left) and (b) Samba printheads (right).....40

Figure 3.5: Scanning electron micrographs (SEM) of inkjet printed metal films on shape memory polymer before (left) and after (right) shrinking (cured and shrunk at 180 °C for 3 minutes). The shrunk (right) SEM strongly reveals a 3D wrinkled structure, providing a large surface area, useful for enhancing sensor performance.....42

Figure 3.6: Inkjet printed (IP) silver (Ag) electrodes on shape memory polymer (SMP) for lead (II) detection utilizing drop on demand dimatix materials printer DMP – 2850. The overall dimension is 31×25×0.52 mm³.....44

Figure 3.7: Inkjet printed Ag-based electrochemical sensor (ECS) with dimension: 31×25×0.52 mm³ - before shrinking and curing (left) and final inkjet printed miniaturized electrochemical sensor with dimension: 13×10×1.52 mm³ - after shrinking and curing (right) at 180°C for 3 minutes.....45

Figure 3.8: Simple step by step fabrication process flow of inkjet printed (IP) gold (Au) electrochemical sensor (ECS): (a) IP ECS on shape memory polymer (SMP) with dimension $13 \times 10 \times 1.52 \text{ mm}^3$ (after shrinking and curing) – silver (Ag) working electrode (WE), Ag counter electrode (CE) and Ag reference electrode (RE), (b) masking technique for bleach (sodium hypochlorite) immersion on Ag RE, (c) IP Ag-based ECS with Ag working electrode (WE), Ag counter electrode (CE) and AgCl reference electrode (RE), (d) Au based IP ECS with dimension $13 \times 10 \times 1.52 \text{ mm}^3$ after Au plating immersion using 24K brush gold solution: Au WE, Au CE, and AgCl RE.....47

Figure 3.9: Experimental setup for inkjet printed electrochemical sensor. Red, green, and black wire of the USB drive are connected with reference, working, and counter electrode terminal of the potentiostat respectively.....49

Figure 4.1: Electrochemical Impedance Spectroscopy (EIS) measurement using phosphate buffer saline (PBS) with pH 7.42.....51

Figure 4.2: Cleaning procedure for inkjet printed gold electrochemical sensor – last cycle of 25 cycles of CV for 0.5 M sulfuric acid (H_2SO_4). Scan rate is 100 mV/s.....52

Figure 4.3: Cyclic Voltammetry (CV) of gold (Au) based electrochemical sensor (ECS) for blank (optimized DI water without lead(II)) – green, 3mM lead (II) (optimized DI water with 3 mM lead (II)) – red, and 14.4 $\mu\text{g/L}$ lead (II) (optimized DI water with 14.4 $\mu\text{g/L}$ lead (II)) – blue) at 100 mV/s.....55

Figure 4.4: Cyclic Voltammetry (CV) of gold (Au) based electrochemical sensor (ECS) for blank (optimized tap water without lead(II)) – green, 3mM lead (II) (optimized tap water with 3 mM lead (II)) – red, and 14.4 $\mu\text{g/L}$ lead (II) (optimized tap water with 14.4 $\mu\text{g/L}$ lead (II)) – blue) at 100 mV/s.....56

Figure 5.1: Plot of (A) $\Delta(\Lambda, \alpha)$ and (B) $K(\Lambda, \alpha)$ with a range of different transfer co-efficient, α ..59

Figure 5.2: Peak to peak separation vs. kinetic parameter, Ψ60

Figure 5.3: Cyclic voltammogram (CV) for inkjet printed gold electrochemical sensor (square working electrode surface area) for 3 mM of ferri(III)cyanide/ferro(II)cyanide in 0.1 M KCl (10, 20, 30, 40, 50, 60, 70, 80, 90, and 100 mV/s).....61

Figure 5.4: Area (mm^2) calculated using Randles-Sevcik quasi reversible equation for 15 different samples (inkjet printed gold plated electrochemical sensors.....61

Figure 5.5: Inkjet printed gold electroplated electrochemical sensor on shape memory polymer (left). The cell consists of gold working electrode (WE) and counter electrode (CE) and silver chloride reference electrode (RE). The lateral and effective electrode surface area are 4 mm^2 and 6.923 mm^2 respectively. The energy dispersive spectroscopy layered image (right) shows the potential coating of gold on silver inkjet printed electrodes.....63

Fig. 5.6: Scanning electron micrographs (SEM) of inkjet printed metal films on shape memory polymer after shrinking, revealing a 3D wrinkled structure, providing a large surface area, useful for enhancing sensor performance.....64

Figure 5.7: Energy dispersive spectroscopy for inkjet printed silver electrode (41.7% silver).....65

Figure 5.8: Energy dispersive spectroscopy for silver chloride (AgCl) reference electrode (7.9% chlorine).....66

Figure 5.9: Energy dispersive spectroscopy for inkjet printed gold plated silver based electrode (9.9% gold).....	66
Figure 5.10. Square wave anodic stripping voltammetry for 30 $\mu\text{g/L}$ (top-left: green), 25 $\mu\text{g/L}$ (top-right: red), 15 $\mu\text{g/L}$ (bottom-left: blue), and 0 $\mu\text{g/L}$ (bottom-right: blank). Modulation amplitude - 280 mV, frequency - 15 Hz, estimated duration - 4.4 s, and scan rate - 45 mV/s, and deposition time - 5 minutes.....	67
Figure 5.11: Calibration curve for inkjet printed shape memory polymer incorporated gold plated electrochemical sensor. The data point for each concentration is a mean of three different data collected using three different sensors.....	68
Figure 5.12: Cyclic voltammogram (CV) for the full range of under potential deposition (UPD) of bismuth (III) on gold plated inkjet printed electrochemical sensor (ECS).....	69
Figure 5.13: Inkjet printed (IP) shape memory polymer (SMP) incorporated gold based electrochemical sensor (ECS) (a) before under potential deposition (UPD) of Bi (III) and (b) after UPD of Bi (III).....	70
Figure 5.14: Commercially available ZP sensor (a) before under potential deposition (UPD) of Bi (III) and (b) after UPD of Bi (III) on gold based electrochemical sensor (ECS).....	70
Figure 5.15: Scanning Electron Micrograph images for bismuth (III) deposited inkjet printed gold plated electrochemical sensor.....	71
Figure 5.16: Energy dispersive spectroscopy for inkjet printed Bismuth (III) deposited inkjet printed working electrode (33.7% bismuth)	72
Figure 5.17: Square wave anodic stripping voltammetry (SWASV) of bismuth (III) plated inkjet printed gold electrodes with different concentrations of lead (II) ions i.e., blank, 5ppb, 10 ppb, 20 ppb, 40 ppb, 60 ppb, 80 ppb, and 100 ppb in 0.1 M HCl. Modulation	

amplitude - 280 mV, frequency - 15 Hz, estimated duration - 4.4 s, and scan rate - 45 mV/s, and deposition time - 5 minutes.....	73
Figure 5.18: Calibration curve for bismuth (III) plated inkjet printed gold plated electrochemical sensor. The data point for each concentration is a mean of three different data collected using three different sensors.....	73
Figure 5.19: Cyclic voltammogram (CV) for in situ Bismuth (III) functionalization on gold plated electrochemical sensor (ECS).	74
Figure 5.20: Square wave anodic stripping voltammetry (SWASV) of inkjet printed gold electrodes with different concentrations of lead (II) ions i.e., blank, 5ppb, 10 ppb, 20 ppb, 40 ppb, 60 ppb, 80 ppb, and 100 ppb including 200 $\mu\text{g/L}$ bismuth (III) salt in 0.1 M HCl. Modulation amplitude - 280 mV, frequency - 15 Hz, estimated duration - 4.4 s, and scan rate - 45 mV/s, and deposition time - 5 minutes.....	75
Figure 5.21: Calibration curve for inkjet printed gold plated electrochemical sensor with 200 $\mu\text{g/L}$ bismuth (III) salt in lead (II) contaminated aqueous solution. The data point for each concentration is a mean of three different data collected using three different sensors.....	75
Figure 5.22: Last cycle of 25 cycles of cyclic voltammogram (CV) for 0.5M H_2SO_4 for 4 times before each measurement. Scan rate is 100 mV/s.....	77
Figure 5.23: Cyclic Voltammetry (CV) of gold (Au) plated electrochemical sensor (ECS) for 5mM lead (II) contaminated 0.1M HCl (optimized DI water) for 4 times at 50 mV/s. The ECS was cleaned with 25 cycles of CV at 100 mV/s using 0.5 M H_2SO_4 prior every use.....	77

Figure 5.24: Square wave anodic stripping voltammetry (SWASV) of gold (Au) plated electrochemical sensor (ECS) for 5mM lead (II) contaminated 0.1M HCl (optimized DI water) for 4 times - modulation amplitude - 280 mV, frequency - 15 Hz, estimated duration - 4.4 s, and scan rate - 45 mV/s, and deposition time - 5 minutes. The ECS was cleaned with 25 cycles of CV at 100 mV/s using 0.5 M H₂SO₄ prior every use.....78

Figure 5.25: Selectivity test for inkjet printed shape memory polymer based gold plated electrochemical sensor in case of lead (II), iron (III), and copper (II) individually...79

Figure 5.26: Selectivity test for inkjet printed shape memory polymer based gold plated electrochemical sensor in case of simultaneous presence of lead (II), cadmium (II) and copper (II).....80

Figure 5.27: Cyclic Voltammetry (CV) of gold (Au) plated electrochemical sensor (ECS) for blank (optimized tap water without lead(II)) – green, 5mM lead (II) (optimized tap water with 5 mM lead (II)) – purple at 100 mV/s.....81

Figure 5.28: Cyclic Voltammetry (CV) of gold (Au) plated electrochemical sensor (ECS) for blank (optimized tap water without lead(II)) – green, 5mM lead (II) (optimized river water with 5 mM lead (II)) – purple at 100 mV/s.....82

Figure B.1: Plot of (A) $\Delta(\Lambda, \alpha)$ and (B) $K(\Lambda, \alpha)$ with a range of different transfer co-efficient....113

Figure B.2: Peak to peak separation vs. kinetic parameter, Ψ113

Figure B.3: Cyclic voltammogram (CV) for inkjet printed gold electrochemical sensor (square working electrode surface area) for 3 mM of ferri(III)cyanide/ferro(II)cyanide in 0.1 M KCl (10, 20, 30, 40, 50, 60, 70, 80, 90, and 100 mV/s).....114

Figure B.4: Peak current vs. square root of scan rate. The slope is defined as diffusion coefficient
(D - cm²/s)115

Figure C.1: Calibration curve for bismuth (III) plated inkjet printed gold plated electrochemical
sensor. The data point for each concentration is a mean of three different data
collected using three different sensors.....118

List of Acronyms

3D.....	Three Dimensional
Ag.....	Silver
AgCl.....	Silver Chloride
Au.....	Gold
AuNDS.....	Gold Nano Dendrites
ABS.....	Acetate Buffer Solution
AM.....	Additive Manufacturing
ANP.....	Advanced Nano Products
ASTM D3359.....	Standard Test Methods for Rating Adhesion by Tape Test
ASV.....	Anodic Stripping Voltammetry
Bi (III).....	Bismuth (III)
BiOCl.....	Bismuth Oxychloride
Cd (II).....	Cadmium (II)
Cu (II).....	Copper (II)
CAD.....	Computer Aided Design
CC.....	Chronocoulometry
CDC.....	Center for Disease Control and Prevention
CE.....	Counter Electrode
CNS.....	Central Nervous System
CML.....	Convergent Microsystems Laboratory
CV.....	Cyclic Voltammetry

DI.....	Deionized
DLS.....	Dynamic Light Scattering
DMC.....	Dimatix Materials Cartridge
DMP.....	Dimatix materials Printer
DO.....	Dissolved Oxygen
DPASV.....	Differential Pulse Anodic Stripping Voltammetry
DPH.....	Department of Public Health
EAAS.....	Electrothermal Atomic Absorption Spectrometry
ECS.....	Electrochemical Sensor
EDS.....	Energy Dispersive Spectroscopy
EESA.....	Effective Electrode Surface Area
EIS.....	Electrochemical Impedance Spectroscopy
Fe (III).....	Iron (III)
FAAS.....	Flame Atomic Absorption Spectrometry
FDA.....	Food and Drug Administration
FDM.....	Fused Deposition Modeling
GCE.....	Glassy Carbon Electrode
GIMP.....	GNU Image Manipulation Program
GUM.....	Guide to the Expression of Uncertainty in Measurement
Hg (II).....	Mercury (II)
HCl.....	Hydrochloric Acid

HMI.....	Heavy Metal Ion
H ₂ O ₂	Hydrogen Peroxide
H ₂ SO ₄	Sulfuric Acid
IARC.....	International Agency for Research on Cancer
ICOES.....	Inductively Coupled Optical Emission Spectrometry
ICPMS.....	Inductively Coupled Plasma Mass Spectrometry
IP.....	Inkjet Printing
KCl.....	Potassium Chloride
LOD.....	Limit of Detection
LOQ.....	Limit of Quantitation
Ni (II).....	Nickel (II)
NIH.....	National Institutes of Health
NIST.....	National Institute of Standards and Technology
NaOCl.....	Sodium Hypochlorite Solution (3%) – Bleach
O ₂	Oxygen
Pb (II).....	Lead (II)
Pd.....	Palladium
Pt.....	Platinum
PBS.....	Phosphate Buffer Saline
PEN.....	Polyethylene Naphthalate
PET.....	Polyethylene Terephthalate
pH.....	Potential of Hydrogen

PI.....	Polyimide
PNS.....	Peripheral Nervous System
PTFE.....	Polytetrafluoroethylene
PVC.....	Polyvinyl Chloride
RE.....	Reference Electrode
ROS.....	Reactive Oxygen Species
R-S.....	Randles-Sevcik
SEM.....	Scanning Electron Microscopy
SLA.....	Sterolithography
SLS.....	Selective Laser Sintering
SMP.....	Shape Memory Polymer
SPE.....	Screen Printed Electrode
SPT.....	Screen Printing Technology
SWASV.....	Square Wave Anodic Stripping Voltammetry
TN.....	Technical Note
UL.....	Underwriters' Laboratories
UPD.....	Under Potential Deposition
USEPA.....	United States Environmental Protection Agency
UTEP.....	University of Texas at El Paso
WE.....	Working Electrode
Zn (II).....	Zinc (II)
ZP.....	Zimmer and Peacock

List of Units

°C.....	Degree centigrade (temperature)
Ω.....	Ohms (resistance)
Ω.□.....	Ohms per square (resistivity)
μA.....	Microamperes (current)
μg/L.....	Microgram per liter (concentration of heavy metal ions)
μg/dL.....	Microgram per deciliter (concentration of heavy metal ions)
cP.....	Centi poise (viscosity)
Hz.....	Hertz (frequency)
K.....	Caratage (purity of gold)
KHz.....	Kilohertz (frequency)
m.....	Meter (length/width/radius/diameter)
mm ²	Square millimeter (area)
mm ³	Cubic millimeter (volume)
mV.....	Millivolts (potential)
mA.....	Milliamperes (current)
mM/m.....	Milli newton per meter (surface tension)
m/s.....	Meter per second (drop speed)
mV/s.....	Millivolts per second (scan rate)
M.....	Molar (concentration of sample analyte)
mM.....	Millimolar (concentration of sample

analyte)

M..... Minutes (time)

ppb..... Parts per billion (concentration of heavy
metal ions)

s..... Seconds (time)

Chapter 1: Inkjet Printed Electrochemical Sensors for Lead Detection

This PhD dissertation research explores inkjet printing technology on shape memory polymer (SMP) substrate for lead (II) detection in aqueous solutions (electrochemical applications). It has been observed from the literature review that inkjet printing on SMP has potential to fabricate 3D metal electrodes. However, literature review on lead (II) – heavy metal ion (HMI) detection always indicates the popularity towards screen printing technology (SPT) or lithography. Lithography is an expensive process that typically requires a cleanroom facility. Contrastingly, SPT is cheaper but inconsistent from batch-to-batch fabrication which results in variations that fail to provide reliable data in case of lead (II) detection. Unfortunately, no studies have been found yet to consider inkjet printed metal electrodes for HMI detection (electrochemical and bio-sensing applications).

It has been demonstrated in this manuscript that inkjet printing on SMP provides a larger surface area and 3D topology to the printed sensors which provides consistent data and higher sensitivity towards lead (II) detection in aqueous solution. This technology – combination of inkjet printing on SMP offers three specific advantages i.e. quick and simple fabrication (simultaneous curing and shrinking), miniaturization, and increased effective electrode surface area despite miniaturization. Therefore, this PhD dissertation research has developed a simple, miniaturized, sensitive, selective, reproducible, and disposable 3D (inkjet printed – additive manufacturing technology) gold (Au) plated electrochemical sensor (ECS) on shape memory polymer (SMP) for aqueous lead (II) detection. Section 1.1 provides a brief overview of the complete dissertation research, Section 1.2 illustrates the rationality for choosing inkjet printing – additive manufacturing technology for ECS fabrication, Section 1.3 demonstrates the exigency of this research – problem statement, Section 1.4 represents detailed specific research goals, Section 1.5

provides a brief discussion about scope and objectives, and Section 1.6 briefly outlines the complete dissertation.

SECTION 1.1. INTRODUCTION

This PhD dissertation research has investigated and developed a simple, miniaturized, sensitive, selective, reproducible, and disposable 3D (inkjet printed – additive manufacturing technology) gold (Au) plated electrochemical sensor (ECS) on shape memory polymer (SMP) for aqueous lead (II) detection. This technology has shown promising output in case of electrochemical sensing (lead (II) detection) due to increased effective electrode surface area ($7.25 \text{ mm}^2 \pm 0.15 \text{ mm}^2$) despite miniaturizing lateral surface area (4.19 mm^2) of the fabricated ECSs – data calculated using 15 different measurements collected from 15 different fabricated inkjet printed ECSs. The effective electrode surface area has been calculated using Randles -Sevcik quasi reversible equation. The design, fabrication processes including printing recipe development for Dimatix Materials Printer (Fujifilm – DMP 2850) in case of both printheads (i.e., legacy – the old one and Samba – newly launched (2021)), optimization including bismuth functionalization, evaluation, uncertainty analysis, and cost analysis of the novel SMP based inkjet printed Au plated sensors have been delineated in this manuscript in detail. Sensor characterization, optimization, and evaluation have been performed using electrochemical analysis i.e., cyclic voltammetry (CV), square wave anodic stripping voltammetry (SWASV), and electrochemical impedance spectroscopy (EIS). The fabricated ECS consists of Au working electrode (WE), Au counter electrode (CE), and silver chloride (AgCl) reference electrode (RE). Immersion Au plating (24K brush gold solution) has been applied on inkjet printed silver (Ag) electrodes to fabricate Au WE and CE. Chlorination using sodium hypochlorite solution (3% v/v) has been utilized to fabricate AgCl reference electrode. Bismuth (Bi (III)) functionalization has been performed in two different

ways i.e., ex situ - a full range of CV (-800mV to -200 mV) - has been conducted to bismuth plate the Au electrode with the solution of 400 $\mu\text{g/L}$ Bi (III) salt and in situ -CV/SWASV have been performed with lead (II) contaminated aqueous solution diluted with 200 $\mu\text{g/L}$ Bi (III) salt. The limit of detection of the fabricated inkjet printed ECSs are 0.64 $\mu\text{g/dL}$ - Bi (III) deposited WE, 0.76 $\mu\text{g/dL}$ - Au electroplated WE, and 1.4 $\mu\text{g/dL}$ -Au electroplated WE with lead (II) contaminated aqueous solution diluted with 200 $\mu\text{g/L}$ Bi (III) salt. The R-squared (R^2) measure of the correlation coefficient value in case of each WEs are 0.999, 0.992, 0.995 respectively. To investigate the potential ECSs reproducibility, EIS measurement for the fabricated ECSs ($64.07 \pm 7.19 \Omega$) has also been conducted using phosphate buffer saline (PBS; pH 7.4) - data calculated using 10 different measurements collected from 10 different fabricated ECSs. Additionally, the green fabricated - mercury free inkjet printed ECSs have been validated using uncertainty analysis following “Type A evaluation of standard uncertainty” approach from “Evaluation of Measurement Data – Guide to the expression of uncertainty in measurement” for 15 different ECS sample in case of reduction factor (%), resistivity measurement ($\Omega\text{-cm}$), and peak current measurement (mA) for electrochemical analysis.

SECTION 1.2. WHY INKJET PRINTED ELECTROCHEMICAL SENSOR?

Inkjet printing – additive manufacturing technology has been chosen as the potential 3D printing method for electrochemical sensor (ECS) fabrication as it offers high resolution, low-cost, low-waste, uniformity in the roll-to-roll fabrication (very rare in popular existing technology i.e. screen printing technology), and, compatibility with a wide variety of polymer substrates. This PhD dissertation research targeted inkjet printing on shape memory polymer (SMP) substrate to fabricate a simple, sensitive, selective, and reusable ECS for lead (II) detection in aqueous solution. According to the United States Environmental Protection Agency, the maximum allowable level

of lead (II) in aqueous solution/drinking water is 1.5 $\mu\text{g/dL}$ (USEPA, 2023). This technology – combination of inkjet printing on SMP based ECS potentially detected a much lower concentration of lead (II) in aqueous solution compared to the USEPA standard. The limit of detection of the fabricated inkjet printed ECSs are 0.64 $\mu\text{g/dL}$ – bismuth (Bi (III)) plated working electrode (WE), 0.76 $\mu\text{g/dL}$ – gold (Au) WE, and 1.4 $\mu\text{g/dL}$ – Au WE with lead (II) contaminated aqueous solution diluted with 200 $\mu\text{g/L}$ Bi (III) salt.

SECTION 1.3. PROBLEM STATEMENT

In April 30, 2019 Centers for Disease Control and Prevention (CDC) reported that 2.0% of the entire population of children in the United States have more than 5 $\mu\text{g/dL}$ blood lead (II) levels [1]. The CDC concluded their results based on the 18% of the United States children blood lead (II) report [1]. Between 1990 to 2010, California Environmental Health Tracking Program and the Department of Public Health (DPH) recognized approximately 1.2 million children between 1 to 5 years with elevated blood lead (II) levels ($>10 \mu\text{g/dL}$) [2]. Unfortunately, only 50 % (607,000) cases were reported to CDC [3]. Many experts predict that the future situation will be worsened significantly further increasing the number of affected children.

Lead accumulates over time in the human body and in plants, and its solubility makes water one of the main sources of contamination, that can provide a continuous stream of the heavy metal. Small amounts of lead (II) exposure to children can cause severe developmental damage such as learning disabilities, behavioral disorientation, hearing loss, speech disorder, and attention deficiency [3, 4]. The neurotoxic effect of lead (II) causes severe damage to both the central nervous system (CNS) and the peripheral nervous system (PNS). Contaminated drinking water is considered as a major source of lead accumulation in human blood. Drinking water is contaminated due to lead containing pipes, faucets, and plumbing features [5]. According to the

US EPA and the International Agency for Research on Cancer (IARC), lead (II) is considered as an extremely poisonous and carcinogenic to the human body [6]. The combination of these factors makes lead a major public health concern both presently and in the future.

Therefore, it is extremely important to have effective and efficient technology which can accurately identify the presence of lead (II) in aqueous solutions and/or blood samples to mitigate this public health threat. Unfortunately, there are a limited number of sensitive, selective, and miniaturized commercial lead (II) detection devices currently that provide consistent results, ensure reliable measurement techniques, and provide a cost-effective measurement [7-9]. Lithography and screen-printing technology (SPT) are considered as the state-of-the-art technologies for manufacturing electrochemical lead (II) sensing elements [10-24]. In recent times, SPT is widely accepted and chosen by many researchers. However, one major limitation of this technology is variation in measurement from batch-to-batch fabrication and materials due to the manufacturing method [25]. On the other hand, lithography (etching and lift-off) is extremely time consuming, expensive, requires a cleanroom facility and sometimes requires hazardous materials.

To overcome the above-mentioned limitations, this PhD dissertation research aimed to fabricate an ECS combining inkjet printing technology with SMP. For the first time, this research has introduced and utilized inkjet printing on SMP technique to fabricate the ECS for heavy metal ions (HMIs) detection in aqueous solution. Actual research on HMIs detection in water started at the beginning of 20th century. Researchers are continuously trying to find out an innovative, reliable, effective, and efficient technology for HMIs detection in drinking water. Nevertheless, it is a clear challenge to find a reliable lead (II) detection technology to serve imminent demand. In this context, it is important to mention that three most popular lead sensing devices were recalled

from the market by the United States Food and Drug Administration (FDA) during the year of 2021 due to inconsistent and unreliable results [26]. In addition, CDC revised the presence of reference blood lead (II) level in human body i.e. 3.5 $\mu\text{g}/\text{dL}$ on May 14, 2021 [27]. It is believed that even a minimum amount of lead (II) is responsible for human health hazards and weakens a generation with compromised intelligence. Thus, this research investigated and developed a lead (II) sensing system which is not only consistent and miniaturized with inkjet printing on SMP but also highly sensitive and would detect target concentration of 1.5 $\mu\text{g}/\text{dL}$, selective (simultaneous detection of other HMIs i.e. copper and iron), and reusable.

SECTION 1.4. RESEARCH GOALS

This dissertation research has four specific research goals i.e., fabricating inkjet printed electrochemical sensor effectively and efficiently, ensuring and experimenting sensitivity and selectivity, and finally validating the sensor. A detail description of each specific research aims/goals including every parameters and characteristics have been sketched out in this section.

1. Innovate/propose/develop a novel approach (reliable and consistent) to fabricate a simple, cost-effective, sensitive, selective, and disposable ECS.
 - Exploring different sizes (regular-mm and micro-below 5mm) and shapes (square and circular) for fabricating the sensors.
 - Measure surface area before and after shrinking – calculate the reduction factor (%) and effective electrode surface area calculation.
 - Explore/optimize the selective surface coating (under potential deposition of bismuth on gold electrode) – Bi functionalization.
 - Measure the resistivity ($\Omega\cdot\text{cm}$) of each fabricated ECSs.
 - Cleaning cycle optimization.

- Characterize and optimize the fabricated ECSs with the potential reported (in other published research) electrochemical analysis i.e. cyclic voltammetry (CV) and anodic stripping voltammetry (ASV) – current vs. potential graph.
 - Finalize ideal/optimum deposition time for electrochemical analysis (CV/ASV).
 - Explore the limit of detection (LOD) and limit of quantitation (LOQ) for the fabricated ECSs.
 - Collect and observe the SEM images and energy dispersive spectroscopy (EDS) to understand the 3D topology of the inkjet printed material (silver nanoparticle conductive ink) of the shrunk ECS.
 - Model peak currents vs. concentration in case of different levels of lead (II) contaminated optimized aqueous solution.
2. Apply and ensure the effectivity of the fabricated ECSs for the lower (i.e. below 15 $\mu\text{g/L}$ - lead) and ultra-trace level (i.e. below 0.1 $\mu\text{g/dL}$ - lead) HMIs detection in the aqueous solution (sensitivity).
 - Experiments are going to be performed for optimized aqueous solution with and without lead (II) contamination.
 3. Verify the efficiency of the fabricated ECS for simultaneous presence of other HMIs – cadmium and mercury (selectivity).
 - The contaminated optimized drinking water sample will be prepared with specific amount of lead, cadmium, and copper together to experiment the selectivity of the fabricated ECS.
 4. Validate the fabricated ECS by conducting uncertainty analysis (considering 15 fabricated ECSs) after sintering and shrinking the ECSs. Reduction factor (%), resistivity

measurement (Ω - \square), and peak measurement (mA) for electrochemical sensing in case of HMIs detection in the drinking water are going to be analyzed following GUM approach.

SECTION 1.5. SCOPE AND OBJECTIVE

The broader aspect of this research is to establish a multi-functional inkjet printed electrochemical microchip sensor (green fabricated and mercury free) incorporating Au-plated SMP for HMIs (lead, copper, and mercury) detection in aqueous solution (blood sample and drinking water). The primary goal to achieve the above-mentioned overarching vision is to analyze/develop a cost-effective, accurate, consistent, and reliable fabrication processes for manufacturing ECSs for lead (II) detection. The next step is to apply the novel/potential technologies to fabricate a simple, cost-effective, sensitive, selective, and disposable ECS for lead (II) detection in the aqueous solution. Appropriate electrochemical analyses (CV and ASV data) in case of HMIs detection need to be collected and analyzed/scrutinized before making further/final progress. The green fabricated ECSs will be finally validated using uncertainty analysis for 15 ECSs samples. Hence, the specific objectives of this research project are consistent and reliable ECS fabrication with increased effective electrode surface area for HMIs detection, ensure high sensitivity and selectivity of the ECS for HMIs detection, maintain green fabrication and cost-effectivity, and validate the fabricated ECS with uncertainty analysis.

SECTION 1.6. OUTLINE

This dissertation focuses on the fabrication of a simple, cost-effective, sensitive, selective, and disposable inkjet printed Au plated ECSs for lead (II) detection in aqueous solutions. The first half of the dissertation discusses about the justification of the research, problem statement, a detail and through background and literature review, limitation and/or challenges of the existing technology, and finally, the fabrication processes of the novel inkjet printed Au plated ECS for

lead (II) detection in aqueous solution. The second half mostly focuses on the optimization, characterization, and validation of the fabricated ECSs.

Chapter 2 covers an overview of the related topics i.e., inkjet printing, printing substrate – shape memory polymer, three-electrode system, electrochemical analysis, and uncertainty analysis. This chapter also provides a detail idea about the current existing technology in the area of heavy metal ion or lead sensing. The thorough literature review provides a clear perception regarding the state-of-the-art technologies, their characteristics, and recent challenges/limitations. Chapter 3 focuses on the fabrication of the inkjet printed ECSs. Chapter 3 consists of 4 different sections. The first section of this chapter illustrates materials and reagents utilized to fabricate the inkjet printed sensors. This section also includes different designs and their efficacy for the printed sensors in case of electrochemical sensing applications. The second section of Chapter 3 details out the printing recipe development tools and techniques i.e., fluid properties characterization of the nanoparticle ink and jetting recipe development and optimization. The third section of this chapter shares the information regarding the characterization of the printing substrate – shape memory polymer. Finally, the fourth section of Chapter 3 provides description of each step of fabrication processes in detail of inkjet printed gold plated ECSs.

Optimization and characterization of the fabricated ECSs are extremely important to utilize the sensors potently in any specific application. Chapter 4 explains broadly about the characterization and optimization in case of resistivity, cleaning cycle, and electrochemical analysis – cyclic voltammetry (CV). Chapter 5 is the result section of this dissertation. This section covers all the potential data collected, analyzed, and observed to understand the behavior, characteristics, strength, and limitations/challenges of the fabricated inkjet printed gold plated

ECSs for lead detection in aqueous solution. This chapter also includes validation technique – uncertainty analysis and cost analysis of the fabricated ECSs.

Chapter 6 concludes this dissertation by providing specific summary of the entire research i.e., problem statement, state-of-the-art technologies, research gap, proposed approach, fabrication processes, characterization, optimization, research findings, contribution to the field, limitations, and potential future scopes. The Appendix sections of this dissertation include theoretical and mathematical descriptions of different equations/models – reduction factor and effective electrode surface area calculation, explanation of different statistical data including regression model in case of determining limit of detection and limit of quantitation of the fabricated sensors, and unit conversions of different sample analytes.

Chapter 2: Background

There are two specific goals of this chapter. First, to provide a brief but complete explanation on the basics of inkjet printing, shape memory polymer (SMP), three-electrode system, electrochemical analysis, and uncertainty analysis in order to make the readers familiar with the technical concepts and terminology. Second, a thorough literature review is presented to determine the state of the art in lead (II)/heavy metal ion (HMI) sensing research in order to contextualize the idea and necessity of using inkjet printing additive manufacturing technology on SMP for fabricating inkjet electrochemical sensors (ECS) for HMI detection.

SECTION 2.1. INKJET PRINTING BASICS

Additive manufacturing (AM) is a process of joining materials layer by layer to make/print 3D objects. The four AM technologies are fused deposition modeling (FDM), selective laser sintering (SLS), stereolithography (SLA), and inkjet printing (IP). It is determined to use inkjet printing to manufacture ECS for lead (II) detection in this research. The inkjet printing technology is chosen based on certain characteristics of the manufactured product such as resolution, surface finish, throughput, and range of usefulness of materials. It is considered as a unique and potential fabrication method to fabricate ECS due to its high resolution, low-cost fabrication, incredible control over the material deposition (drop on demand), and multi-material characteristics. It allows direct patterning of structure from metal nanoparticle conductive inks utilizing piezoelectric inkjet cartridge. After simple steps of curing and sintering (heat treatment processes) the deposited ink pattern turns into a conductive film. Figure 2.1 illustrates the processes of inkjet printed ECS pattern.

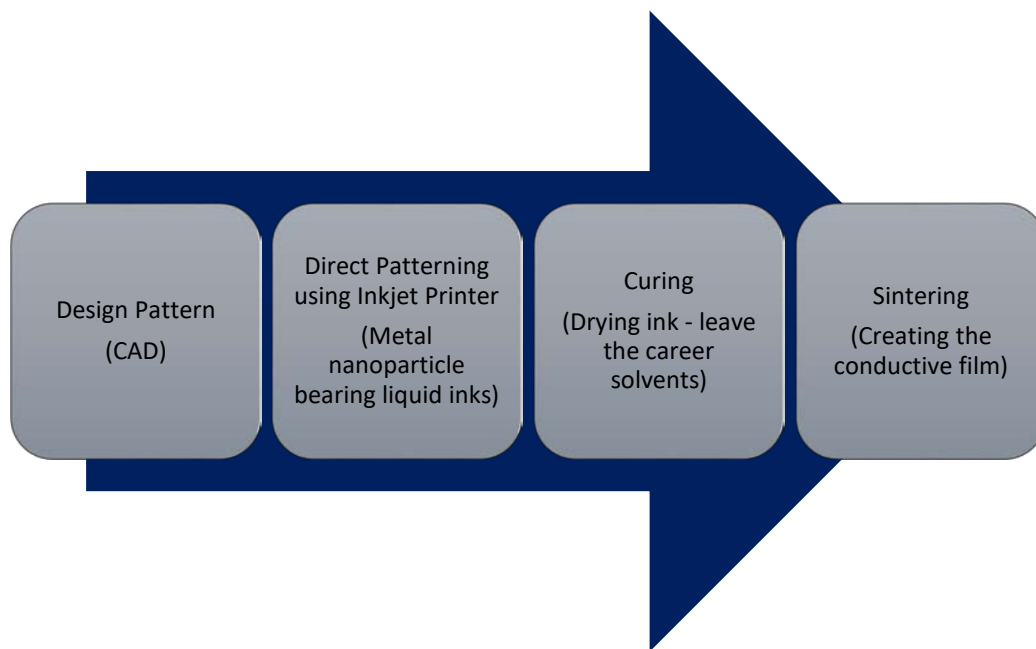


Figure 2.1: Inkjet printing (IP) - additive manufacturing (AM) processes for electrochemical sensor (ECS) fabrication.

SECTION 2.2. SHAPE MEMORY POLYMER

Shape memory polymer (SMP) can be defined as a polymer that can recover deformation and/or apply force in response to a stimulus such as heat, light, solvent, etc. Basically, recovering deformation is not the property of SMP rather it is the effect caused by appropriate programming (heating and applying stimulus) and polymer structure. Figure 2.2 illustrates different stages which provides information about the transformation cycle of SMP. The reason for applying force at higher temperature (above glass transition temperature) is that it provides chain mobility to reshape polymer microstructure. On the other hand, the polymer is stored at lower temperature (below glass transition temperature) because it restricts chain mobility (preserves microstructure of polymer strictly). SMPs are commonly made from polystyrene or polyolefin. In case of electrochemical (ECS) fabrication, the pattern is inkjet printed on SMP substrate. Then SMP is shrunk as well as the metal ink is sintered by applying higher temperature (greater than glass

transition temperature and lower than melting point) simultaneously. When, the contraction occurs on the substrate, the 3D printed pattern is also contracted. Hence, 3D microstructure is fabricated in a simple, cost-effective, and time efficient way.

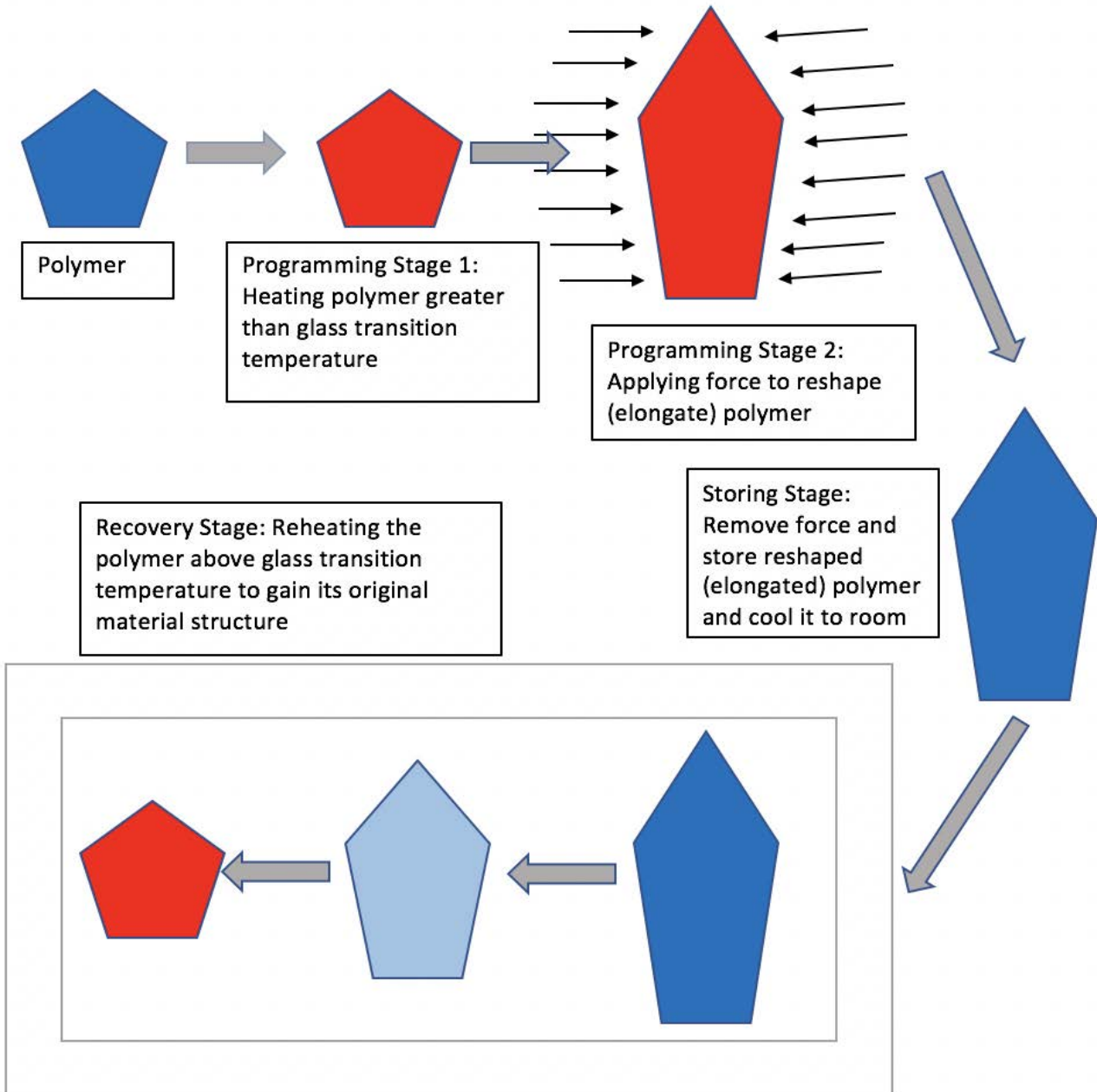


Figure 2.2: Shape memory polymer (SMP) cycle consists of three stages: programming, storing, and recovery stage.

SECTION 2.3. THREE ELECTRODE SYSTEM

The three-electrode system consists of a cell with one working electrode (WE), one counter electrode (CE), and one reference electrode (RE). This system is used in different types of voltammetry to observe current as a function of the applied potential. In this setup, the charge/current flows between working and counter electrode and the potential of the working electrode is measured with respect to the reference electrode. The three-electrode system eliminates the error in the electrode potential due to polarization current. An additional reference electrode is utilized in this setup to make the system stable. The working electrode in this research is a gold (Au) plated silver (Ag) based inkjet printed electrode. A specific potential is set at the working electrode so that it makes the contact with the analyte. The working electrode potential is controlled by the constant potential of reference electrode. In this research the reference electrode is silver chloride (AgCl) reference electrode. The reference electrode does not pass any current. The applied potential on the Au working electrode surface should be adequate enough to conduct oxidation-reduction or reduction-oxidation. Finally, the Au counter electrode passes the currents by completing the circuit. This current rate is limited by the electron transfer capacity on the gold working electrode surface.

SECTION 2.4. ELECTROCHEMICAL ANALYSIS

In this research, cyclic voltammetry (CV), square wave anodic stripping voltammetry (SWASV), and electrochemical impedance spectroscopy (EIS) have been performed on the fabricated ECSs for electrochemical analysis. In any kind of voltammetry, current is measured as a function of voltage/potential. In case of CV, a sweeping potential is applied across working and reference electrode. Because of the sweeping voltage, there comes a point when there will be enough positive charge on the electrode surface. In this phenomenon, the sample analyte in the

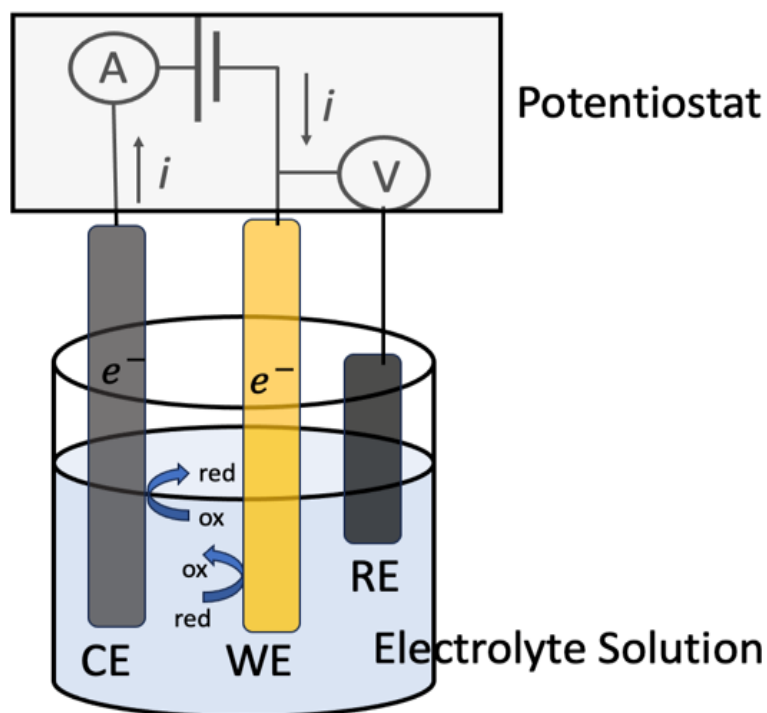


Figure 2.3: Three electrode system with working electrode – WE, counter electrode – CE, and reference electrode – RE.

solution i.e., lead ion (II) in this research is going to lose an electron. Whenever there is an electron transfer, there will be current flowing through the system. The oxidation peak represents the maximum number lead (II) ions oxidizing per second. The decaying current in the oxidation cycle represents less amount of available lead (II) ions to lose electron. When the sweeping potential starts decreasing there will be enough negative potential on the working electrode surface. In this circumstance, it will start donating the electrons to the lead (II) ions in the sample solution. This is defined as reduction. And the reduction peak represents maximum number of lead (II) ions reduced per second. As the layer gets depleted, a gradual increase in current is observed. And when there is no ion left for reduction, the cycle is complete. So, the forward sweep represents the stripping/oxidation of lead (II) ion and the reverse sweep represents the reduction/deposition

of lead (II) ion. CV is fast, cost-effective, and potential for higher concentration measurement. Figure 2.4 represents step by step processes of CV and Figure 2.5 shows actual CV for 5mM of lead (II) contaminated optimized DI water.

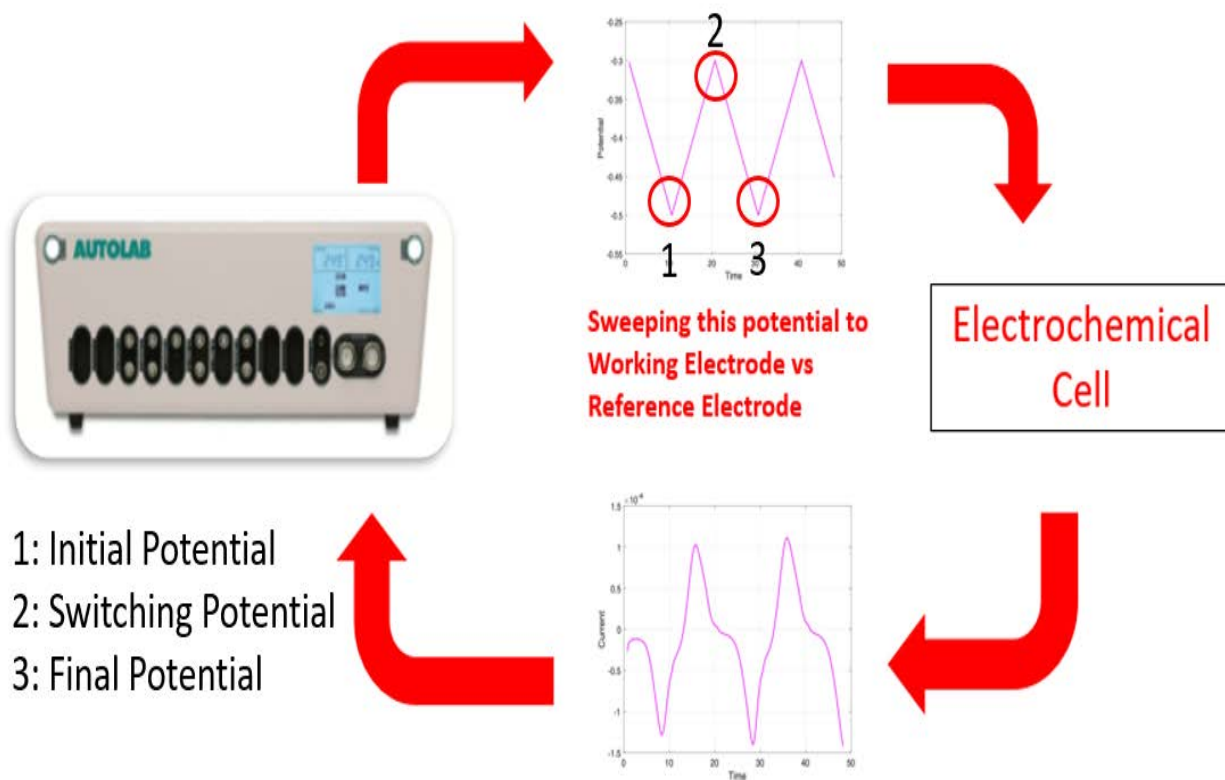


Figure 2.4: Step by step processes of cyclic voltammetry.

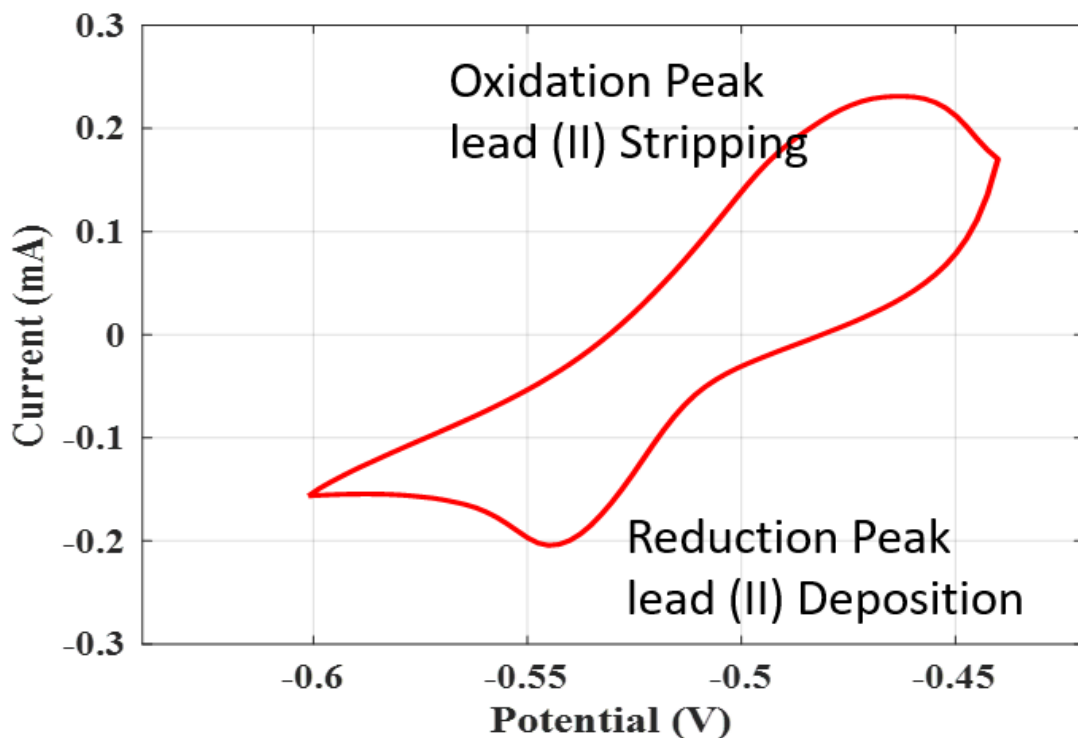


Figure 2.5: Cyclic voltammogram for 5 mM of lead (II) contaminated optimized (0.1 M HCl) DI water.

ASV consists of two steps i.e., deposition and stripping. In deposition metal or ion is deposited on the working electrode and in the stripping the ion is oxidized or stripped selectively from the electrode. Eventually, the potential difference in the sample solution is measured. In ASV, the linear potential is applied to counter electrode so that the current can flow from the working to counter electrode. On the other hand, the potential between working and reference electrode represent the potential in the cell. At the beginning, a large negative potential to working electrode is applied for few minutes to plate the electrode with sample analyte in the solution i.e., lead ion (II) in this research. In the next step i.e., in the stripping part, the deposited ions are selectively removed from the working electrode by oxidizing it. If the peak current is not significant enough the deposition time needs to be optimized. Deposition time is proportional to current and hence current is proportional to the concentration of lead (II) ions present in the sample

solution. ASV is comparatively slow and expensive but extremely helpful to determine lower concentration and selectivity. It can be utilized appropriately to perform selectivity for up to 5 different ions present simultaneously in the same sample solution. Figure 2.6 represents actual CV for 5mM of lead (II) contaminated optimized DI water.

EIS offers different types of electrical and mechanical data of electrochemical system. It has been widely used in case of characterizing different electrochemical and biosensors. In this electrochemical analysis, a sinusoidal signal i.e., ac voltage or current is applied over a wide range of frequencies and the sinusoidal response is observed in case of applied disturbance in the state of equilibrium. In this system, a signal excitation is applied for measuring impedance response. The impedance is divided into two parts i.e., real and imaginary. The graphical plot of imaginary impedance vs. real impedance is defined as Nyquist plot. On the other hand, a graphical representation of impedance magnitude vs. frequency is defined as Bode plot. This particular graphical plot is extremely popular in engineering community and has been utilized in this research. Figure 2.7 represents impedance vs. frequency characteristics in case of gold-plated inkjet printed ECSs in case of phosphate buffer saline (PBS; pH 7.42).

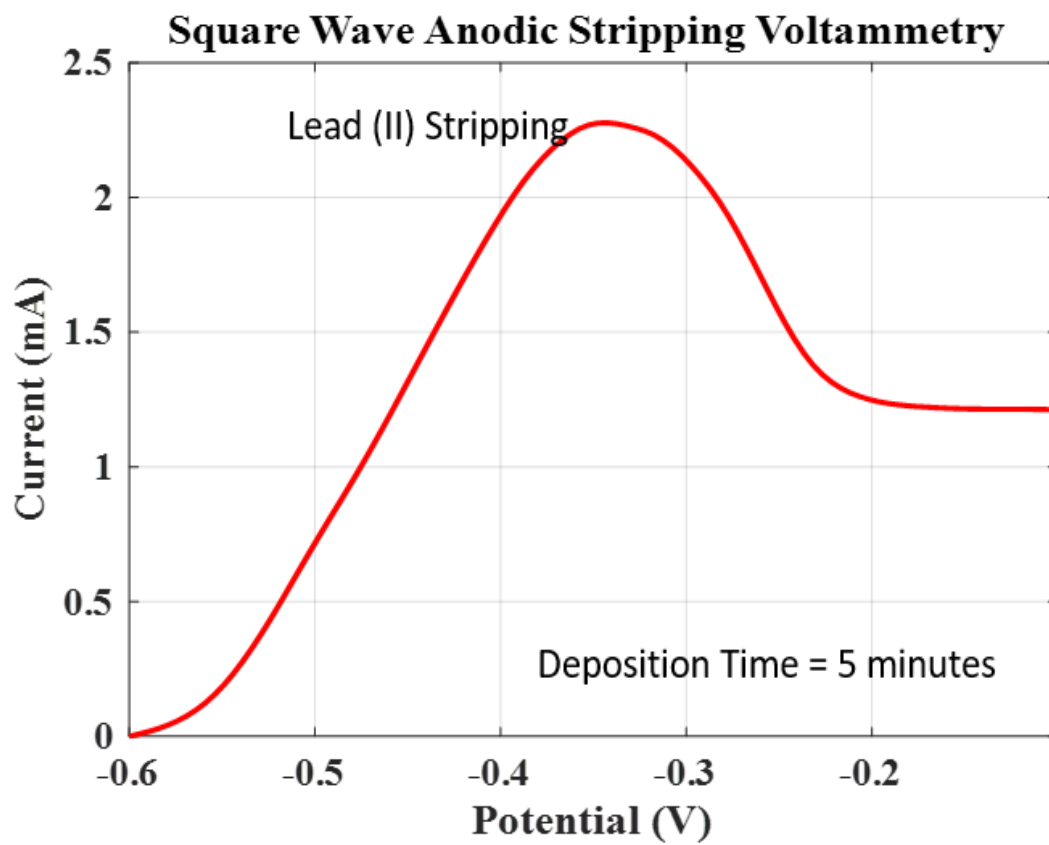


Figure 2.6: Square wave anodic stripping voltammetry for 5 mM of lead (II) contaminated optimized (0.1 M HCl) DI water.

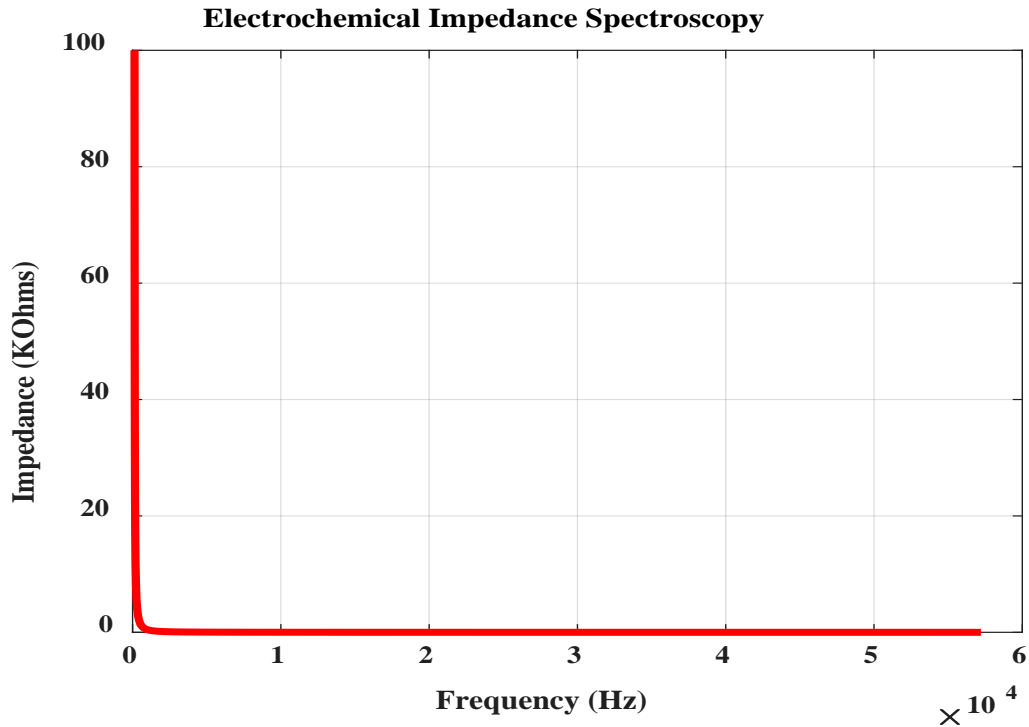


Figure 2.7: Impedance vs. Frequency response using electrochemical impedance spectroscopy measurement in case of phosphate buffer saline (PBS) with pH 7.42.

SECTION 2.5. UNCERTAINTY ANALYSIS

In this research, “Type A evaluation of standard uncertainty” approach from “Evaluation of Measurement Data – Guide to the expression of uncertainty in measurement (GUM)” has been used to determine the uncertainty in the raw data. As, arithmetic mean or average is the best available estimate of the expected value out of all possible observations, this has been used as the input estimate to determine the measurement results. The experimental variance of the observations has been estimated by the probability distribution of each occurrences. The calculated experimental standard deviation illustrates the dispersion of each observation from their mean. The variance and standard deviation of the mean have been determined by considering the experimental variance and experimental standard deviation out of the total number of

observations/occurrences. This variance of mean is defined as Type A variance and the standard deviation of the mean is defined as Type A standard uncertainty.

The best available estimate of a group of observations is the average or arithmetic mean of the total number of observations (in this study, total number of observations, $n = 15$ as 15 sensors/samples have been considered individually for uncertainty analysis). The average/mean has been calculated by,

$$\text{observation}_{\text{mean}} = \left(\frac{1}{n}\right) \sum_{j=1}^n \text{observation}_j \quad (2.1)$$

The individual observations contain different values because of random variations in the influence quantities (digital reading, processing time, temperature, and activation energy of diffusion). The experimental variance of the observations, which estimates the variance σ^2 of the probability distribution of the reduction factor has been determined by,

$$\sigma^2(\text{observation}) = \left(\frac{1}{n-1}\right) \sum_{j=1}^n (\text{observation}_j - \text{observation}_{\text{mean}})^2 \quad (2.2)$$

The experimental standard deviation (SD) has been determined from the square root of the estimated variance. Finally, in order to consider the best estimate, Type A variance (experimental variance of the mean) has been determined by,

$$\sigma^2(\text{observation}_{\text{mean}}) = \frac{\sigma^2(\text{observation})}{n} \quad (2.3)$$

Finally, Type A standard uncertainty has been calculated by taking the square root of the Type A variance.

SECTION 2.6. HISTORY AND STATE OF THE ART

The direct or indirect presence of highly toxic heavy metal ions (HMIs) in drinking water causes severe damage to human health, plants, and animals. It is well documented that highly toxic HMIs such as lead (Pb), arsenic (As), mercury (Hg), cadmium (Cd), antimony (Sb), and

chromium (Cr) are producing a significant impact to human health. Figure 2.8 shows maximum allowable rate of HMIs in aqueous solution decided and approved by USEPA (2022). It is important to detect the presence of HMIs level in samples precisely in order to protect and preserve the environment. Therefore, scientists have been making a continuous effort to mitigate the pollution of the environment by detecting HMIs in aqueous solution.

Recent researches try to find out what is the most effective and efficient solution on this very eminent issue which endangers human life. The reliable certified standard analytical methods (electrothermal atomic absorption spectrometry – EAAS, flame atomic absorption spectrometry – FAAS, inductively coupled plasma mass spectrometry – ICPMS, and inductively coupled optical emission spectrometry – ICOES) available in today’s world to assess the lead (II) concentration in aqueous solution is time consuming, expensive, bulky, and overall inefficient [7-9]. Therefore, several researches are wandering since the beginning of 20th century to mitigate the pollution of environment by detecting HMIs in aqueous solution effectively and efficiently.

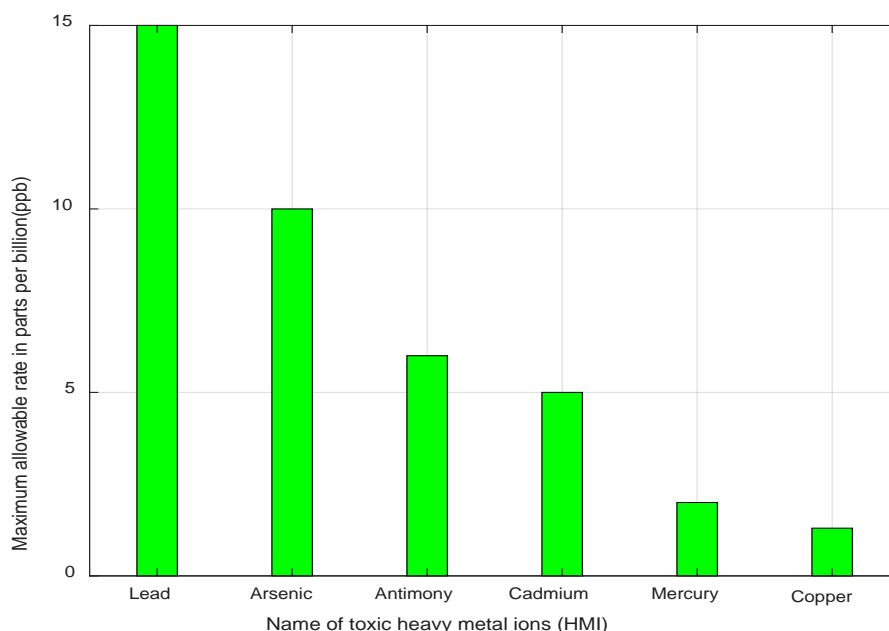


Figure 2.8: Maximum allowable rate of HMIs in aqueous solution by USEPA (2023).

Electrochemical stripping analysis is a sensitive and remarkable technique for ultra-trace level HMIs detection and can be easily coupled with inexpensive but efficient instruments [9]. Table 2.1 summarizes potential state of the art researches/systems to detect HMIs in aqueous and/or electrochemical solution using electrochemical stripping analysis. High sensitivity, short response time, specificity, and relatively low production cost makes ECSs eventually a reliable and convenient source of research for detecting HMIs in aqueous solution. Several manufacturing technologies such as electrochemical deposition [9, 10, 16, 19, 20], screen printing technology (SPT) [11-15, 17, 22, 23], and lithography [21, 24] have been applied to ECSs fabrication during the last 20 years. SPT is chosen and accepted by most of the manufacturers/researchers due to its cost-effectivity, favorable quality (only in case of bulk fabrication), flexibility of their design, and reproducibility [11-15, 17, 22, 23]. However, this technology has compromised performance such as varying quality (in case of batch to batch fabrication and materials), material waste, low resolution, and necessity for unique screen for each individual design [25, 28]. On the other hand, electrodeposition, lithography, ultrasonication, etc. are expensive, inconsistent, requires clean room facilities and/or hazardous materials.

Table 2.1: State of the Art Potential Electrochemical Sensors (ECSs) for Heavy metal ions (HMIs) Detection.

Year	ECS/System	Fabrication Technology/ Manufacturing Company	Measurement Technique	Detection Limit ($\mu\text{g/L}$)	Deposition Time (minutes)	Reference
2000	Bismuth coated carbon electrode	Deposition of bismuth on glassy carbon electrode (Goodfellow Co., Oxford, UK)	ASV	Pb - 1.1 Cd - 0.3	Pb - 2 Cd - 10	[10]
2005	Gold electrode	Screen printed electrode (SPE)	Square Wave Anodic Stripping Voltammetry (SWASV)	Pb - 0.5	Pb - 3	[11]
2010	Bismuth deposited carbon electrode	SPE	Differential Pulse Anodic Stripping	Pb - 278 Cd - 208	Pb - 5 Cd - 5	[12]

			Voltammetry (DPASV)			
2013	Bismuth based porous carbon electrode	SPE	ASV	Pb - 0.03 Cd - 0.34	Pb - 5 Cd - 5	[13]
2016	Phenanthroline-based flexible carbon electrode	SPE	Cyclic Voltammetry (CV)	Pb - 13906	-	[14]
2017	Bismuth deposited thin gold film-based electrode	SPE	Differential Pulse Anodic Stripping Voltammetry (DPASV)	Pb - 222.5	Pb - 6	[15]
2017	Cobalt oxide nanosheets on indium tin oxide substrate	Electrochemical deposition and annealing method	DPASV	Pb - 0.52	-	[16]
2017	Copper based electrode	SPE	ASV	Pb - 4.4	Pb - 5	[17]
2018	GCE modified by a thin layer of graphitic carbon nitride	Ultrasonication and drop casting	ASDPV and CV	Pb - 0.00002 Cd - 0.0009	Pb - 11.6 Cd - 11.6	[18]
2019	GCE modified with 3D nanoporous silica incorporated with poly furfural	Co-electro polymerization on GCE	CV, DPV, and ASV	Pb - 100	Pb - 5.83	[19]
2019	Gold nano dendrites (AuNDs) incorporated graphite pencil lead electrode	Electro-deposition of AuNDs on the surface of graphite pencil lead	ASDPV	Pb - 0.12 Cu - 0.19 Hg - 0.18	Pb - 5 Cu - 5 Hg - 5	[20]
2019	Micropillar array incorporated gold based working electrode	Lithography	CV and ASV	Pb - 1	Pb - 5	[21]
2020	Gold Electrode	SPE	SWASV	Pb - 7.3 Cu - 5.1 Hg - 4.3	Pb - 1 Cu - 1 Hg - 1	[22]
2021	Flexible copper-biopolymer nanocomposite electrode	SPE	SWASV	Pb - 7.2	Pb - 5	[23]
2021-2022	Inkjet printed gold plated electrode	Inkjet Printing	CV and SWASV	Pb - 7.2	Pb - 7.2	[29][30] [31] [32] [33]

Pb – lead (II); Cd – cadmium (II); Zn – zinc (II); Cu – copper (II); Hg – Mercury (II);

Inkjet printed electrodes have a wide variety of applications in today's electronic era i.e., electrochemical and biosensors [34-35], batteries [36-37], power electronic devices [38-41], and

integrated circuits [42]. For electrochemical and biosensing applications, elemental materials in addition to carbon-based materials – graphene and carbon nanotubes have received significant attention and consideration due to electrical conductivity, mechanical stability, chemical function ability, and environmental compatibility [43]. Recently, inkjet printed elemental materials based electrochemical and biosensors have been utilized widely due to its specific characteristics – high resolution, low-cost, low waste, mechanical flexibility, and wide variety of printable inks (gold, silver, platinum, palladium etc.) and substrates (glass, polymer, paper, ceramic etc.). Inkjet printing offers the same functionality (electrochemical and mechanical) compared to commercially available electrochemical and biosensors fabricated using conventional techniques i.e., lithography and screen-printing technology. Table 2.2 shows potential electrochemical applications of inkjet printed additive manufactured electrochemical sensors.

Table 2.2: Inkjet Printed Electrochemical Sensors (ECSs) for Different Applications.

Year	Application	Ink	Substrate	Sintering method	Reference
2005	H ₂ O ₂	Ag	PVC	Chemical	[44]
2011	Cancer biomarker protein	Au	Kapton	Thermal, 200 °C	[45]
2012	O ₂	Au and Ag	Cellulose	Thermal, 60°C	[46]
2013	pH and glucose	Au and Ag	Paper	Thermal, 200 °C	[47]
2013	Cancer biomarker protein	Au	PI	Thermal, 200 °C	[48]
2013	CRP antigen	Au	Paper	Photonic	[49]
2014	DNA hybridization	Au	Paper	Photonic	[50]

2015	Free chlorine	Ag	Glass	Thermal, 120 °C	[51]
2015	Salmonella	Au and Ag	PET	Photonic	[52]
2016	pH	Pd	Glass/PI	Thermal, 200 °C	[53]
2016	pH and DO	Au and Ag	PI	Thermal, 200 °C	[54]
2016	K ⁺	Au	Paper	Photonic	[55]
2017	S ²⁻	Ag	PEN	Thermal, 120 °C	[56]
2018	pH	Pd and Ag	Glass	Thermal, 200 °C	[57]
2019	pH and glucose	Pt and Ag	PEN	Thermal, 180 °C	[58]
2019	Pb ²⁺	Bi (inorganic salt)	PET	Photonic plasma	[59]
2019	Hg ²⁺	Au	PI	Thermal, 380 °C	[60]
2019	DNA	Au	PET	Plasma	[61]
2020	Ni ²⁺	Ag and Au	Paper	Thermal, 160 °C	[62]
2021	Paraquat	Ag	Paper	Thermal, 120 °C	[63]
2022	DO and ROS	Ag and Au	Glass	Thermal, 120 °C	[64]
2023	Blood biomarkers for Alzheimer's disease	Graphene modified with gold	Ceramic	Thermal, 37 °C	[65]

Gold – Au; Silver – Ag; Palladium – Pd; Platinum – Pt; Oxygen – O₂; Nickel – Ni²⁺; Dissolved oxygen – DO; Reactive oxygen species – ROS; Sulfide – S²⁻; Lead – Pb²⁺; Bismuth – Bi; Mercury – Hg²⁺; Hydrogen peroxide – H₂O₂ ;Potential of hydrogen – pH; PI

– Polyimide; PEN – Polyethylene naphthalate; PET - Polyethylene terephthalate; PVC – Polyvinyl chloride

Materials also play a significant role in terms of ECS fabrication. Historically, mercury was initially considered as a potential material in order to manufacture ECSs due to its high hydrogen potential [9]. However, in order to maintain the green environment, scientists have started to find out the alternatives of mercury [7, 66]. Researchers have shown interests towards different types of materials such as bismuth (Bi) [7, 10, 12, 13, 15], gold (Au) [11, 20-22, 29-33, 37], carbon (C) [18, 19], copper (Cu) [17, 23], and boron doped diamond [68]. These materials have been used enormously to observe their capacity and performance to replace mercury. Figure 2.9 represents the percentage of ECSs fabricated from different types of materials for HMIs detection [7].

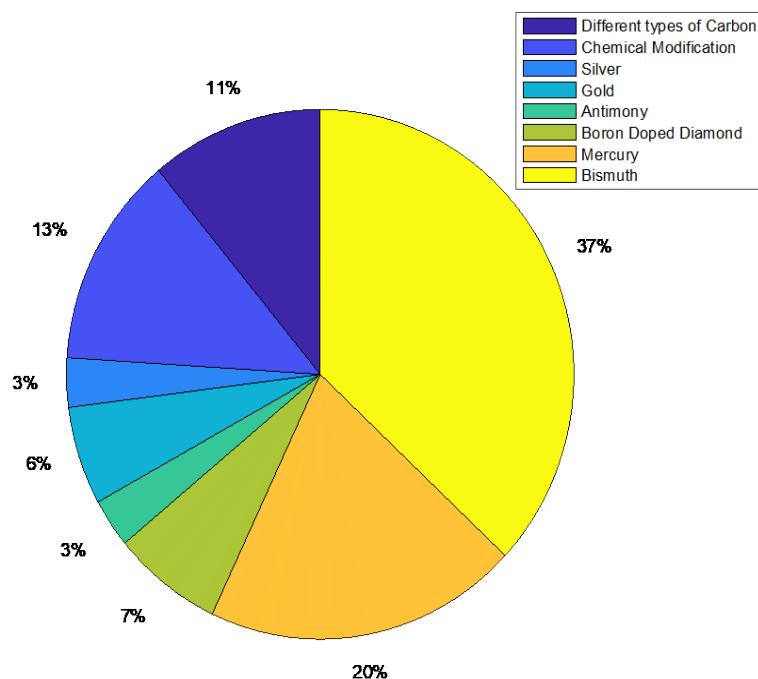


Figure 2.9: Percentage of various materials' contribution for electrochemical sensor (ECS) fabrication for HMIs detection.

It is observed that, in order to manufacture and establish green ECSs for HMIs detection researchers significantly focused on Bi (37%) due to its environment friendly characteristics and good analytical performance. However, some analysts focused on other materials as well to observe their effectiveness for ECSs in case of HMIs detection. However, Bi is considered as one of the most promising materials in case of heavy metal ions (HMIs) detection. Bi is a potential alternate of mercury. It has significant material properties i.e., wide potential window, inertness towards dissolved oxygen in the test medium, ability to form alloy with HMIs, and low toxicity [69]. Bi can be functionalized in case of HMIs detection in three different ways – ex situ, in situ, and bulk modification [70-72]. In the ex situ processes, Bi is deposited on the working electrode following under potential deposition at a specific potential before HMIs detection. In the in-situ processes, Bi is deposited on the working electrode with the target HMIs simultaneously. Bulk modification of the working electrode occurs by the fabrication of the electrode with a mixture of active material and Bi with a specific ratio. Table 2.3 shows the detail information regarding Bi functionalized ECS in case of different HMIs detection.

Table 2.3: State of the Art Potential Bismuth Modified Electrochemical Sensors (ECSs) for Heavy metal ions (HMIs) Detection.

Year	ECS/System	Fabrication Technology	Matrix	Measurement Technique	Detection Limit ($\mu\text{g/L}$)	Deposition Time (minutes)	Reference
2004	Nafion coated bismuth plated electrode	Bismuth electrode deposition followed by spread coating of Nafion	Urine, wine, tap water	Square Wave Anodic Stripping Voltammetry (SWASV)	Pb – 0.1 Cd – 0.1 Zn – 0.4	10	[73]
2005	Graphite epoxy composite electrode containing in-built bismuth precursor	Graphite paste containing bismuth salt placed in a PVC sleeve body	Buffer solution	SWASV	Pb – 19.1 Cd – 35.8	2	[74]

2006	Copper/ Nafion/ Bismuth electrode	Electro-deposition of bismuth on copper substrate	Ground water	Differential Pulse Anodic Stripping Voltammetry (DPASV)	Pb – 0.62 Cd – 0.68	10	[75]
2008	Electro chemical reduction of bismuth oxide electrode	Screen printed electrode (SPE)	River water	SWASV	Pb – 2.3 Cd – 1.5	5	[76]
2009	Nafion film modified bismuth coated glassy carbon electrode (GCE)	Chemical reduction followed by electrodeposition	Sewerage water	SWASV	Pb – 2.47 Cd – 1.39 Cr – 5.27	2	[77]
2010	Bismuth modified carbon nano tube (CNT) with poly composite film	Electrodeposition of bismuth on CNT	Lake water	DPASV	Pb – 0.04 Cd – 0.02	2	[78]
2014	Bismuth deposited graphene oxide reduced ionic liquid doped electrode	SPE	Rice	SWASV	Pb – 0.10 Cd – 0.08	2	[79]
2014	Multifiber microelectrode with bismuth film	Double deposition and stripping	Buffer solution	SWASV	Pb – 0.037 Cd – 5.04×10^{-3}	5	[80]
2014	Bismuth electrode based on electrochemically reduced graphene oxide	SPE	Milk	DPASV	Pb – 0.8 Cd – 0.5	5	[81]
2015	GCE coated with multi walled carbon nanotube (MWCNT)	Electro-deposition of bismuth on GCE	Tap and well water	DPASV	Pb – 0.40 Cd – 0.20	7	[82]
2015	Bismuth doped mesoporous carbon xerogel deposited GCE	Sol-gel method coupled with drying and thermal pyrolysis	Well water	SWASV	Pb – 0.07 Cd – 5060	3	[83]
2015	Bismuth film electrode based on activated graphene	Electrodeposition of bismuth using 0.1 M acetate buffer solution	Tap water	DPASV	Pb – 0.05 Cd – 0.07	5	[84]
2016	Bismuth oxide doped mesoporous carbon electrode	Drop casting of bismuth on GCE	Lake water	SWASV	Pb – 3.65×10^{-4} Cd – 1.77×10^{-4}	~3	[85]

2016	Bismuth working electrode on oxidized silicon wafer	Photolithography	Lake water	SWASV	Pb – 0.18	0.5	[86]
2016	Graphene bismuth nanocomposite GCE	Electrodeposition of exfoliated graphene oxide and bismuth deposition	Tap water	DPASV	Pb – 0.11 Cd – 0.18 Zn – 1.80	5	[87]
2016	Nafion/ionic liquid/ graphene composite modified carbon electrode	SPE	Drinking water	SWASV	Pb – 0.8×10^{-4} Cd – 0.6×10^{-4} Zn – 0.9×10^{-4}	2	[88]
2018	Bismuth plated reduced graphene oxide and CNT composite flexible electrode	Photolithography	Drinking water	SWASV	Pb – 0.2 Cd – 0.6	2.5	[89]
2019	Modified nano porous bismuth electrode	Electroplating of bismuth and tin	Acetate buffer solution	SWASV	Pb – 1.5 Cd – 1.3	5	[90]
2020	Bismuth nanoparticle loaded cobalt ferrite GCE	Drop casting	Tap water	SWASV	Pb – 2.42 Cd – 1.50	5	[91]
2022	Bismuth film deposited carbon paste electrode	Under potential deposition of bismuth	Acetate buffer solution	SWASV	Pb – 0.5 Cd – 0.3	3	[92]
2022	Bismuth oxide surface decorated nano porous bismuth GCE	Drop casting	Tap water	SWASV	Pb – 0.02 Cd – 0.03	3	[93]

Pb – lead (II), Cd – cadmium (II), Zn – zinc (II), Cr – chromium (IV)

In this research Bi and Au plated working electrode, Au counter electrode and Ag/silver chloride (AgCl) reference electrode have been fabricated and analyzed. Although it is observed from the pie chart that researchers have used Au in a very inconsequential way for lead (II) detection, it has been chosen as a base material for the working and counter electrodes due to its significant electrochemical properties such as biocompatibility, large surface area, high surface energy, and interface dominating properties [29-32]. Due to biocompatibility and large surface area, the Au plated ECSs have shown high sensitivity and selectivity. Improved sensitivity and selectivity happen due to high surface energy and interface dominating properties. It should also

be noted that, in this research cost-effective ECSs fabrication has been a major concern. Hence, the Au electrodes have been fabricated using Au electrodeposition on silver inkjet printed electrodes on SMP. The performance of the electrodeposited Au electrodes is potential enough compared to bare Au electrodes (performances have been compared in case of optimized cleaning procedure with 0.5 M sulfuric acid) to receive further considerations for other electrochemical/bio sensing applications.

The ECSs are characterized/optimized using different electrochemical analysis such as cyclic voltammetry (CV) [14, 18, 19, 21] and anodic stripping voltammetry (ASV) [9-13, 15-23] to understand different facts in detecting HMIs such as selectivity, sensitivity, reliability, as well as reproducibility. In this research, both approaches are going to be applied in the case of green fabricated inkjet printed Au plated ECSs.

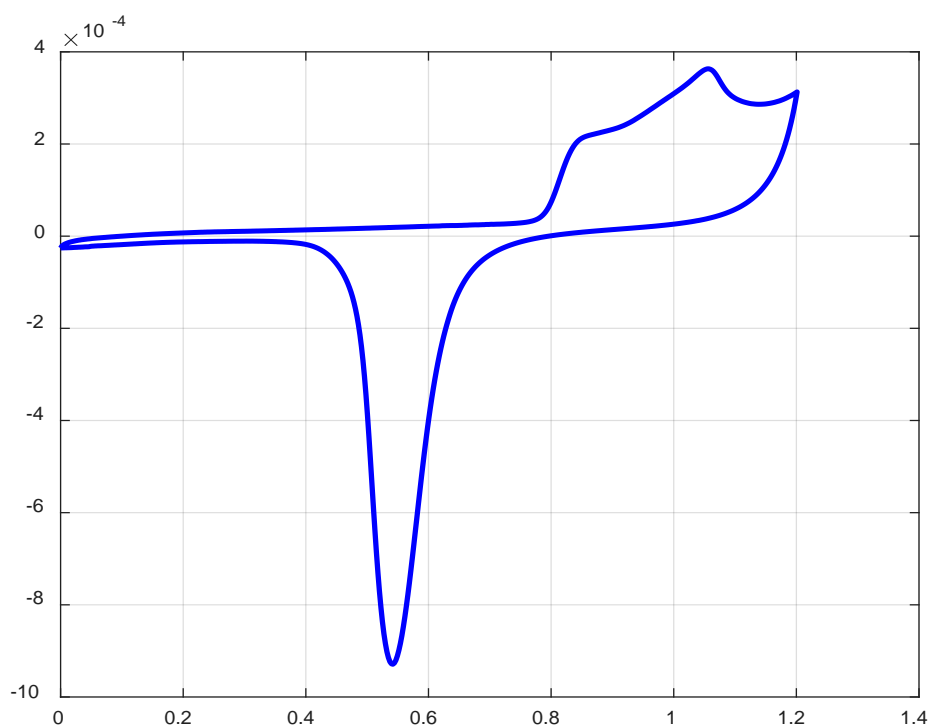


Figure 2.10: Cyclic voltammetry (CV) for inkjet printed gold plated electrochemical sensor (ECS) using 0.5 M sulfuric acid (H_2SO_4). Scan rate is 100 mV/s.

SECTION 2.7. SUMMARY

This chapter has provided detail background description of related topics i.e., inkjet printing, shape memory polymer, three electrode system, electrochemical analysis, and uncertainty analysis. A thorough literature review has been delineated regarding HMIs detection. Literature review has been performed from different point of view i.e., reviewing/exploring all the potential ECSs for HMIs detection, focusing on only inkjet printed ECSs for different applications, observing different materials/metals utilized for fabricating ECSs, reviewing the performance of bismuth coated/plated ECSs, and finally potential electrochemical analysis for optimizing and characterizing fabricated ECSs. Literature review based on different perspective has been outlined in the form of tables to provide conceptual and contextual ideas to the readers regarding ECSs for HMIs detection in detail.

Chapter 3: Fabrication of Inkjet Printed Electrochemical Sensor

This chapter focuses on the fabrication of inkjet printed gold-plated ECSs thoroughly. A detail description of apparatus and reagents including vendor details as well as electrochemical sensor design have been provided in Section 3.1. Section 3.2 covers all the inkjet printing recipe development i.e., details of fluid properties measurement of nanoparticle inks and jetting recipe development for Dimatix materials printer DMP 2850. DMP 2850 operates with piezoelectric drop-on-demand (DOD) printheads. Previously, Dimatix used to manufacture Legacy printheads (8-12 cP). Recently, they have launched a new printhead with different properties (2021) – Samba printheads (4-8 cP). All the detail information regarding both printheads have been reported in this section. In addition, the jetting recipes have been developed for both printheads to ensure future production/research of the inkjet printed ECSs as Dimatix has stopped manufacturing Legacy printheads. Shape memory polymer (SMP) has been utilized as a printing substrate for fabricating inkjet printed ECSs. Section 3.3 represents detail characterization of SMP. Finally, Section 3.4 describes step by step fabrication processes of inkjet printed gold-plated SMP incorporated ECSs.

SECTION 3.1. MATERIALS AND METHODS

Section 3.1.1. Apparatus and Reagents

Deionized ultra-filtered water was collected from Fisher Chemical. Conductive 50 nm diameter silver nanoparticle ink (ANP-DGP-40-LT-15-C) was obtained from Advanced Nano Products Co., LTD. Low cost consumer grade polystyrene shape memory polymer substrate (MagicShrink) and sodium hypochlorite solution – 3% (bleach) were arranged from local store. Hydrochloric acid solution (1N) (Cat. # SA481) was collected from Thermo Fisher Scientific, Fair Lawn, NJ, US. Lead (II) Chloride (Cat. # 7758-95-4) was obtained from Sigma Aldrich, St. Louis,

MO, US. Brush Gold Solution (24K) and Electro-Cleaner Solution were collected from Gold Plating Services, Inc., Layton, UT, US. Digital Multimeter (Tektronix DMM 4050) has been used to perform resistivity measurement for each fabricated sensor sample. Drop on demand inkjet printer DMP 2850 at Convergent Microsystems Laboratory (CML), the University of Texas at El Paso (UTEP) has been used for this research to inkjet print the electrochemical sensors using 10 pL piezoelectric cartridges i.e., Legacy and the newly launched Samba (2021) with integrated reservoir and heater. Keithley 2450-EC, Graphical Potentiostat, 200 V, 1 A, 20 W has been utilized to characterize the fabricated electrochemical sensor with cyclic voltammetry (CV) potentiodynamic electrochemical measurement technique. In addition, the square wave anodic stripping voltammetry (SWASV) and electrochemical impedance spectroscopy (EIS) have been performed using Autolab PGSTAT302N from Dr. Cabrera's lab, UTEP. Finally, a scanning electron microscope (SEM) Hitachi SU 3500 SEM equipped with a STEM detector from Polymer Extrusion Lab (PEL), UTEP has been utilized to observe and analyze the characteristics – scanning electron micrograph (SEM) images and energy dispersive spectroscopy (EDS) of fabricated novel inkjet printing and shape memory polymer incorporated gold-plated electrochemical sensors for lead (II) detection in aqueous solutions.

Section 3.1.2. Design of the Sensor

The electrochemical sensor pattern was designed using computer aided drafting (CAD) tool such as GIMP 2.10.24. This design was then converted into printer-identified image (bitmap image for the Dimatix Fujifilm inkjet printer) where the image was a combination of pixels. The inkjet printer was then operated by controlling unit (PC-based software) to eject/inkjet printed silver nanoparticle ink according to the bitmap CAD design to achieve a coherent pattern on shape memory polymer (SMP). The fabricated novel inkjet printed and SMP incorporated gold (Au)

plated electrochemical sensor (ECS) consists of a three electrodes cell with Au working electrode, Au counter electrode, and silver chloride (AgCl) reference electrode. The overall dimension of the designed and inkjet printed electrochemical sensor is $31 \times 25 \times 0.52 \text{ mm}^3$. The working electrode area of the designed electrochemical sensor is 20.25 mm^2 .

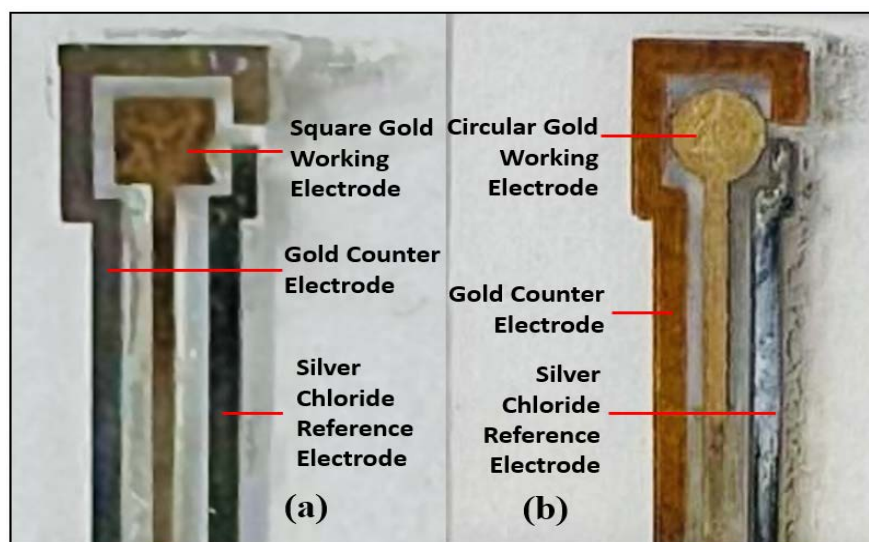


Figure 3.1: Inkjet printed shape memory polymer (SMP) incorporated gold plated electrochemical sensors (ECSs) for lead (II) detection: (a) square working electrode and (b) circular working electrode.

Both circular working electrode (popular in literature) and square working electrode have been designed and fabricated. Figure 3.1 (a) and (b) represents inkjet printed Au plated ECSs for both square and circular working electrodes respectively. Effective electrode surface area (EESA) has been calculated for both square and circular inkjet printed Au plated ECSs. EESA has been calculated based on quasi reversible Randles-Sevcik equation. The EESAs of the square and circular shape working electrodes are 7.25 mm^2 (lateral area – 4.19 mm^2) and 6.52 mm^2 (lateral area - 3.291 mm^2) respectively which justify our previously reported claim to have increased EESA even after miniaturization of the Au plated inkjet printed ECSs. The EESA calculation has been described in detail in Section 5.1 and Appendix B. However, as the square working electrode

appeared to have larger EESA, the further investigation and experiments in this research have been conducted with square Au plated inkjet printed electrodes. Figure 3.2 and 3.3 represent the cyclic voltammetry (CV) analysis at different scan rates (required for EESA calculation) respectively.

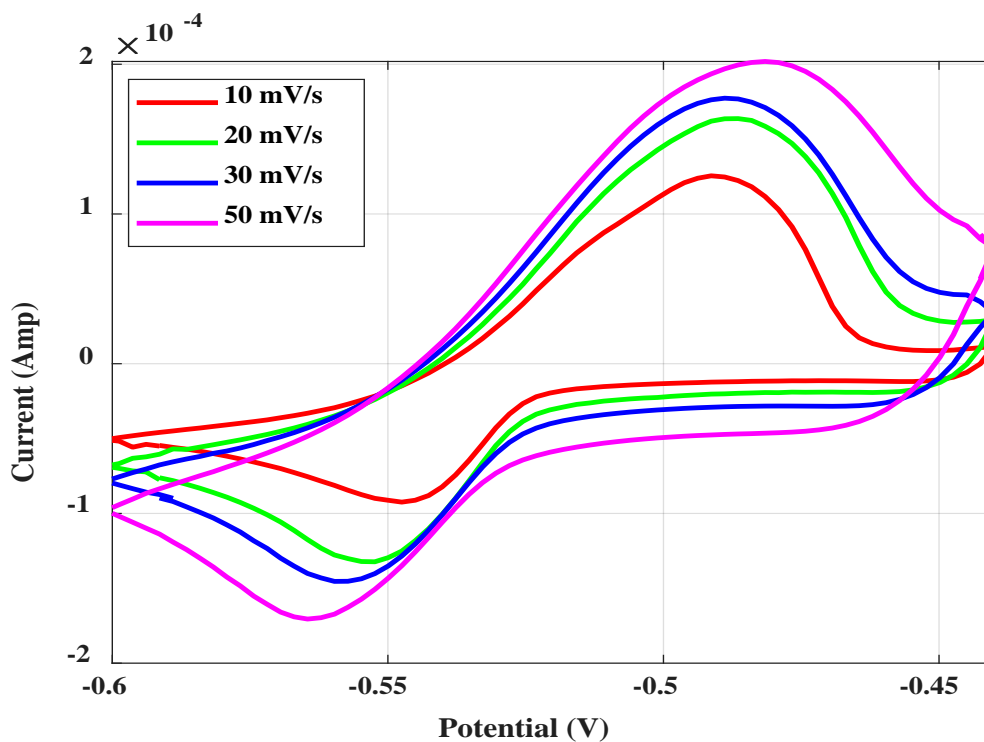


Figure 3.2: Cyclic voltammogram (CV) for inkjet printed gold electrochemical sensor (square working electrode surface area) for 5 mM of lead (II) contaminated optimized (0.1 M HCl) deionized water for different scan rate (10, 20, 30, and 50 mV/s).

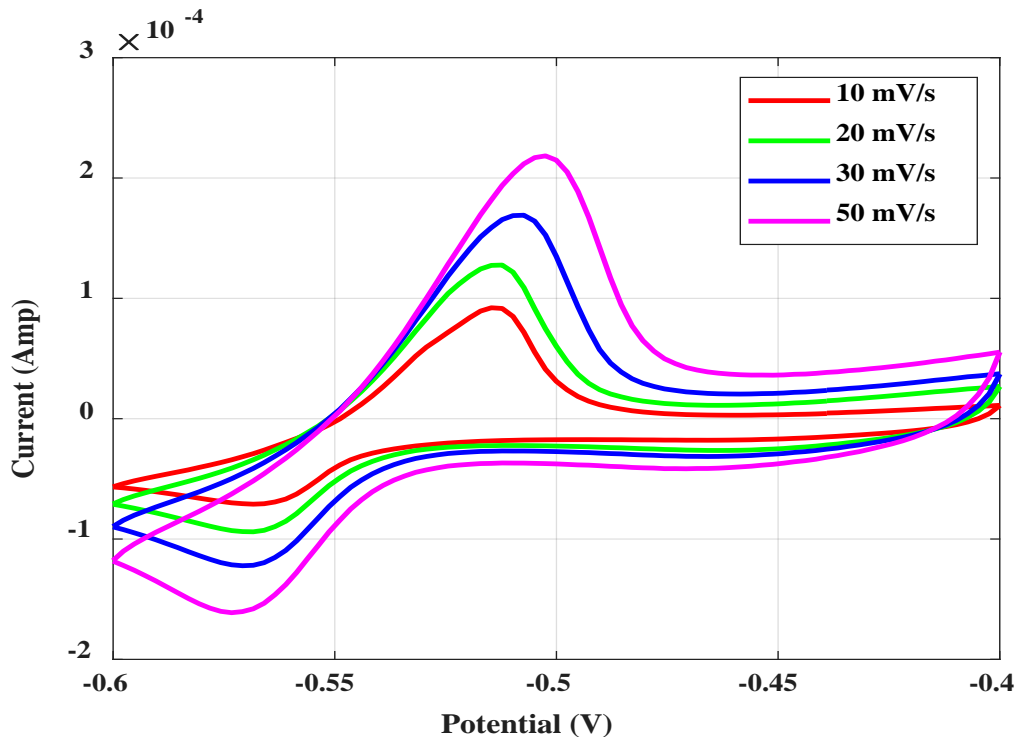


Figure 3.3: Cyclic voltammogram (CV) for inkjet printed gold electrochemical sensor (circular working electrode surface area) for 5 mM of lead (II) contaminated optimized (0.1 M HCl) deionized water for different scan rate (10, 20, 30, and 50 mV/s).

SECTION 3.2. INKJET PRINTING RECIPE DEVELOPMENT

Section 3.2.1. Fluid Properties of Nanoparticle Ink

In this research, silver (Ag) nanoparticle conductive ink has been utilized to inkjet print electrochemical (ECS) patterns on shape memory polymer (SMP) substrate. Ag ink has been chosen due to its high compatibility with Fujifilm Dimatix Materials inkjet printer (DMP 2850) and excellent fluid properties. It also offers high cost-effectivity and conductivity. It is considered as one of the best performing ink in case of inkjet deposition. This highly conductive nanoparticle ink has been characterized based on its fluid properties i.e., viscosity, surface tension, particle size measurement, and pH value. Ink viscosity has been analyzed using a Brookfield Ametek LV-DVE viscometer (spindle 00 and 30 rpm). The Enhanced UL Adapter accessory and a recirculating water bath has been utilized to allow for 16 ml sample volumes to be measured with viscosities

down to 1cP. The viscosity of the ink has then been captured as a function of temperature. Surface tension measurements have been performed with a BZY-201 tensiometer using the Wilhelmy platinum plate technique. Prior to each measurement, the plate has been cleaned in solvent (isopropanol) and then heated using an alcohol burner. In this method, dynamic contact angle is measured while immersing and withdrawing the vertically suspended platinum plate. Dynamic light scattering (DLS) measurements have been performed using a Precision Detectors PD2000LS dynamic light scattering system using a quartz cuvette for particle size measurement of Ag nanoparticle conductive ink. The observation has been obtained using a 10⁶x dilution of commercially available Ag ink. The viscosity, surface tension, particle size, and pH value of the Ag ink are 11.6 cP, 32.3 mN/m, 17.7 nm, and 10 respectively. All the fluid properties measurements have been performed at room temperature (20°C). The adhesion test for Ag ink has been performed using ASTM D3359 (ASTM 2009) on SMP substrate. It has shown excellent adhesion property for SMP substrate. Finally, the sintering process is extremely simple and fast in case of Ag nanoparticle ink. It takes 10-20 minutes to convert the Ag nanoparticle ink into a conductive film at 150°C – 180°C. In this research the Ag inkjet printed patterns on SMP have been sintered and cured at 180°C in 3 minutes only.

Section 3.2.2. Recipe Development for Inkjet Printheads

The performance of silver (Ag) nanoparticle conductive ink has been evaluated based on inkjet printing using Fujifilm Dimatix DMP-2850. The jetting parameters have been investigated thoroughly and developed for the Ag ink. During this research, it was learned that the manufacturer had discontinued their older style print heads – Legacy printheads (DMC-11610/11601) and were migrating all systems to their newer Samba G3L print heads. Hence, initial development began on the legacy print heads, and then migrated to the newer style print

heads. The legacy printhead used for inkjet printing Ag was DMC-11610 (10 pL) which had 16 nozzles spaced 254 μm apart. On the other hand, the Samba G3L printhead has 12 nozzles spaced 338.67 μm apart. Before loading the ink into a syringe (3ml) and performing the printing tests, the inks were filtered with 0.2 μm 25mm diameter polytetrafluoroethylene (PTFE) filter. SMP has been used as a printing substrate to print the nanoparticles conductive ink. The viscosity requirement of the new head (4-8 cP) is much lower than the DMC-11610 (10-12 cP). To use the new heads, after upgrading DMP 2850 printer, one needs to follow the same procedure as with the old heads but be sure to select the Samba 12 nozzle head when loading the cartridge. Also, these new heads appear to have wetting issues if wiped with isopropanol, so this has been avoided. Inkjet printing parameters have been optimized based on different print heads i.e. platen temperature for both printheads has been chosen as 35 $^{\circ}\text{C}$, cartridge temperature has been optimized between 30 - 35 $^{\circ}\text{C}$, jetting voltage has been ranged from 22-26 V, jetting frequency and meniscus set point for Legacy and Samba printheads has been chosen as 5 kHz and 0.5 as well as 5 kHz and 5 respectively. The cartridge print height has been selected as 1 mm. Figure 3.4 represents the waveforms for Ag ink in case of both Legacy and Samba printheads. The drop spacing used for printing different patterns with both print heads and Ag ink was 64.5 μm - drop diameter of Ag ink on SMP is \sim 75 μm . Table 3.1 exhibits the detail of jetting recipes for both printheads.

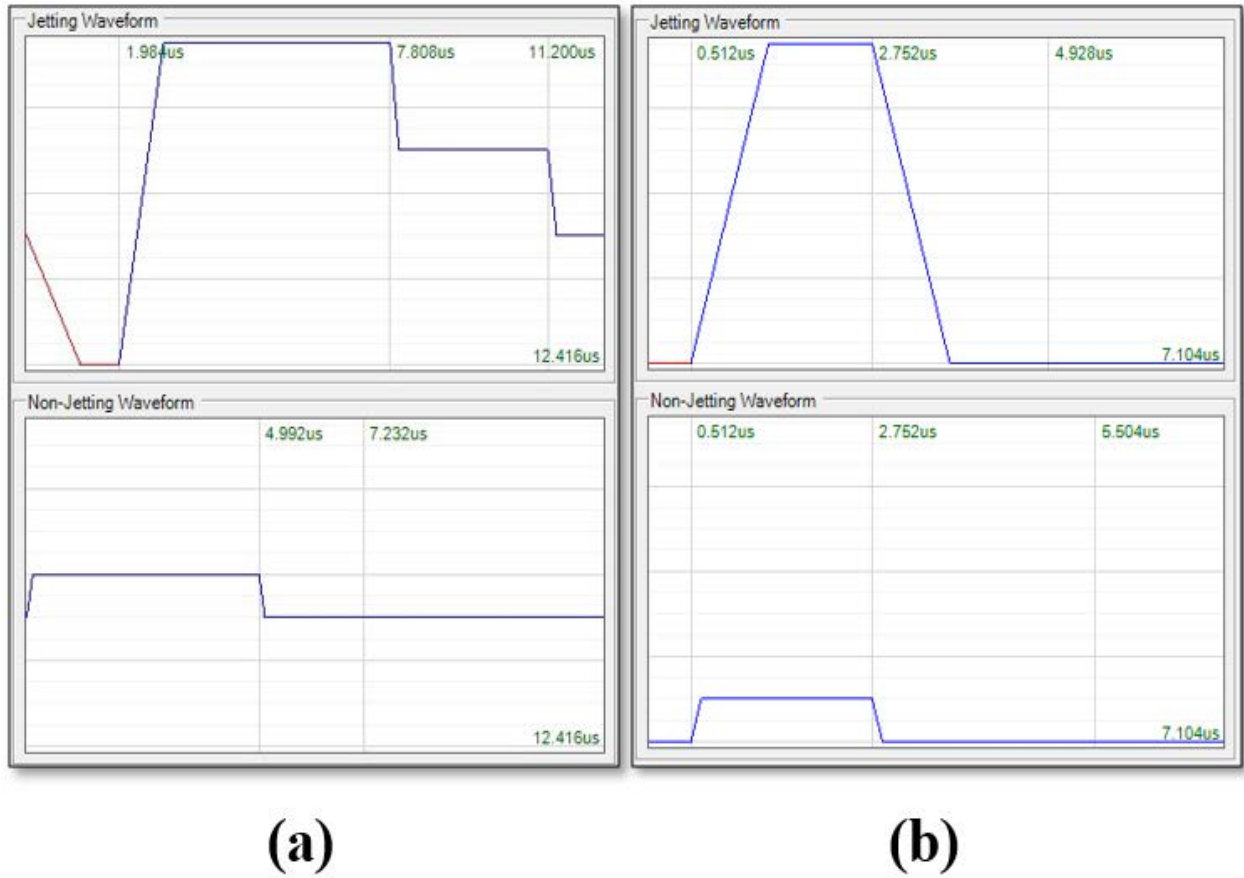


Figure 3.4: Waveform data for the silver nanoparticle conductive ink (a) DMC-11610 (left) and (b) Samba printheads (right).

Table 3.1: Inkjet Printing Recipes (Fujifilm Dimatix DMP 2850) of Silver Nanoparticle Conductive Ink.

Nanoparticle Ink	Optimized Inkjet Printing Parameters	Inkjet Printhead	Drop Speed (m/s)
Silver	Platen temp – 35 °C Cartridge temp – 35 °C Jetting Frequency – 5 kHz Jetting voltage – 22V Meniscus set point – 0.5	Legacy	~4.8
Silver	Platen temp – 35 °C Cartridge temp – 38 °C Jetting Frequency – 5 kHz Jetting voltage – 26V Meniscus set point – 5	Samba	~7.3

SECTION 3.3. CHARACTERIZATION OF SHAPE MEMORY POLYMER SUBSTRATE

Inkjet printing electrodes on shape memory polymer (SMP) substrate allows for 3D electrode formation in a single process step at low temperature and atmospheric pressure. In this research, thermally contracting SMP has been utilized to print electrochemical sensor (ECS) electrode patterns using inkjet printing silver (Ag) nanoparticle ink. The Ag nanoparticle ink electrode geometry has been sintered and shrunk simultaneously by placing it into an oven for 3 minutes. It has been observed that the reduction factor (%) of the processed ECS (sintered and shrunk) achieves up to 58% approximately and creates a complex 3D metal topology which is difficult to obtain using conventional electrode fabrication techniques [96-98]. The detail of reduction factor (%) has been included in Appendix A. In order to observe the shrinking characteristics of the SMP film used for this research (MagicShrink), 18 different samples (1 cm by 1 cm) were shrunk at six different temperatures (140°C to 190°C) for 3 minutes. It has been observed that, the shrinking mechanism is similar and stable for each sample. The reduction factor of the shrunk film is 0.58 for each sample.

In this research, nanoparticle Ag ink (ANP DGP-40-LT-15-C) has been used to inkjet printing ECS pattern. This nanoparticle ink becomes conductive by curing it at 150°C ~180°C for 10 to 20 minutes. But it has been perceived that the desired conductivity can be achieved only within 3 minutes at 140°C to 190°C with SMP (simultaneous curing and shrinking mechanisms). Resistivity measurements of the SMP fabricated electrodes have been performed to characterize the process impact on thin-film performance. Scanning electron micrograph (SEM) images have been utilized to further characterize the 3D microstructure and topology created by inkjet printing on SMP fabrication process for ECS at different process temperatures. Figure 3.5 shows SEM

images of inkjet printed Ag ECSs on SMP before (left) and after (right) shrinking and curing the electrodes.

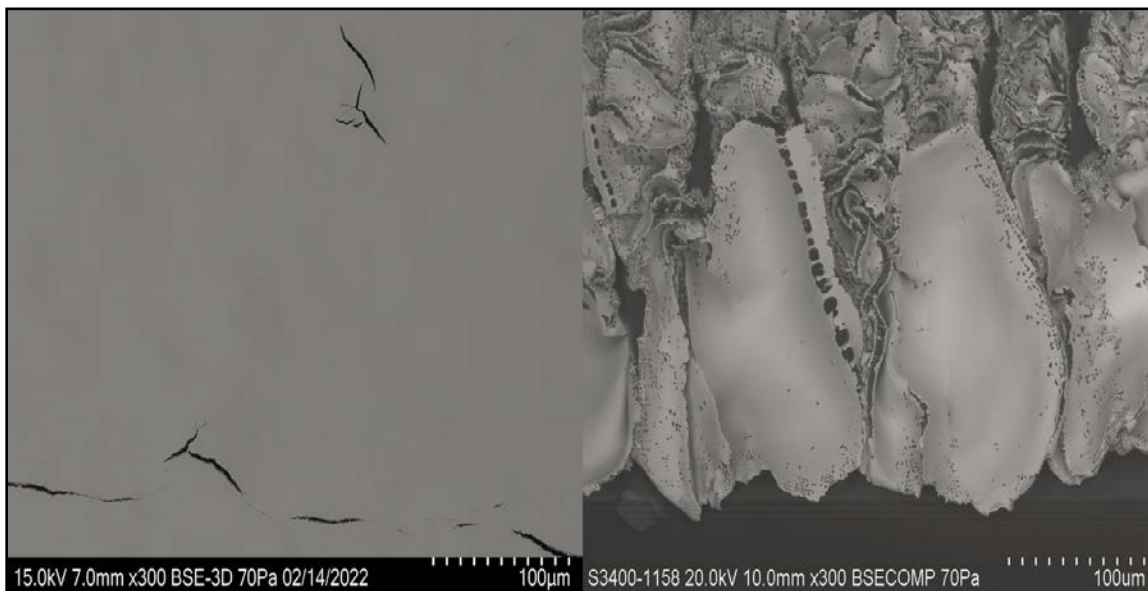


Figure 3.5: Scanning electron micrographs (SEM) of inkjet printed metal films on shape memory polymer before (left) and after (right) shrinking (cured and shrunk at 180 °C for 3 minutes). The shrunk (right) SEM strongly reveals a 3D wrinkled structure, providing a large surface area, useful for enhancing sensor performance.

Fabricating ECSs on SMP with inkjet printing technology has shown promising potential to improve electrochemical sensing. The inkjet printing on SMP process demonstrates significant 3D geometry of silver electrode which represents an increased electrode surface area for ECSs. It is difficult to fabricate similar ECSs with 3D topology using conventional techniques. However, this efficient technology i.e., inkjet printing on SMP has potential to be considered for other electrochemical and biological applications due to increased device surface area. Table 3.2 represents shrinking characteristics in case of Ag inkjet printed electrodes.

SECTION 3.4. FABRICATION PROCESSES

The CAD designed electrochemical sensor (ECS) has been inkjet printed using 50 nm diameter silver (Ag) nanoparticle conductive ink. The primary CAD design was a bitmap image which has been converted into 9 bitmap images (pixelation technique) to avoid the coalescence between two adjacent droplets [94-95]. Pixelation technique has been performed using MATLAB R2020b.

Table 3.2: Shrinking Characteristics of Inkjet Printed (Silver Nanoparticle Ink) SMP based Electrochemical Sensors.

Samples ID	Temperature (°C)	Duration (minutes)	Initial Dimension (mm)	Final Dimension (mm)	Size Changing Factor Reduction: - Increment: +
1	180	3	Length: 31	Length: 13.5	Length: - 0.56
			Width: 25	Width: 10	Width: - 0.6
			Height: 0.52	Height: 1.53	Height: + 1.94
2	180	3	Length: 24.5	Length: 10	Length: - 0.59
			Width: 20	Width: 7.5	Width: - 0.62
			Height: 0.52	Height: 1.50	Height: + 1.88
3	180	3	Length: 29	Length: 13	Length: - 0.55
			Width: 23.5	Width: 10	Width: - 0.57
			Height: 0.52	Height: 1.44	Height: + 1.92

The reported sensor has been inkjet printed using 10 pL nozzles of DMP – 2850 allowing 10% overlapping fashion of the inkjet droplets to obtain a consistent pattern without wasting the printing materials. Droplet sizes varies with different substrates based on their surface and adhesive property. The combination of pixelation and overlapping approach showed promising

result in case of homogeneity and uniformity in printed patterns on the shape memory polymer (SMP) substrate. High resolution and non-contact inkjet printing has been performed at overall 35°C (platen and cartridge temperature).

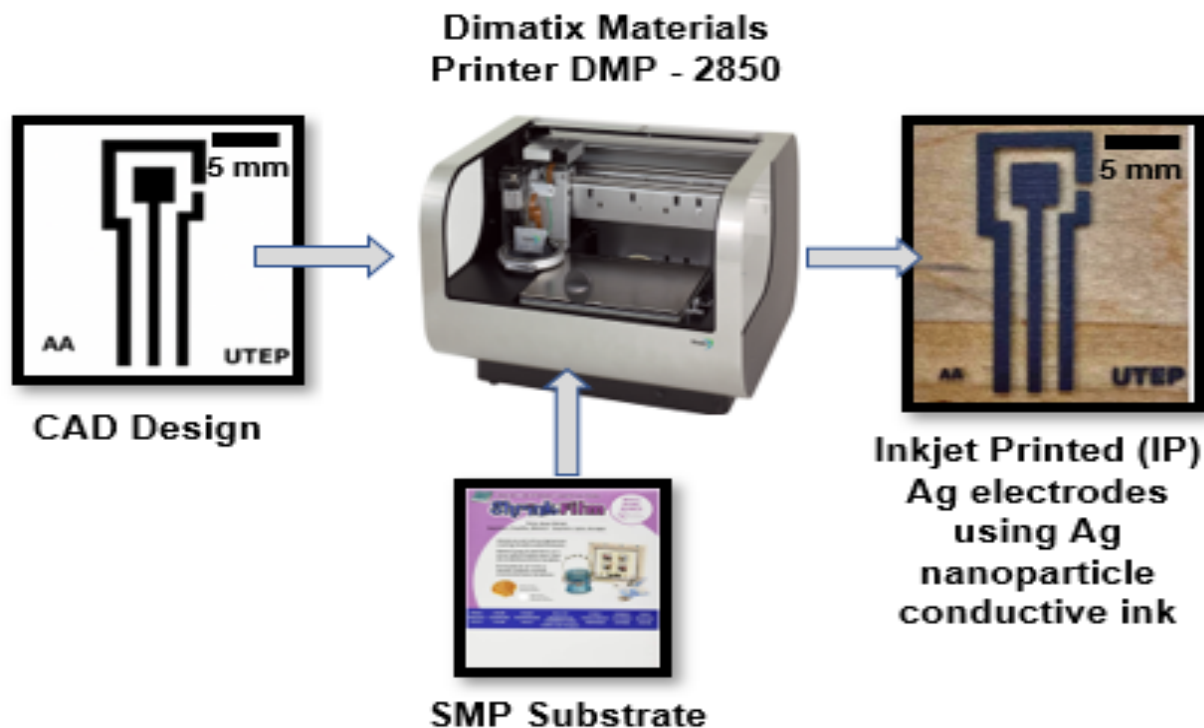


Figure 3.6: Inkjet printed (IP) silver (Ag) electrodes on shape memory polymer (SMP) for lead (II) detection utilizing a drop on demand Dimatix DMP – 2850 materials printer. The overall dimension is $31 \times 25 \times 0.52 \text{ mm}^3$.

Initially, the SMP substrate sheet has been pretreated with ethanol rinse. It has been dried with compressed air at room temperature. This clean pretreated SMP sheet has been placed on the platen of the DMP – 2850 to inkjet print Ag conductive electrodes. After patterning the Ag electrodes on the SMP substrate, the SMP sheet was cut into small pieces. The lateral dimension of each small sample was $31 \times 25 \times 0.52 \text{ mm}^3$ containing a cell of three Ag electrodes (working, counter, and reference electrodes). Figure 3.6 shows the CAD design and inkjet printed Ag electrodes on SMP. Each Ag ECS pattern with dimensions of $31 \times 25 \times 0.52 \text{ mm}^3$ has been placed

in a preheated laboratory oven at 180°C for 3 minutes. In this study, patterned Ag ECSs have been cured and shrunk simultaneously with approximately 58% reduction factor in lateral dimensions of the device. The final dimension of the fabricated Au plated SMP incorporated inkjet printed ECS after shrinking/sintering process was 13×10×1.52 mm³ with working electrode surface area 4.19 mm². Figure 3.7 represents inkjet printed Ag based ECS before and after the sintering process.

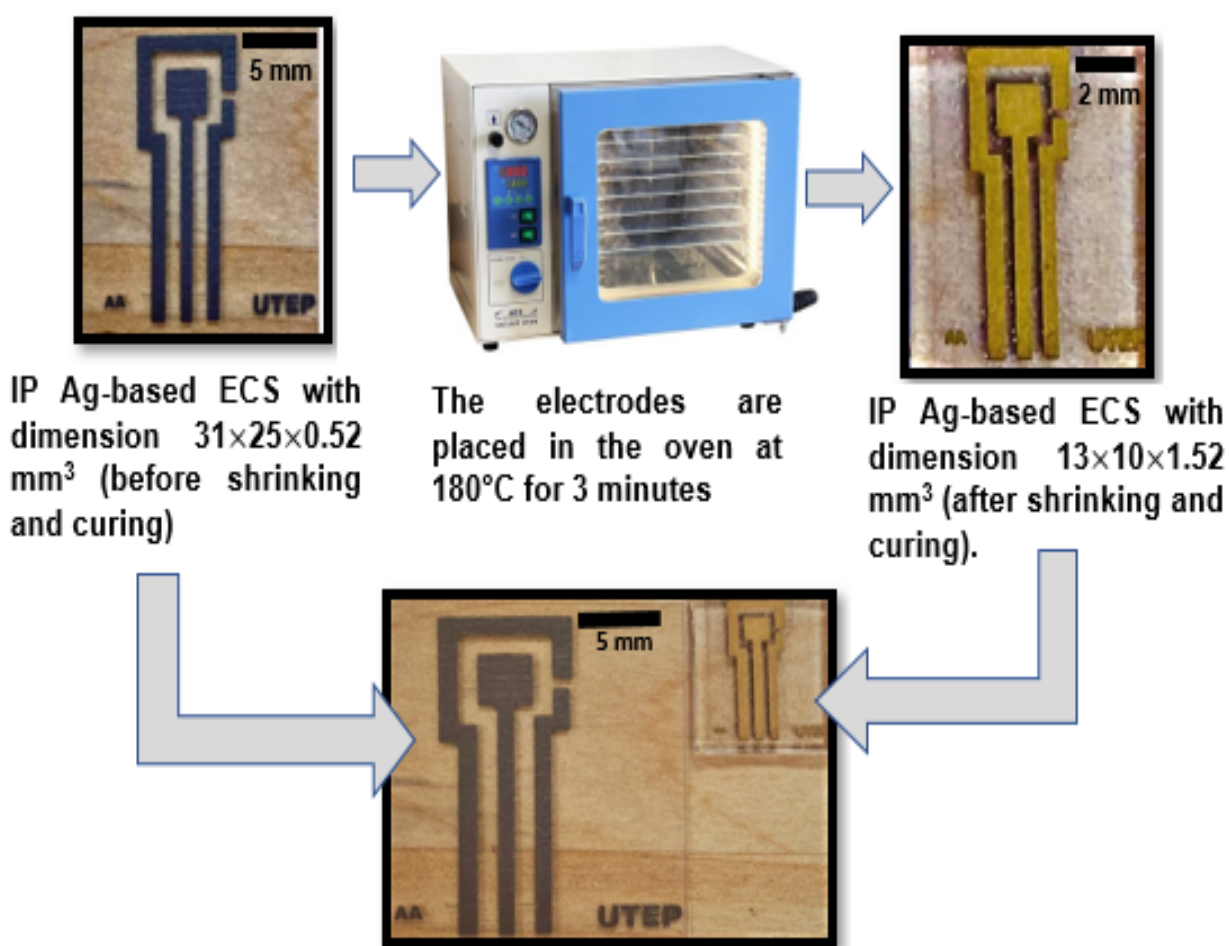


Figure 3.7: Inkjet printed Ag-based electrochemical sensor (ECS) with dimension: 31×25×0.52 mm³ - before shrinking and curing (left) and final inkjet printed miniaturized electrochemical sensor with dimension: 13×10×1.52 mm³ - after shrinking and curing (right) at 180°C for 3 minutes.

The fabricated inkjet printed SMP incorporated Au plated ECS contains one Au working electrode, one Au counter electrode, and one AgCl reference electrode. Au working and counter electrodes are fabricated using gold (24K brush) immersion plating technology. 7 VDC power supply has been utilized to clean the inkjet printed sintered (cure and shrunk) Ag electrodes (working and counter electrodes) with electrode cleaner solution. After cleaning the electrodes, they have been rinsed thoroughly with deionized (DI) water for 60 seconds. 6 VDC power supply has been applied to the working and counter electrodes after immersing them into the 24K brush gold solution for 60 seconds. After gold plating the electrodes, they have been rinsed with DI water again for 60 seconds and gently dried with compressed natural air.

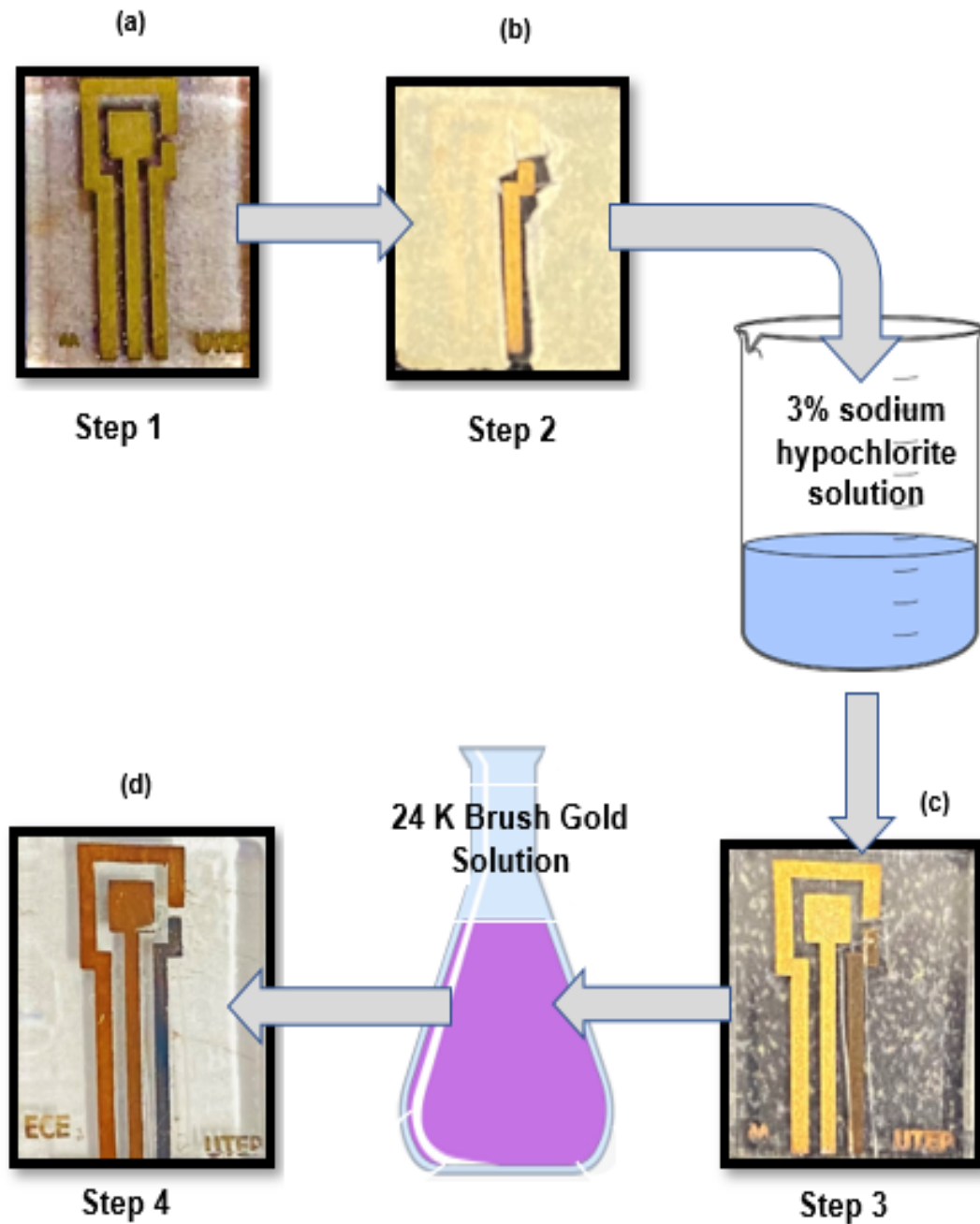


Figure 3.8: Simple step by step fabrication process flow of inkjet printed (IP) gold (Au) electrochemical sensor (ECS): (a) IP ECS on shape memory polymer (SMP) with dimension $13 \times 10 \times 1.52 \text{ mm}^3$ (after shrinking and curing) – silver (Ag) working electrode (WE), Ag counter electrode (CE) and Ag reference electrode (RE), (b) masking technique for bleach (sodium hypochlorite) immersion on Ag RE, (c) IP Ag-based ECS with Ag working electrode (WE), Ag counter electrode (CE) and AgCl reference electrode (RE), (d) Au based IP ECS with dimension $13 \times 10 \times 1.52 \text{ mm}^3$ after Au plating immersion using 24K brush gold solution: Au WE, Au CE, and AgCl RE.

The AgCl reference electrode has been fabricated using chlorination technique [28, 47, 98]. Ag reference electrode has been immersed in the sodium hypochlorite solution (bleach) – 3% without further dilution for approximately 30 seconds (until Ag electrode becomes purple). As, it was desired to chlorinate only the reference electrode, masking tape has been applied on the counter and working electrodes. The combination of inkjet printing on SMP increased enough adhesion of the Ag electrodes to tolerate the chlorination process. After chlorination, the sensors have been rinsed using DI water for 30 seconds. ECSs have been gently dried using natural compressed air after gentle removal of the mask. Figure 3.8 explains step by step procedures for fabricating the Au plated mercury free inkjet printed ECS (CAD design, inkjet printing, curing, and shrinking, chlorination, and gold plating immersion process). Finally, Figure 3.9 shows the actual technique to connect the fabricated inkjet printed Au plated ECSs with the potentiostat for conducting electrochemical analysis.

SECTION 3.5. SUMMARY

In this chapter, all the fabrication details have been covered thoroughly. This chapter started with the information regarding required apparatus and reagents including the description of the vendors. The ECSs have been inkjet printed using Fujifilm Dimatix printer – DMP 2850. Fluid properties i.e., viscosity, surface tension, particle size, and pH value have been investigated to understand the compatibility of the silver nanoparticle conductive ink in case of utilizing DMP 2850. Jetting recipes have been developed for both Legacy and newly launched Samba printheads. The characterization of the printing substrate has been detailed in this chapter. The shrinking characteristics and mechanisms (optimized time, temperature, and reduction factor) have been introduced - ~58% reduction factor is achieved by curing the printed sensors at 180 °C only for 3 minutes. The optimized parameters have been determined based on 15 different samples/ECSs. Finally, a detail and thorough step by step fabrication processes have been presented in this chapter

i.e., inkjet printing, curing/shrinking, applying bleach immersion for silver chloride (AgCl) inkjet printed reference electrode, and applying gold immersion (24K) for fabricating gold-plated inkjet printed working and counter electrodes of ECSs.

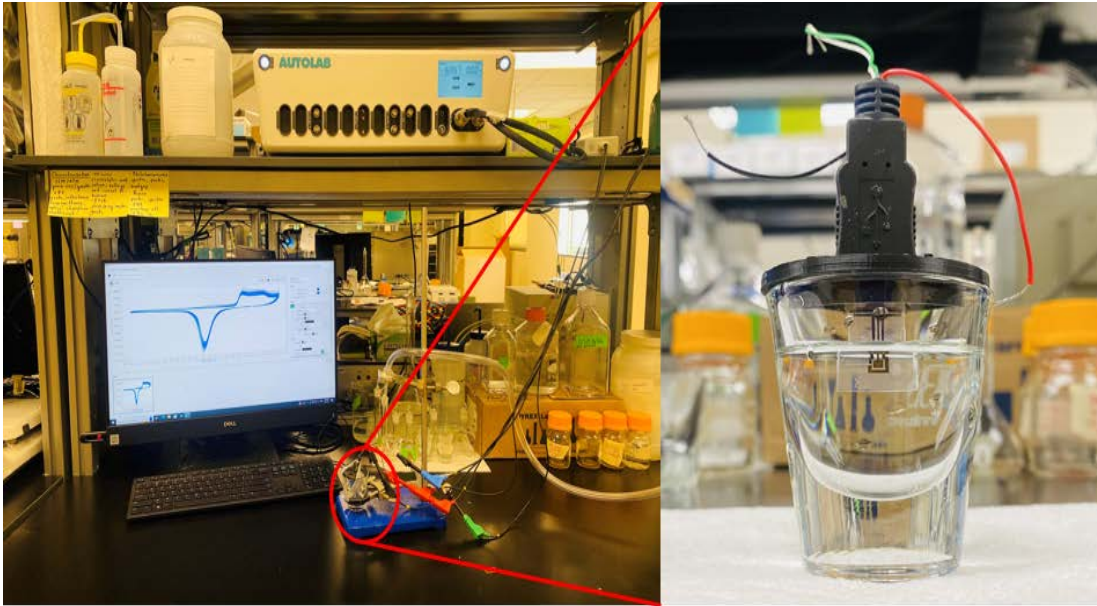


Figure 3.9: Experimental setup for inkjet printed electrochemical sensor. Red, green, and black wire of the USB drive are connected with reference, working, and counter electrode terminal of the potentiostat respectively.

Chapter 4: Optimization and Characterization of the Inkjet Printed Electrochemical Sensor

This chapter covers optimization and characterization of inkjet printed gold-plated ECSs. Section 4.1 covers the information regarding resistivity. Resistivity has been calculated using 2-probe method with digital multimeter (DMM). However, measuring resistivity with DMM does not provide actual idea of the fabricated inkjet printed ECSs. Hence, EIS measurements have been performed using PBS with pH 7.42. Section 4.2 describes about the optimized cleaning cycle. One major concern regarding printed sensor is their intolerance towards conventional cleaning cycle with 0.5 M H₂SO₄ which is extremely important for any type of electrochemical and biosensing applications. However, the inkjet printed gold-plated ECSs have shown excellent tolerance and performance in case of cleaning the electrode (compared to screen printed electrodes) and the cleaning cycle has been optimized based on the performance for the inkjet printed ECSs. Finally, Section 4.3 provides detail information regarding the characterization of the ECSs in case of electrochemical analysis i.e., cyclic voltammetry (CV) and square wave anodic stripping voltammetry (SWASV).

SECTION 4.1. RESISTIVITY

Electrode resistance measurement is extremely important in case of electrochemical sensing. Resistivity of the inkjet printed electrochemical sensor (ECS) has been measured using two-probe device and a digital multimeter [99]. 5 samples (inkjet printed Au plated ECSs) have been utilized to observe the overall performance of the inkjet printed electrodes for resistivity measurement. It has been observed that for each sample the resistance is consistent and suitable (low enough) to conduct further electrochemical analysis.

Table 4.1: Resistivity of The Silver Patterns for Multiple Samples.

Sample No.	1	2	3	4	5	Average
Resistivity ($\Omega\text{-}\square$)	4.3	4.6	3.9	4.3	4.8	4.4 ± 0.3

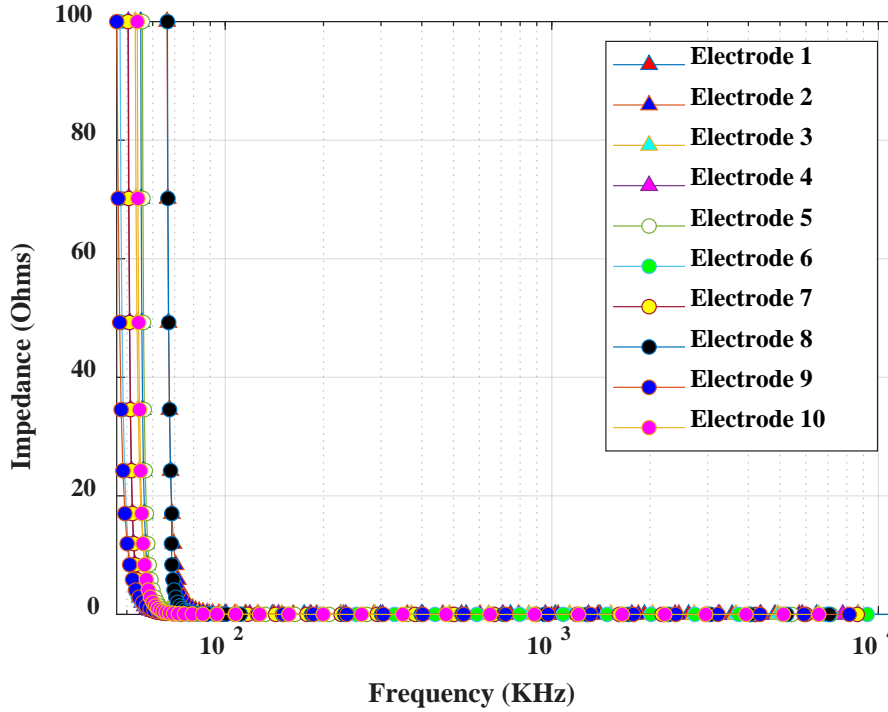


Figure 4.1: Electrochemical Impedance Spectroscopy (EIS) measurement using phosphate buffer saline (PBS) with pH 7.42.

Table 4.1 indicates the average resistivity ($\Omega\text{-}\square$) for 5 different inkjet printed Au plated ECSs. Electrochemical impedance spectroscopy (EIS) measurements are also extremely important to understand the reproducibility of the system. In this research EIS measurements have been performed on 10 different sensors utilizing phosphate buffer saline (PBS) with pH 7.42. The mean impedance of the 10 sensors was 64.07Ω with a standard deviation of 7.19Ω . This measurement shows excellent reproducibility of the fabricated inkjet printed Au plated ECS. Figure 4.1 represents EIS measurement for 10 different ECSs with a broad range of frequency i.e., 0.1 Hz to 100 KHz.

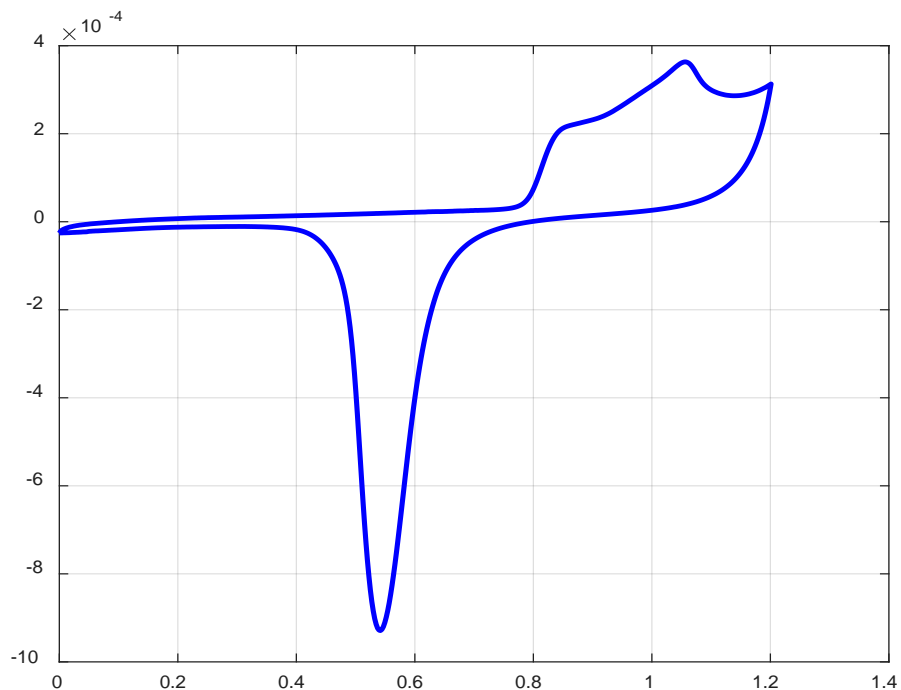


Figure 4.2: Cleaning procedure for inkjet printed gold electrochemical sensor – last cycle of 25 cycles of CV for 0.5 M sulfuric acid (H₂SO₄). Scan rate is 100 mV/s.

SECTION 4.2. CLEANING CYCLE

Pre-processing is extremely important in case of electrochemical analysis. Any type of contaminant can make the data i.e., cyclic voltammetry (CV) or square wave anodic stripping voltammetry (SWASV) noisy, inaccurate, inconsistent, and unreliable. The fabricated inkjet printed gold (Au) plated electrochemical sensors (ECSs) have been pretreated to get rid of the oxidized layer, improve sensitivity, reproducibility, and get a stable base line. The traditional cleaning process is tedious, harsh, and unnecessary for inkjet printed Au plated ECSs. The pretreatment process in this research is based on other reported investigation regarding Au ECSs [100-101]. However, the cleaning procedure for the inkjet printed Au plated ECSs has been optimized (modified based on the experiments) with 25 cycles of CV analysis using 0.5 M H₂SO₄ (sulfuric acid) with 100 mV/s scan rate and 0/+1.2 V potential range specifically for inkjet printed

SMP incorporated silver (Ag) based Au plated ECSs. It provides a constant concentration of the chloride (Cl^-) ions in the electrolyte medium. It also creates stability for the inkjet printed Ag based AgCl reference electrode. Figure 4.2 represents the last cycle of 25 cycles of CV for 0.5 M H_2SO_4 . The consistent narrow reduction peak ensures the potential sensitivity/performance of the IP Au plated ECSs. It has also been observed that the behavior of the IP Au plated electrode is consistent and similar to bare gold electrodes which opens the potential opportunity to utilize our low-cost consistent and reliable fabrication approach – 24 K brush Au electroplating Ag inkjet printed electrodes for further electrochemical and bio-applications.

SECTION 4.3. ELECTROCHEMICAL ANALYSIS

Cyclic voltammetry (CV), square wave anodic stripping voltammetry (SWASV), and electrochemical impedance spectroscopy (EIS) have been performed on the fabricated ECSs for electrochemical analysis. 0.1M HCl has been utilized as a supporting electrolyte while performing the electrochemical analysis (CV and SWASV). HCl is significantly important to detect HMIs in aqueous solution. It provides a constant concentration of the chloride (Cl^-) ions in the electrolyte medium. It has been determined to experiment the fabricated electrochemical sensors (ECSs) with both the optimized solution (0.1M HCl) with and without lead (II) to observe its potential to perform further development. EIS has been conducted with phosphate buffer saline (pH 7.42) as an electrolyte. This electrolyte has been prepared using 0.1M sodium chloride, 0.1 M potassium chloride, 0.1 M disodium phosphate, and 0.1M potassium dihydrogen phosphate on July 11, 2022. EIS measurements have been performed for the ECSs to evaluate their performance in terms of impedance at different frequency range. The impedance response has been recorded with 10 mV with the frequency range from 0.1 Hz to 100 KHz. The CV has been performed using Keithley 2450 SM. The SWASV and EIS have been conducted using Autolab PGSTAT302N. The

optimized parameters for SWASV are modulation amplitude - 280 mV, frequency - 15 Hz, estimated duration - 4.4 s, and scan rate - 45 mV/s, and deposition time - 5 minutes.

Initially to characterize the performance of the fabricated gold (Au) plated electrochemical sensors (ECSs), 3 mM lead (II) has been diluted with 0.1 M HCl to prepare the samples (both deionized (DI) and tap water). The Au electrochemical sensors have been utilized to conduct cyclic voltammetry (CV) electrochemical analysis for blank, 3mM, and 14.4 $\mu\text{g/L}$ lead (II) contaminated aqueous solution (optimized with 0.1 M HCl) – USEPA approved lead (II) level in drinking water is 15 $\mu\text{g/L}$. Figures 4.3 and 4.4 illustrate the performance of the analysis with 100 mV/s scan rate and -0.6/-0.2 V potential range in case of lead (II) contaminated DI and tap water respectively. HCl with 0.1 M has been utilized as a supporting electrolyte while performing the electrochemical analysis i.e., CV. HCl is significantly important to detect heavy metal ions in aqueous solution. It has been noted that the CV graph for blank does not contain any oxidation/stripping peak in case of both DI and tap water. However, 3 mM and 14.4 $\mu\text{g/L}$ lead (II) contaminated aqueous solution shows a pair of oxidation and reduction peaks for both optimized DI and tap water. Reduction/cathodic peak (~ -480 mV) represents bulk deposition and oxidation/anodic (~ -445 mV) peak represents bulk stripping of the lead (II) ion in the optimized aqueous solution (0.1M HCl) i.e., DI and tap water.

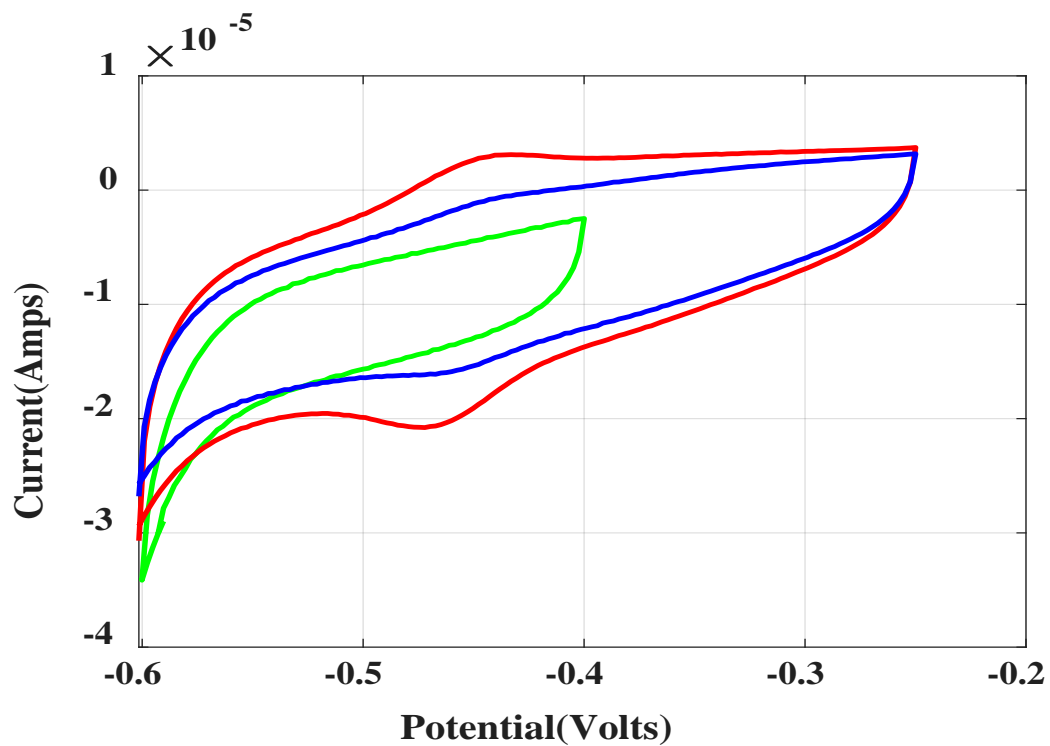


Figure 4.3: Cyclic Voltammetry (CV) of gold (Au) plated electrochemical sensor (ECS) for blank (optimized DI water without lead(II)) – green, 3mM lead (II) (optimized DI water with 3 mM lead (II)) – red), and 14.4 $\mu\text{g/L}$ lead (II) (optimized DI water with 14.4 $\mu\text{g/L}$ lead (II)) – blue) at 100 mV/s.

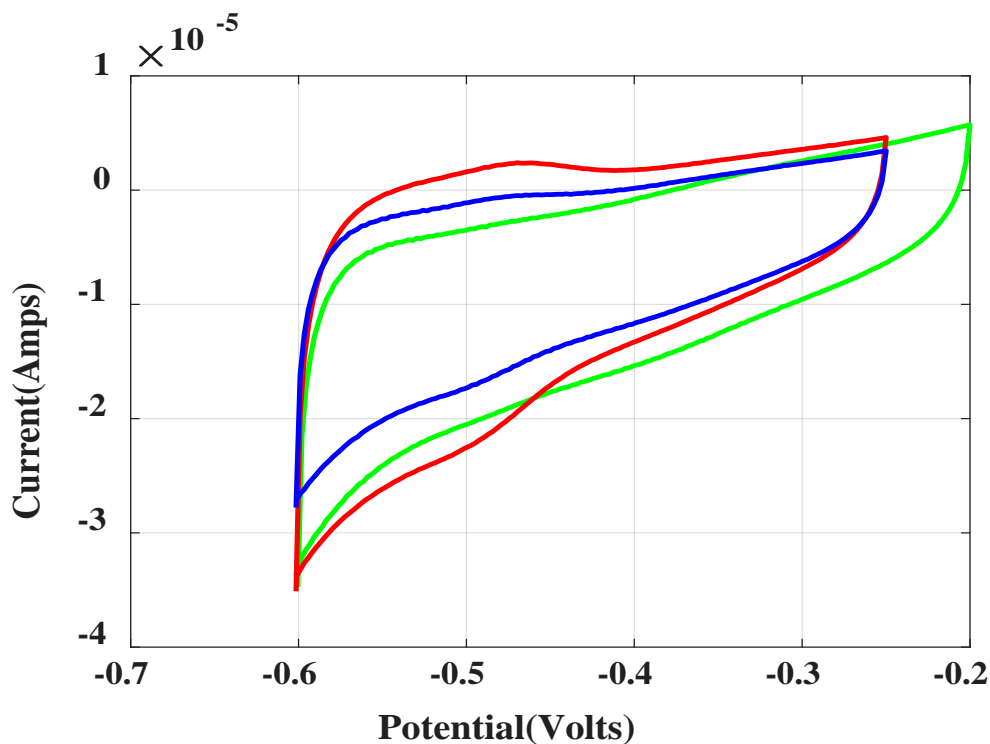


Figure 4.4: Cyclic Voltammetry (CV) of gold (Au) plated electrochemical sensor (ECS) for blank (optimized tap water without lead(II)) – green, 3mM lead (II) (optimized tap water with 3 mM lead (II)) – red), and 14.4 $\mu\text{g/L}$ lead (II) (optimized tap water with 14.4 $\mu\text{g/L}$ lead (II)) – blue) at 100 mV/s.

SECTION 4.4. SUMMARY

Resistivity with 2-probe method and EIS measurements with potentiostat have been conducted with fabricated inkjet printed ECSs. EIS measurement represents that the mean impedance of the 10 ECSs is 64.07Ω with a standard deviation of 7.19Ω . This data shows excellent performance of the fabricated sensors for any electrochemical and/or biosensing applications. This phenomenon also represents the reproducibility of the fabricated sensors. This chapter has included the optimization of the cleaning cycle in detail. 25 cycles of CV with 0.5 M H_2SO_4 has been optimized and showed excellent performance for inkjet printed gold-plated ECSs. Finally, electrochemical analysis has been characterized in this chapter as well. CV and SWASV have been considered as 2 potential voltammetric techniques to perform further electrochemical analyses.

Chapter 5: Results – Inkjet Printed Gold Plated Electrochemical Sensors

This chapter consists of all the results/data obtained using inkjet printed gold-plated ECSs. Section 5.1 covers effective electrode surface area (EESA) calculation. EESA is important in case of electrochemical or biosensing applications as this electrical surface area is different than geometric or mechanical surface area. EESA is defined as an actual area where electron exchange takes place. A mathematical model has been developed for the fabricated inkjet printed ECSs based on EESA and geometric/mechanical area of the working electrode. Section 5.2 covers a detail result sections for inkjet printed gold-plated ECSs i.e., scanning electron micrograph images (SEM), energy dispersive spectroscopy (EDS), CV, SWASV, limit of detection (LOD) and limit of quantitation (LOQ). Section 5.3 describes about the processes of bismuth functionalization in detail. This section also covers results/data obtained utilizing bismuth coated inkjet printed ECSs i.e., SEM, EDS, CV, SWASV, LOD, and LOQ. A detail description of reusability, selectivity, and compatibility with real samples i.e., tap water and river water have been provide in Section 5.4, 5.5, and 5.6 respectively. Uncertain analysis is extremely important to validate any sensor. Uncertainty analysis – GUM approach has been introduced in Section 2.5 (Chapter 2). In this research, inkjet printed ECSs have been fabricated using Gum approach for 15 samples (ECSs). Section 5.7 represents detail analysis regarding uncertainty analysis. Finally, Section 5.8 shows cost analysis of the fabricated inkjet printed ECSs.

SECTION 5.1. EFFECTIVE ELECTRODE SURFACE AREA

Effective electrode surface area (EESA) is defined as an active area of working electrode where the electron exchange takes place. It is different than geometric surface area and generally exceeds the physical areas of small electrodes considering a higher number of chemically reactive sites [102-103]. It is directly related with most of the parameters of the electrode reaction which makes it an important phenomenon to discuss and analyze for the fabricated electrochemical sensors (ECS). Nanostructured electrode surface plays an important role in surface enlargement

[104-112]. The geometric area of the electrodes can be determined visually using techniques such as scanning electron microscopic (SEM) images. But this determination does not resemble the idea of true EESA or electrochemically active electrode area [113].

Hence, it is important to analyze/compute this characteristic which is an important quality control parameter. Several methods and techniques have been reported for EESA calculation throughout the time for solid and liquid electrodes [114-118]. However, computing EESA in case of screen-printed electrode (SPE) and/or inkjet printed electrode is still an area that requires further attention, consideration, and development due to lack of analytical ideas regarding the size and morphology of the fabricated electrodes [116]. To the best of my knowledge EESA calculation of inkjet printed electrochemical sensor has never been previously reported. Cyclic voltammetry (CV) and chronocoulometry (CC) are considered as two appropriate techniques to analyze EESA for printed electrodes. In this research CV has been taken into consideration for EESA calculation. Modified and previously reported Randles-Sevcik (R-S) equations for reversible, quasi-reversible, and irreversible electrochemical processes (CV) at 25 °C are given below [119-128]:

$$I_p(\text{reversible}) = 2.69 \times 10^5 n^{3/2} AC \sqrt{Dv} \quad (5.1)$$

$$I_p(\text{quasi-reversible}) = (2.69 \times 10^5 n^{3/2} AC \sqrt{Dv}) K(\Lambda, \alpha) \quad (5.2)$$

$$I_p(\text{irreversible}) = 2.99 \times 10^5 n^{3/2} AC \sqrt{Dv\alpha} \quad (5.3)$$

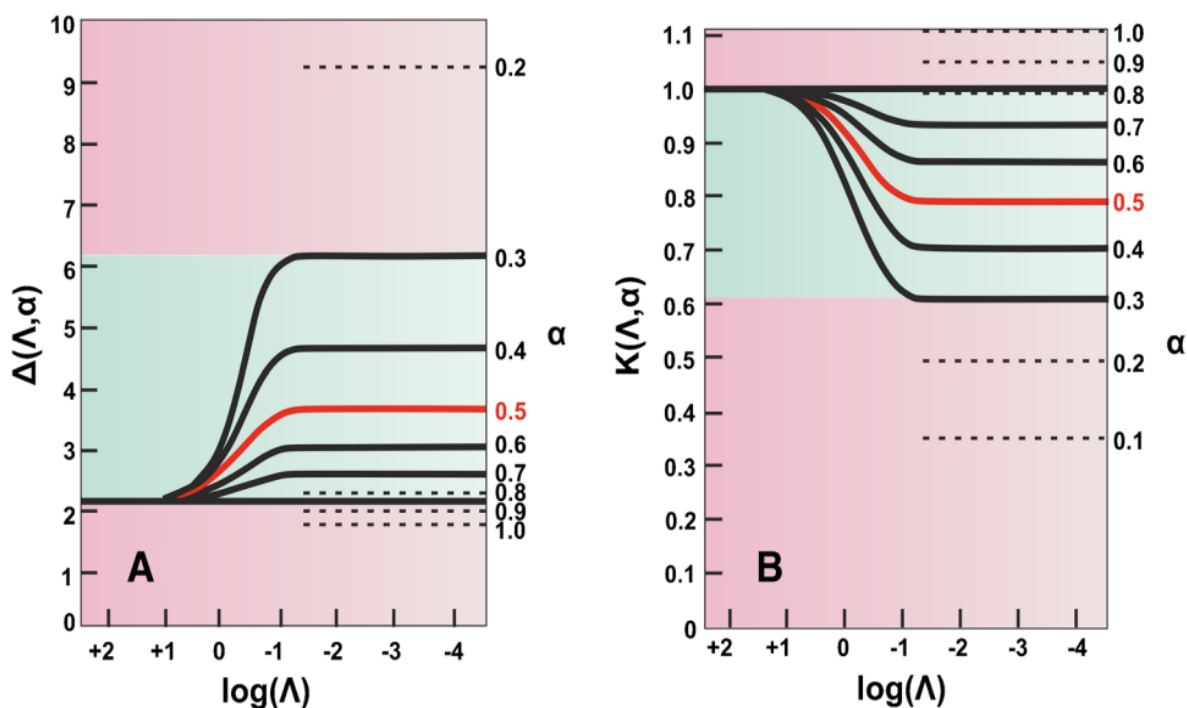


Figure 5.1: Plot of (A) $\Delta(\Lambda, \alpha)$ and (B) $K(\Lambda, \alpha)$ with a range of different transfer co-efficient, α - [127, 128].

Where, I_p is forward peak (anodic/stripping) current (amps), n is the number of electrons in the electrochemical process, A is effective electrode surface area (cm^2), C is the concentration (mol/cm^3), D is diffusion coefficient (cm^2/s), and v is scan rate (V/s). The diffusion co-efficient can be estimated from the slope of the plot of I_p vs \sqrt{v} . In the quasi-reversible equation, $K(\Lambda, \alpha)$ is a dimensionless parameter which is defined by calculating Ψ , $\log(\Lambda)$, and $\Delta(\Lambda, \alpha)$ respectively. Ψ is determined from Nicholson plot based on peak to peak separation [127]. In equation 5.5, E_p and $E_{p/2}$ are peak potential and half wave peak potential respectively. Figures 5.1 represents $\Delta(\Lambda, \alpha)$ and $K(\Lambda, \alpha)$ with respect to function of $\log(\Lambda)$. Figure 5.2 is utilized for determining the value of Ψ based on the peak to peak separation of CV plot.

$$\log(\Lambda) = \log(\Psi\sqrt{\pi}) \quad (5.4)$$

$$\Delta(\Lambda, \alpha) = \frac{E_{P/2} - E_P}{26} \quad (5.5)$$

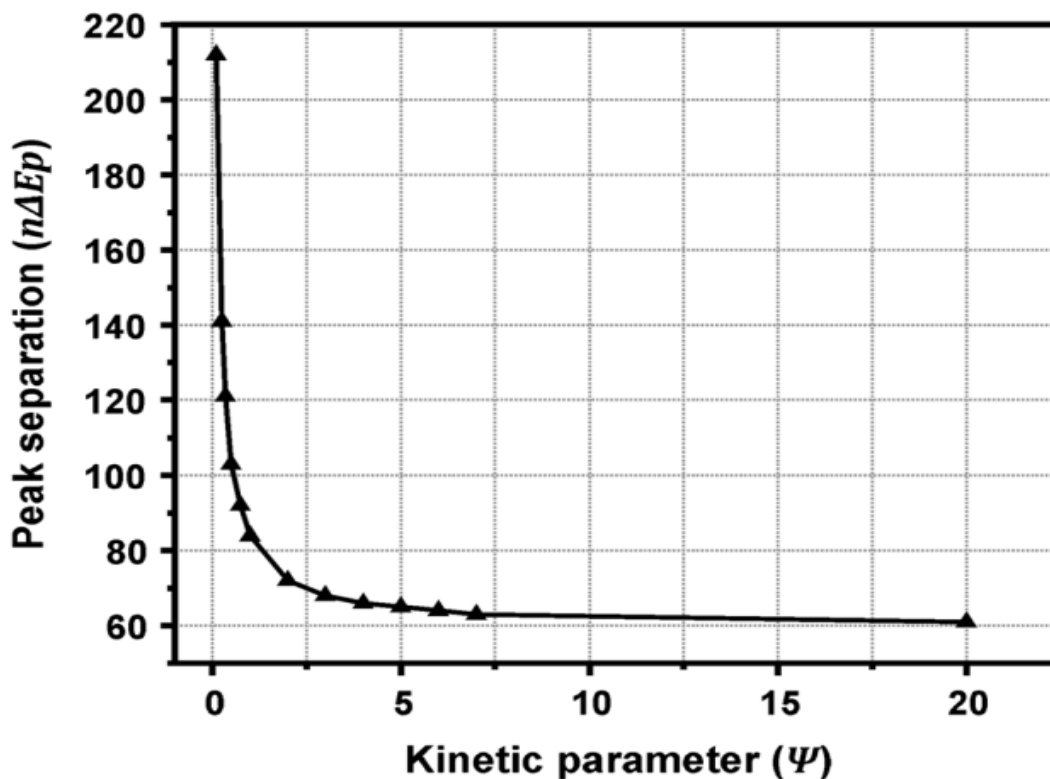


Figure 5.2: Peak to peak separation vs. kinetic parameter, Ψ [127, 128].

It is important to select appropriate equation to compute this parameter based on the CV plot – reversible if the peak to peak separation is lower than 63mV (in practice) and independent of scan rate as well as quasi-reversible if the peak to peak separation is in between 63 mV and 200 mV and dependent of scan rate [27]. In this research EESAs have been calculated for inkjet printed electrode utilizing conventional 3mM ferri(III)cyanide/ferro(II)cyanide in 0.1 M KCl. From Figures 5.3 it has been observed that the CV plots are quasi-reversible. The calculated EESAs of the square working electrode is $7.25 \text{ mm}^2 \pm 0.15 \text{ mm}^2$ (lateral area - 4 mm^2) which justifies our previously reported claim to have increased effective electrode surface area even after miniaturization of the Au ECSs in case of inkjet printing on shape memory polymer (SMP)

substrate. The EESA has been calculated based on 15 different samples – inkjet printed Au plated ECSs – Figure 5.4.

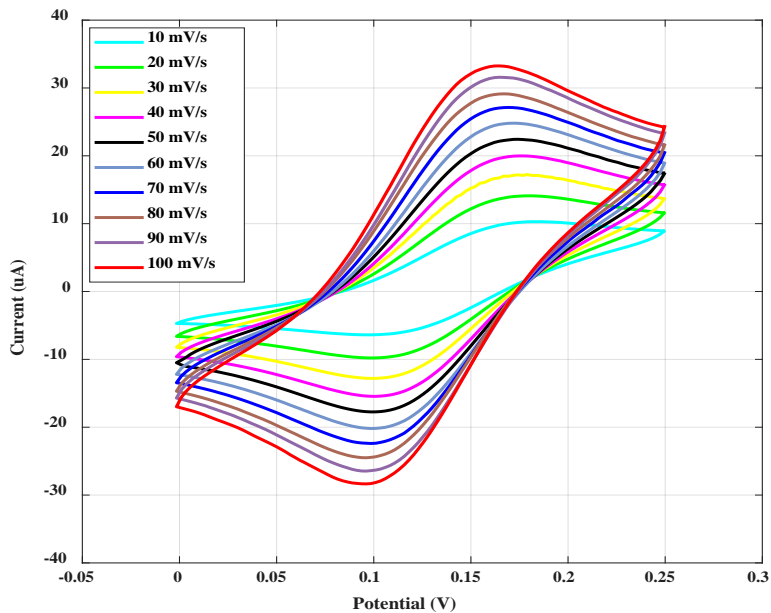


Figure 5.3: Cyclic voltammogram (CV) for inkjet printed gold electrochemical sensor (square working electrode surface area) for 3 mM of ferri(III)cyanide/ferro(II)cyanide in 0.1 M KCl (10, 20, 30, 40, 50, 60, 70, 80, 90, and 100 mV/s).

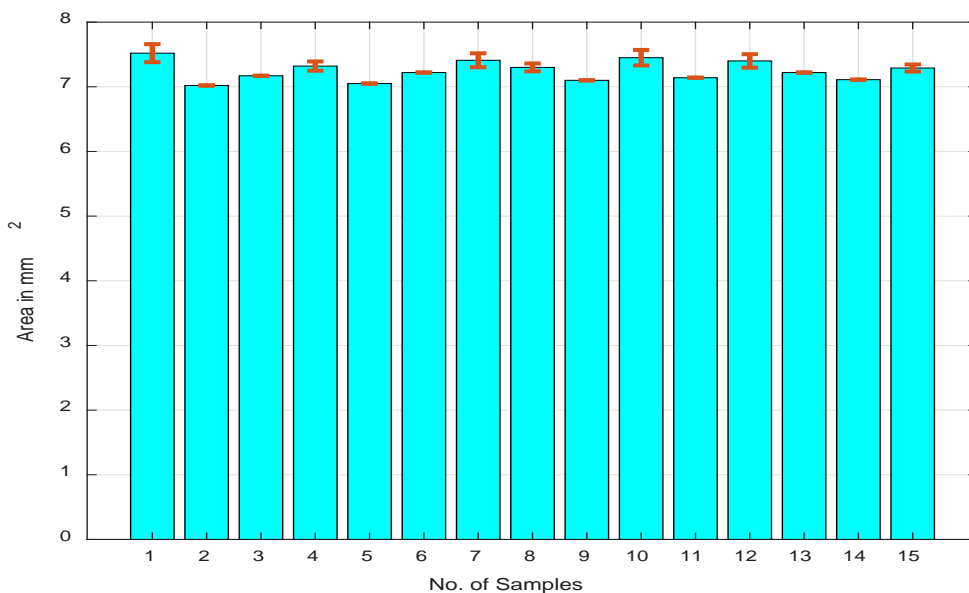


Figure 5.4: Area (mm²) calculated using Randles-Sevcik quasi-reversible equation for 15 different samples (inkjet printed gold plated electrochemical sensors).

From the characterization of the utilized SMP substrate, it has been observed that the mechanical/lateral area (A_{shrunk}) of inkjet printed ECS (cured/shrunk) has been reduced up to ~58% (both in length and width) compared to as-printed mechanical/lateral area ($A_{as-printed}$) – equation 5.6 after curing and shrinking the printed ECSs. As printed area of the inkjet printed gold plated electrode is 20.25 mm² and the shrunk lateral area is 4.19 mm². Hence, the reduction factor in case of working electrode area is ~79%. Equation 5.7 proclaims the relationship between as-printed and shrunk ECSs. Electrical area or EESA has been calculated using Randles-Sevcik quasi reversible equation. It has been observed that the electrical area or EESA ($A_{electrical}$) increases with ~73% compared to mechanical or lateral area (A_{shrunk}) of the fabricated shrunk ECSs. Equations 5.9 and 5.10 represent the relationship between both pairs i.e., electrical and shrunk mechanical area as well as electrical and as printed mechanical areas. This mathematical model provides potential flexibility to design inkjet printed micro electromechanical systems (MEMS) i.e., ECSs in the broader aspect.

$$\frac{A_{as-printed} - A_{shrunk}}{A_{as-printed}} = \sim 79.31\% \quad (5.6)$$

$$A_{as-printed} - A_{shrunk} = \sim 0.7931 A_{as-printed}$$

$$A_{shrunk} = \sim 0.207 A_{as-printed}$$

$$A_{as-printed} = \sim 4.83 A_{shrunk} \quad (5.7)$$

$$\frac{A_{electrical} - A_{shrunk-mechanical}}{A_{shrunk-mechanical}} = \sim 73\% \quad (5.8)$$

$$A_{electrical} - A_{shrunk-mechanical} = \sim 0.73 A_{shrunk-mechanical}$$

$$A_{electrical} = \sim 1.73 A_{shrunk-mechanical}$$

$$A_{shrunk-mechanical} = \sim 0.58 A_{electrical} \quad (5.9)$$

$$A_{as-printed} = \sim 2.79 A_{electrical} \quad (5.10)$$

SECTION 5.2. GOLD PLATED INKJET PRINTED ELECTROCHEMICAL SENSOR

This section describes the data/results i.e., scanning electron micrograph (SEM) images, energy dispersive spectroscopy (EDSs), square wave anodic stripping voltammetry (SWASV) for different concentration of lead (II) contaminated optimized deionized (DI) water, and calibration curve to determine limit of detection (LOD) for a simple, miniaturized, reproducible, and disposable 3D inkjet printed gold (Au) plated electrochemical sensor (ECS) – Figure 5.5. The LOD of the Au plated ECS is $7.6 \mu\text{g/L}$ (below USEPA approved detection limit – $15 \mu\text{g/L}$). The sensor consists of Au working electrode, Au counter electrode, and silver chloride (AgCl) reference electrode.

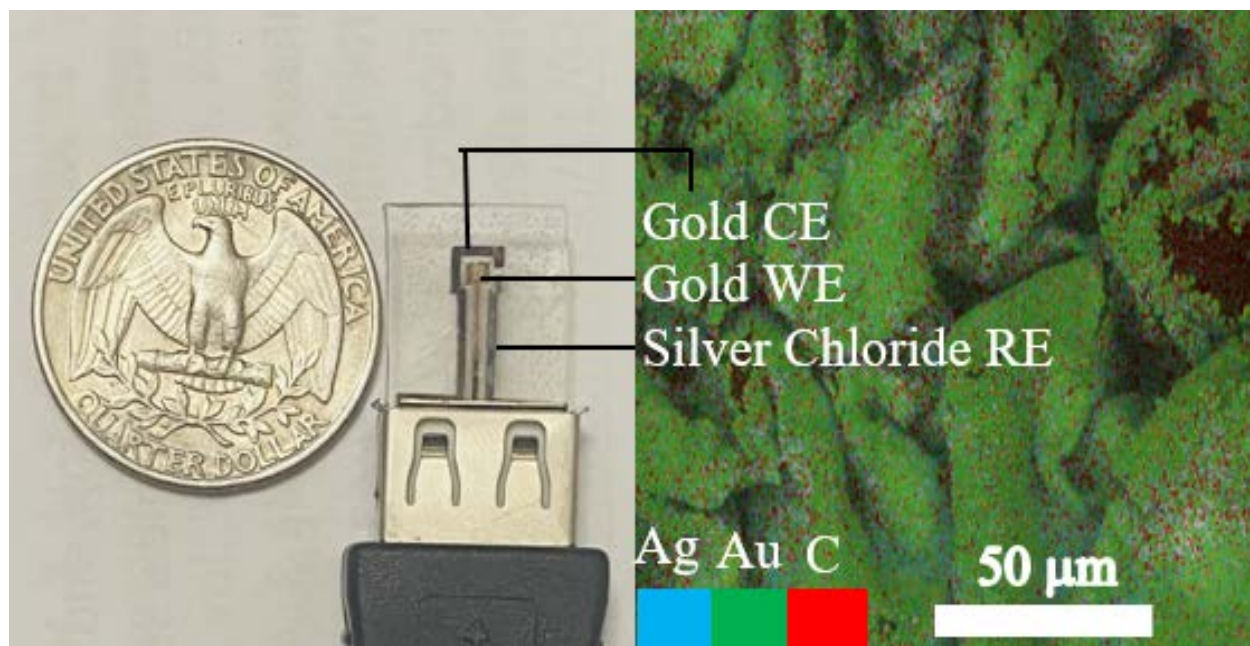


Figure 5.5: Inkjet printed gold electroplated electrochemical sensor on shape memory polymer (left). The cell consists of gold working electrode (WE) and counter electrode (CE) and silver chloride reference electrode (RE). The lateral and effective electrode surface area are 4.19 mm^2 and 7.25 mm^2 respectively. The energy dispersive spectroscopy layered image (right) shows the potential coating of gold on silver inkjet printed electrodes.

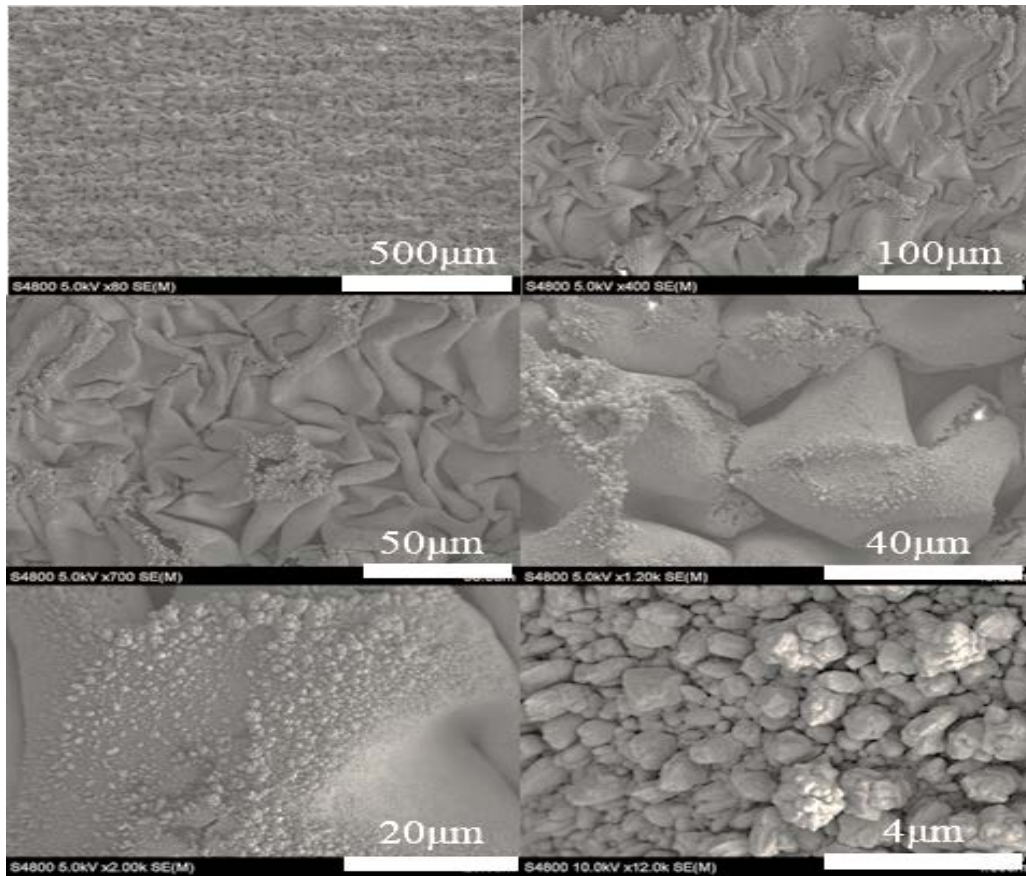


Fig. 5.6: Scanning electron micrographs (SEM) of inkjet printed metal films on shape memory polymer after shrinking, revealing a 3D wrinkled structure, providing a large surface area, useful for enhancing sensor performance.

SEM image is a significant tool to observe the characteristics (3D topology and composition) of any material. In this research, Hitachi SU 3500 SEM has been used to characterize the 3D topography of the materials i.e., Au used to fabricate the reported sensor. Figure 5.6 reveals highly textured 3D geometry of different materials of the fabricated sensors after curing and shrinking. Complex surface topology such as squeezing in the vertical direction, tangled, serpentine, and melted geometric properties of different materials are observed in Figure 5.4 due to shape memory polymer (SMP) substrate contraction and heating. Squeezed 3D geometry of the inkjet printed nanoparticle ink in the presented SEM image explains the reason for having

increased actual (electrical) effective electrode surface area (EESA) despite miniaturizing the lateral dimension or mechanical area of the Au plated inkjet printed ECSs.

EDSs of the fabricated Au plated and silver (Ag) based working electrode as well as AgCl reference electrode have been observed to understand/analyze the effectivity of the Au plating – 24K brush gold solution and chlorination – 3% sodium hypochlorite solution technology respectively in case of inkjet printed ECS fabrication utilizing SMP. Figures 5.7, 5.8, and 5.9 represent the EDSs for Ag working electrode, AgCl reference electrode, and Au working electrode respectively. It is observed that in case of Ag working electrode only the presence of Ag (41.7%) is prominent other than carbon and oxygen. In case of AgCl reference electrode the presence of Ag (42.2%) and Cl (7.9%) are significant. The presence of Au (9.9%) also showed the evidence of gold plating operation in case of Au plated working electrode. The presence of other material i.e., carbon and oxygen were present due to environment and sulfur was visible due to wavelength misinterpretation by the software.

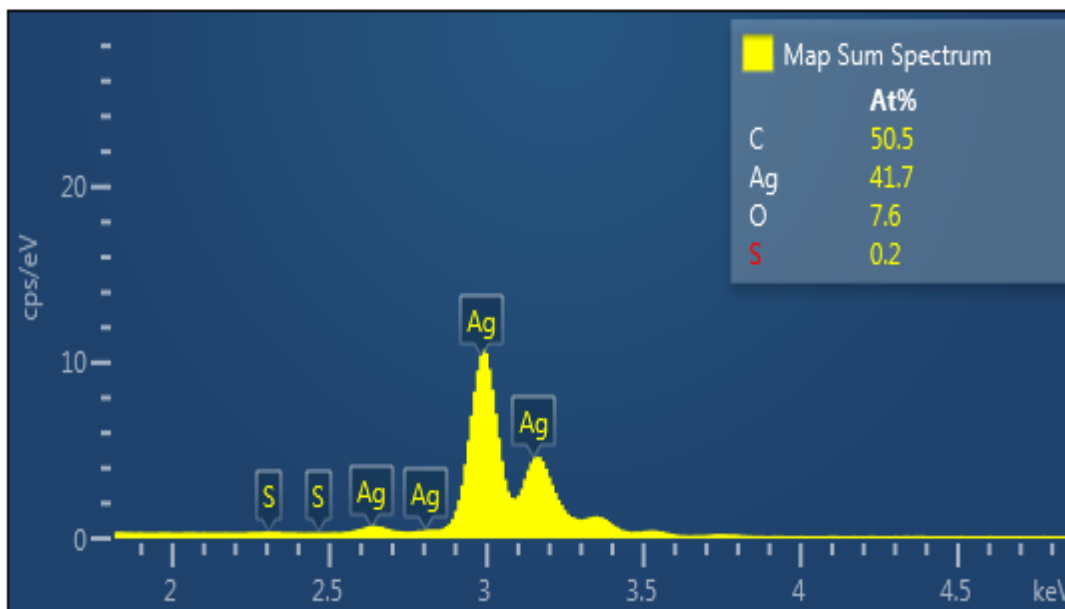


Figure 5.7: Energy dispersive spectroscopy for inkjet printed silver electrode (41.7% silver).

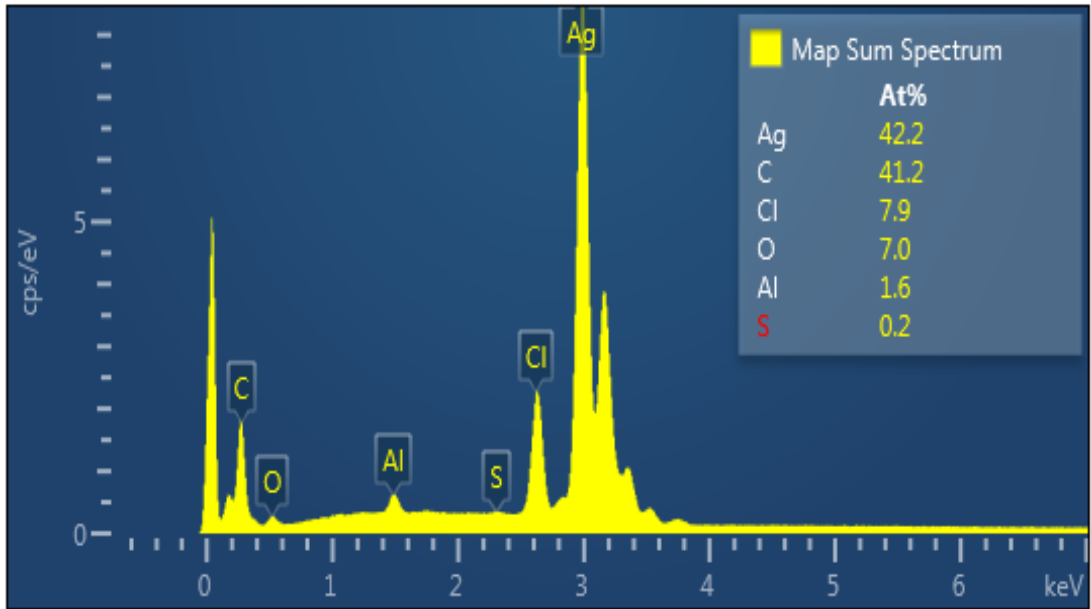


Figure 5.8: Energy dispersive spectroscopy for silver chloride (AgCl) reference electrode (7.9% chlorine).

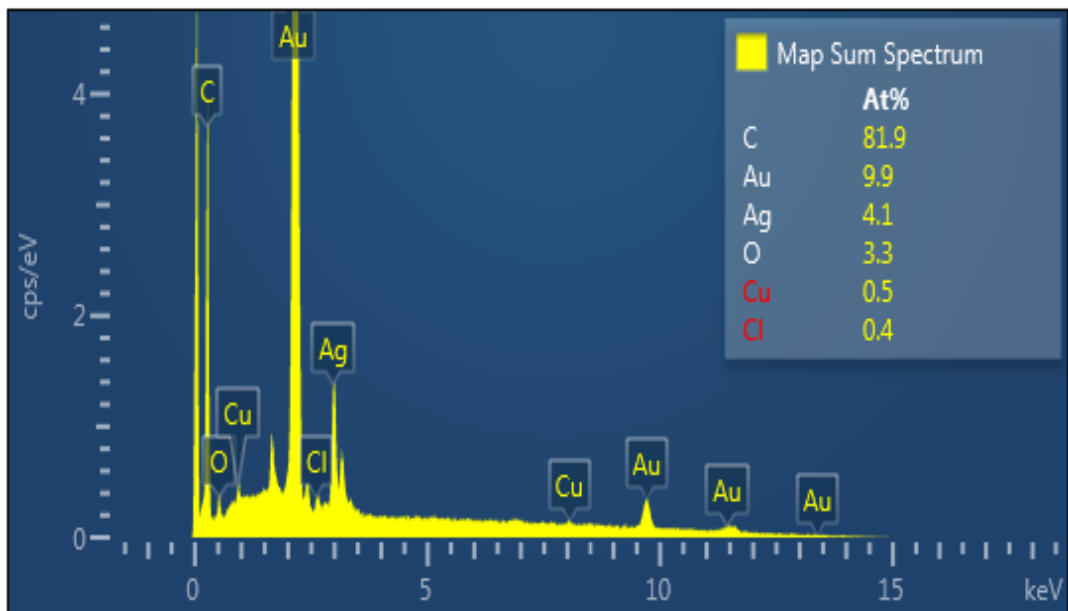


Figure 5.9: Energy dispersive spectroscopy for inkjet printed gold plated silver based electrode (9.9% gold).

After optimization and characterization, Au plated inkjet printed SMP incorporated ECSs have been utilized to detect lead (II) ion in aqueous solution i.e., $30 \mu\text{g/L}$, $25 \mu\text{g/L}$, $15 \mu\text{g/L}$, and $0 \mu\text{g/L}$ lead (II). Figure 5.10 represents SWASV in case of different concentrations. Based on

this electrochemical analysis, the calibration curve has been obtained with higher linearity ($R^2 = 0.99$). Figure 5.11 represents the calibration curve of the fabricated inkjet printed Au plated ECS. The limit of detection of the fabricated sensor is $7.61 \mu\text{g/L}$. The detail calculation of limit of detection has been presented in Appendix C.

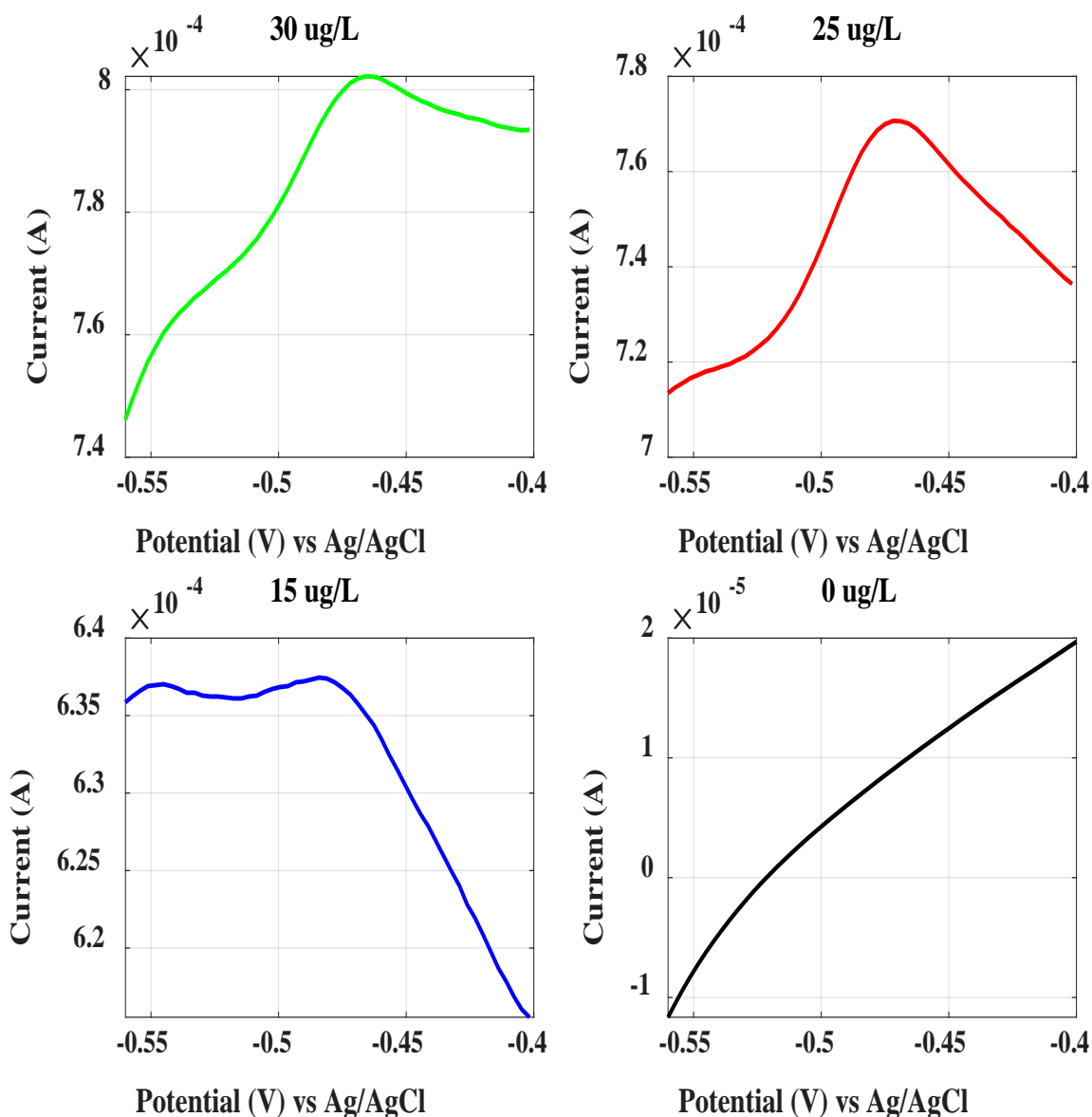


Figure 5.10. Square wave anodic stripping voltammetry for $30 \mu\text{g/L}$ (top-left: green), $25 \mu\text{g/L}$ (top-right: red), $15 \mu\text{g/L}$ (bottom-left: blue), and $0 \mu\text{g/L}$ (bottom-right: blank). Modulation amplitude - 280 mV , frequency - 15 Hz , estimated duration - 4.4 s , and scan rate - 45 mV/s , and deposition time - 5 minutes .

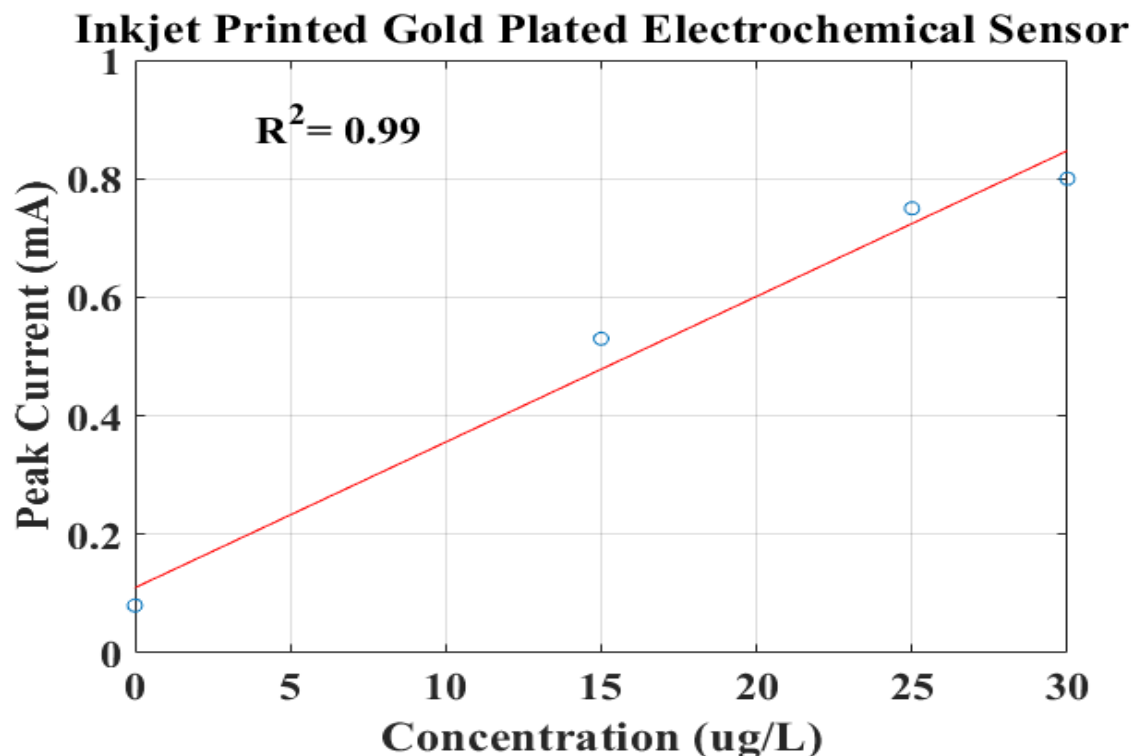


Figure 5.11: Calibration curve for inkjet printed shape memory polymer incorporated gold-plated electrochemical sensor. The data point for each concentration is a mean of three different data collected using three different sensors.

SECTION 5.3. BISMUTH FUNCTIONALIZATION

This section describes the bismuth – Bi (III) functionalization on inkjet printed gold (Au) plated electrochemical sensor (ECS). Bi (III) functionalization has been considered to improve electrochemical sensing performance of lead (II) detection in optimized deionized (DI) water – 0.1 M HCl. The electrochemical cell considered in this part is the same inkjet printed Au plated electrode – consists of a three electrodes cell: An Au counter electrode (CE), an Au working electrode (WE), and a silver chloride (AgCl) reference electrode (RE). The WE has been modified with Bi (III) by two different procedures: (a) ex situ - under potential deposition (UPD) of Bi (III) with a full cycle of cyclic voltammetry (CV) electrochemical analysis and (b) in situ - addition of 200 $\mu\text{g/L}$ Bi (III) to a sample analyte of optimized DI water contaminated with lead (II).

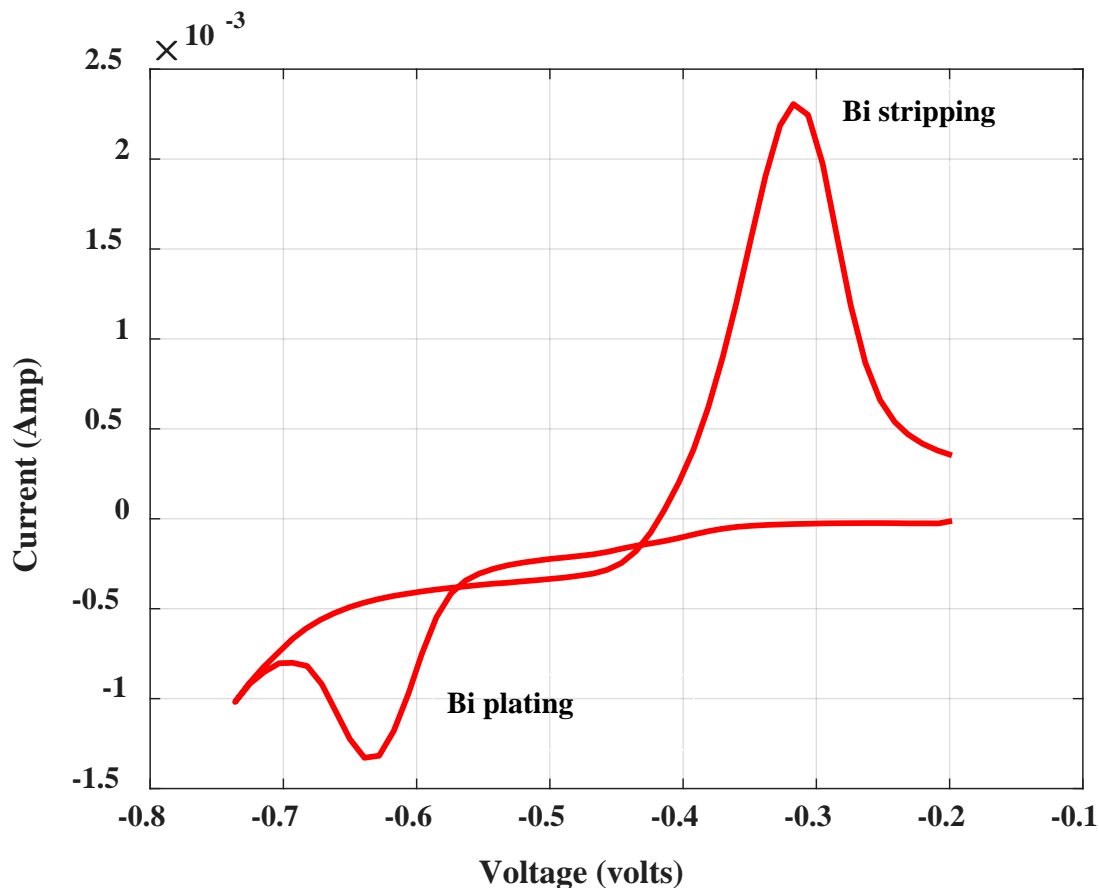


Figure 5.12: Cyclic voltammogram (CV) for the full range of under potential deposition (UPD) of bismuth (III) on gold plated inkjet printed electrochemical sensor (ECS).

Bi (III) is an environment friendly material. It plays an important role for heavy metal ion (HMI) detection. The advantages of Bi (III) coated electrodes in case of HMIs detection are less toxicity, high capacity for fused-alloy formation, less interference of the dissolved oxygen in the test medium, and wide negative potential window. The Au working electrode is Bi (III) coated by electroplating a film of Bi (III) on the surface of the electrode. This process can be performed in two different ways such as ex situ and in situ. This research has focused on both procedures to understand their effectivity towards improved electrochemical sensing performance. In the ex situ

procedure, the electroplating has been conducted prior to the electrochemical sensing analysis. In this research, the ex situ Bi (III) plating has been performed in two steps.

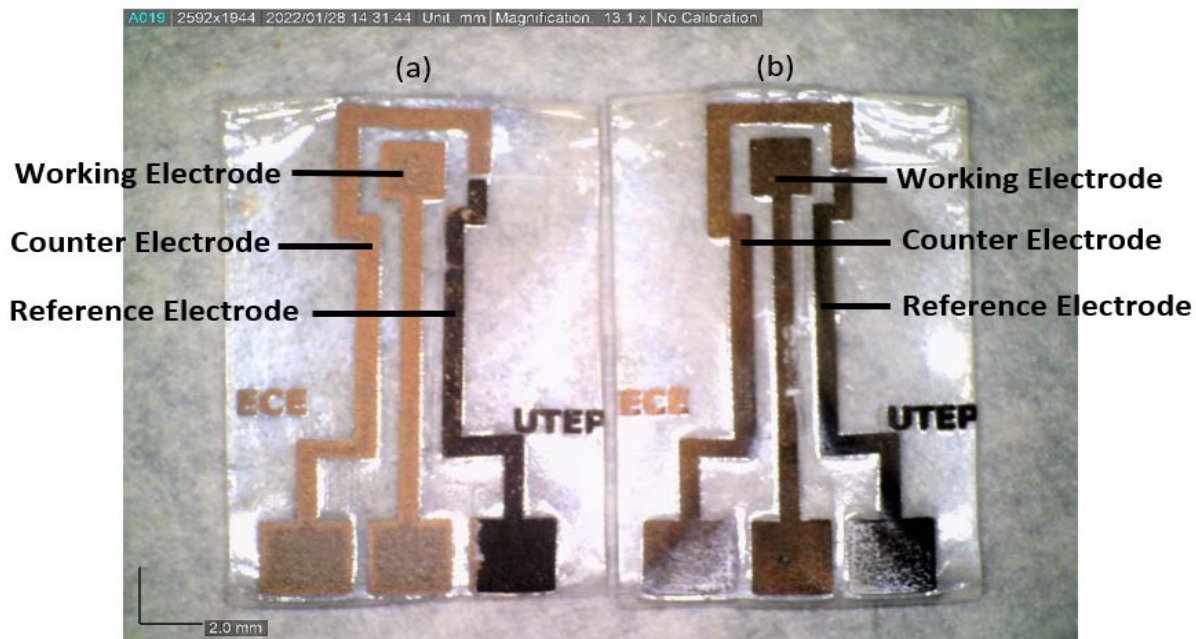


Figure 5.13: Inkjet printed (IP) shape memory polymer (SMP) incorporated gold based electrochemical sensor (ECS) (a) before under potential deposition (UPD) of Bi (III) and (b) after UPD of Bi (III).

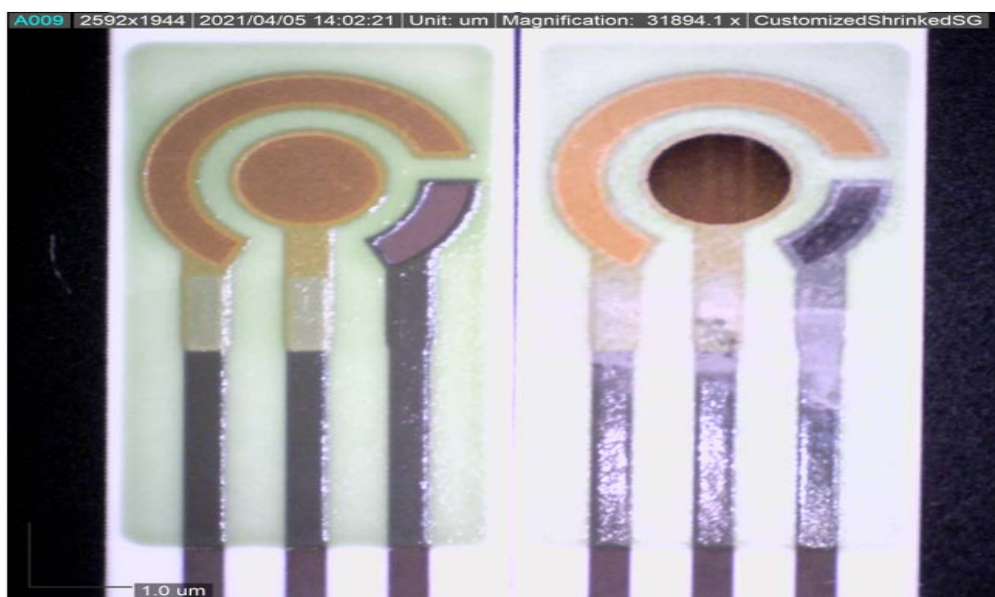


Figure 5.14: Commercially available ZP sensor (a) before under potential deposition (UPD) of Bi (III) and (b) after UPD of Bi (III) on gold based electrochemical sensor (ECS).

In the first step, the solution of bismuth (III) chloride (BiCl_3) and DI water (H_2O) has been prepared – $400 \mu\text{g/L}$ Bi (III) contaminated DI water. BiCl_3 is soluble in DI water due to hydrolyses and produces BiOCl and HCl . In the next step, a full cycle of CV analysis has been performed on the Au plated IP SMP incorporated working electrodes to deposit thin Bi (III) film on the electrodes based on UPD. Figure 5.12 shows one full cycle of CV for UPD of Bi (III) on Au plated WE. Figures 5.13 and 5.14 indicate the thin film of Bi (III) on Au working electrode (dark brown) for both inkjet printed (UTEP) and commercially available (ZP) ECSs respectively. Figures 5.15 and 5.16 represent scanning electron micrograph (SEM) images and energy dispersive spectroscopy (EDS) of Bi (III) coated/deposited inkjet printed WE. Successful UPD of Bi (III) is evident in both characterizations i.e., 3D topology of Bi (III) salt is present in SEM images and 33.7% Bi (III) has been identified in EDS.

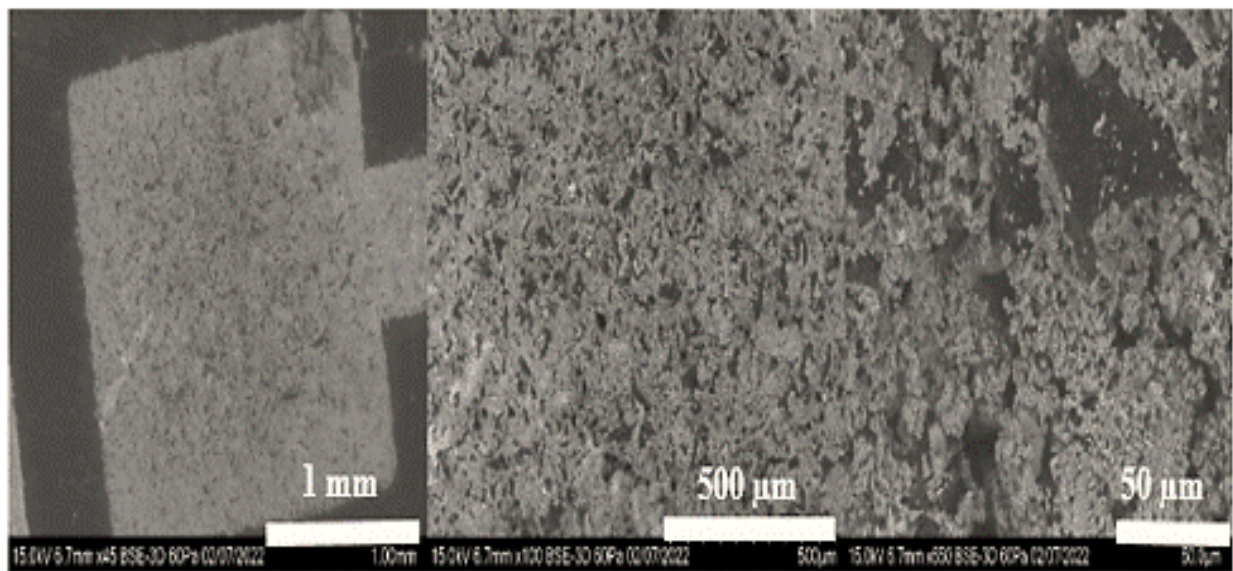


Figure 5.15: Scanning Electron Micrograph images for bismuth (III) deposited inkjet printed gold plated electrochemical sensor.

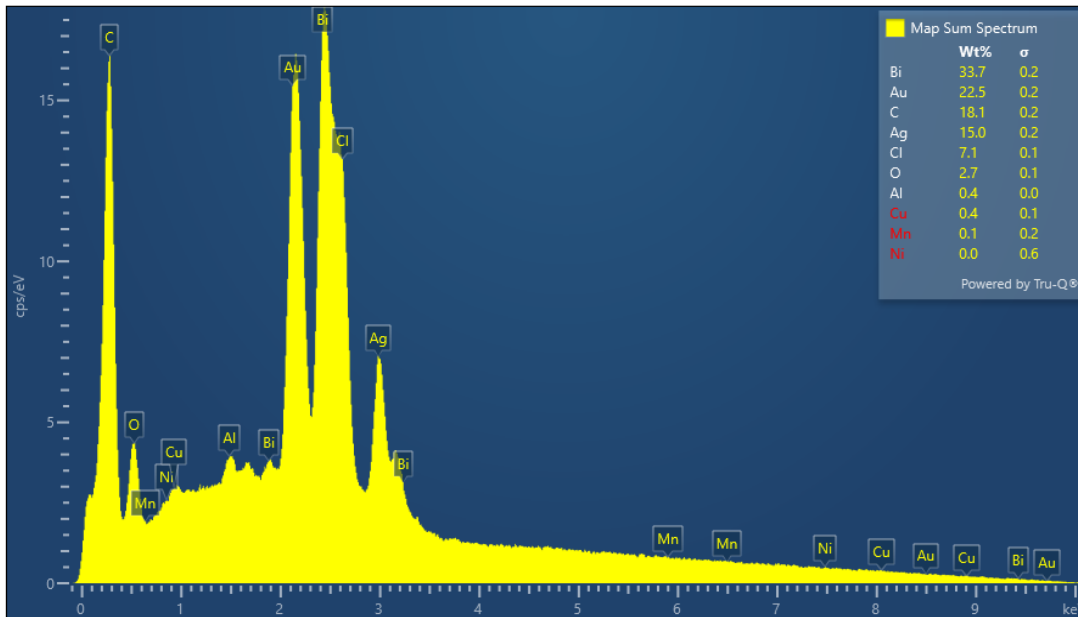


Figure 5.16: Energy dispersive spectroscopy for inkjet printed Bismuth (III) deposited inkjet printed working electrode (33.7% bismuth).

After Bi (III) coating the electrodes have been applied to electrochemical sensing such as lead (II) detection in the optimized DI water (0.1 M HCl) for different concentration i.e., blank, 5 ppb, 10 ppb, 20 ppb, 40 ppb, 60 ppb, 80 ppb, and 100 ppb (1 ppb = 1 $\mu\text{g/L}$). Figures 5.17 and 5.18 illustrate the performance of Bi (III) coated inkjet printed electrodes in case of square wave anodic stripping voltammetry (SWASV) and calibration curve respectively. The limit of detection (LOD) for Bi (III) deposited inkjet printed electrode is 6.39 $\mu\text{g/L}$ – USEPA approved lead (II) level in drinking water is 15 $\mu\text{g/L}$.

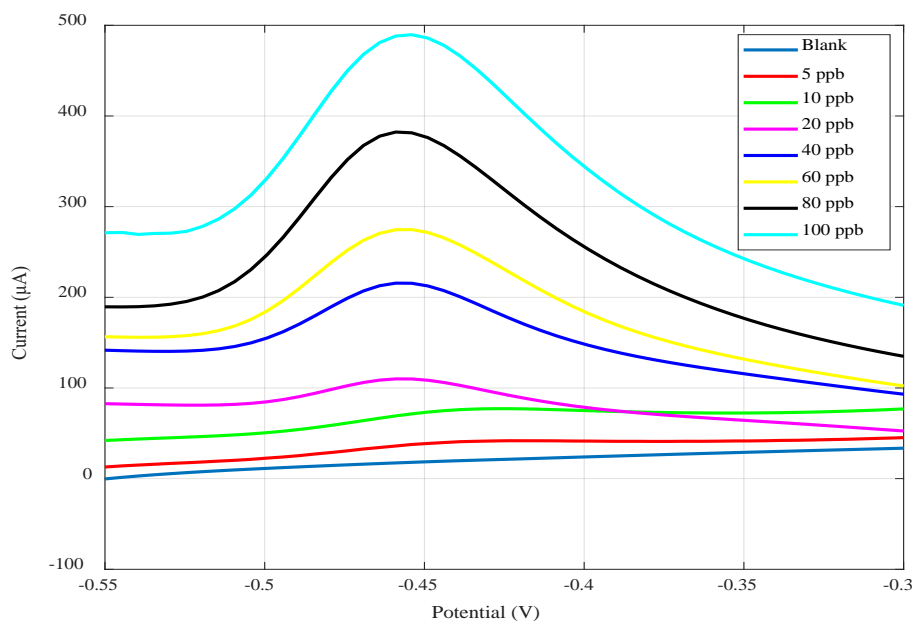


Figure 5.17: Square wave anodic stripping voltammetry (SWASV) of bismuth (III) plated inkjet printed gold electrodes with different concentrations of lead (II) ions i.e., blank, 5 ppb, 10 ppb, 20 ppb, 40 ppb, 60 ppb, 80 ppb, and 100 ppb in 0.1 M HCl. Modulation amplitude - 280 mV, frequency - 15 Hz, estimated duration - 4.4 s, and scan rate - 45 mV/s, and deposition time - 5 minutes.

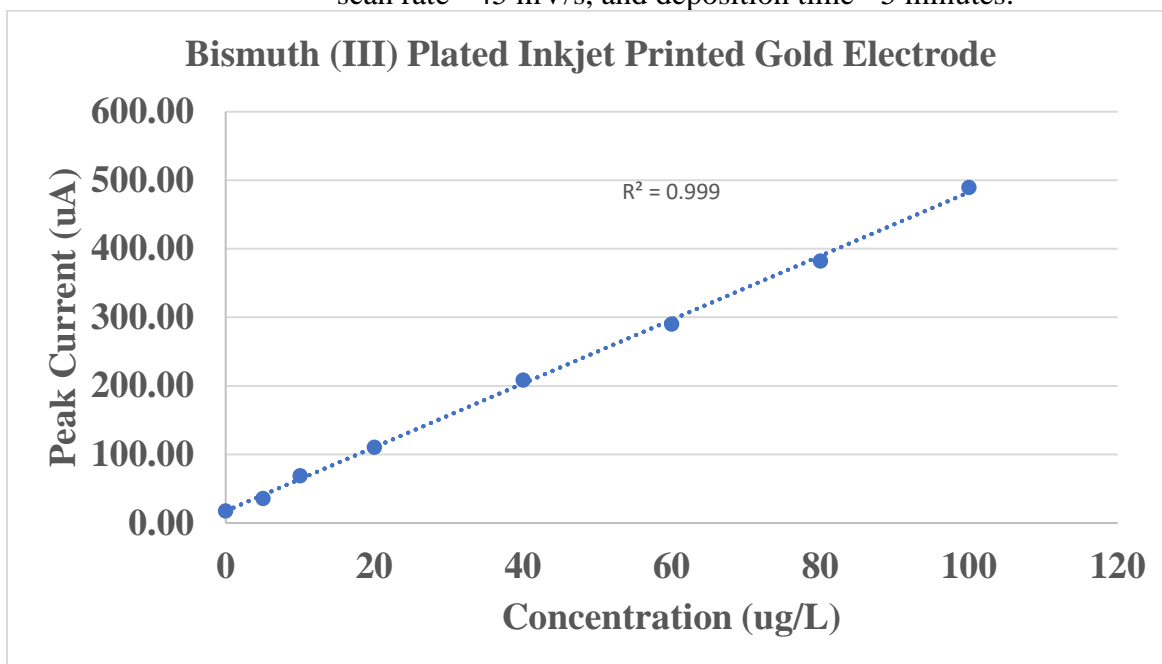


Figure 5.18: Calibration curve for bismuth (III) plated inkjet printed gold plated electrochemical sensor. The data point for each concentration is a mean of three different data collected using three different sensors.

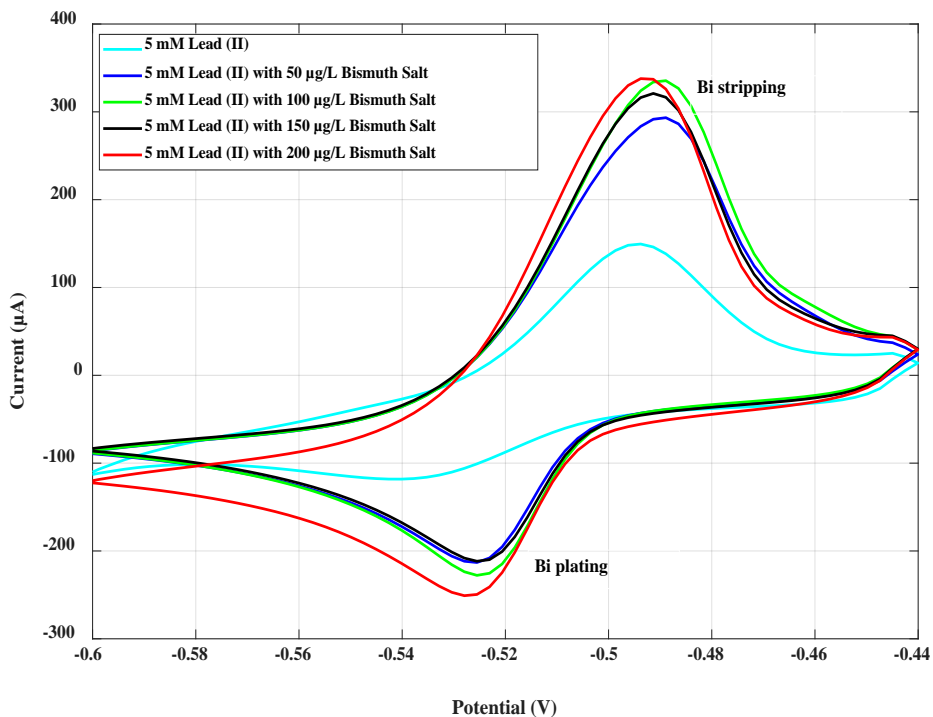


Figure 5.19: Cyclic voltammogram (CV) for in situ Bismuth (III) functionalization on gold plated electrochemical sensor (ECS).

In the in-situ procedure, the Bi (III) deposition on inkjet printed Au plated electrode has been conducted simultaneously with the electrochemical sensing i.e. lead (II) detection process. Different concentration of Bi (III) i.e., 50 µg/L, 100 µg/L, 150 µg/L, and 200 µg/L have been added with the sample analyte of lead (II) contaminated optimized DI water – 5 mM lead (II). Figure 5.19 represents CV for different concentration of Bi (III) diluted in 5 mM lead (II) contaminated optimized DI water. It is observed from the CV analysis that 200 µg/L of Bi (III) performs better in terms of oxidation/reduction peaks. Hence, 200 µg/L concentration of Bi (III) has been chosen for further electrochemical analysis i.e., SWASV for different concentration of lead (II). Figure 5.20 shows SWASV for different concentration of lead (II) contaminated optimized DI water added with 200 µg/L Bi (III). The LOD for inkjet printed Au plated ECS in

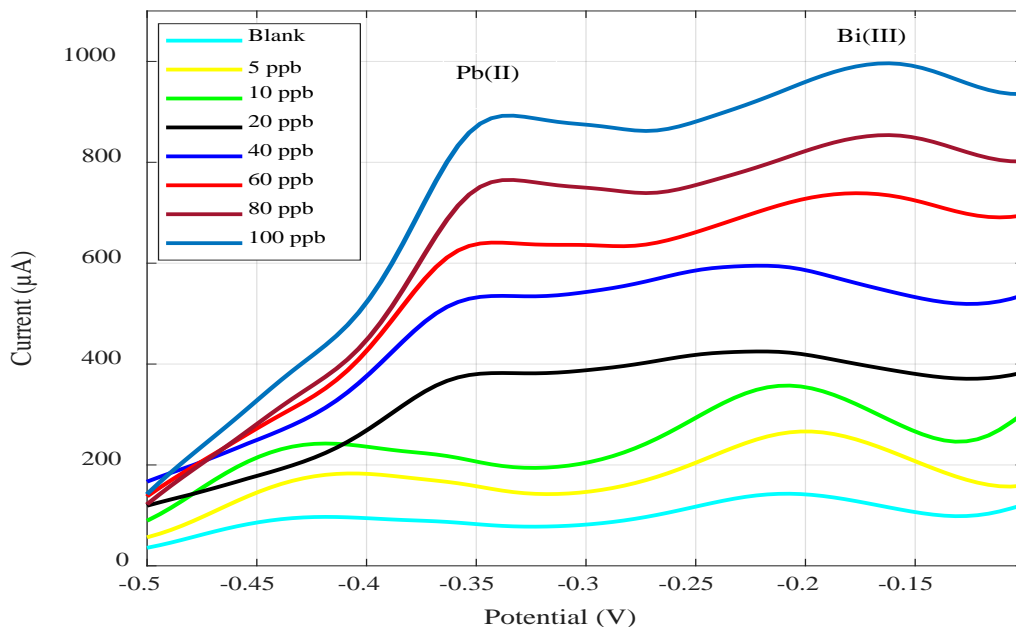


Figure 5.20: Square wave anodic stripping voltammetry (SWASV) of inkjet printed gold electrodes with different concentrations of lead (II) ions i.e., blank, 5ppb, 10 ppb, 20 ppb, 40 ppb, 60 ppb, 80 ppb, and 100 ppb including 200 µg/L bismuth (III) salt in 0.1 M HCl. Modulation amplitude - 280 mV, frequency - 15 Hz, estimated duration - 4.4 s, and scan rate - 45 mV/s, and deposition time - 5 minutes.

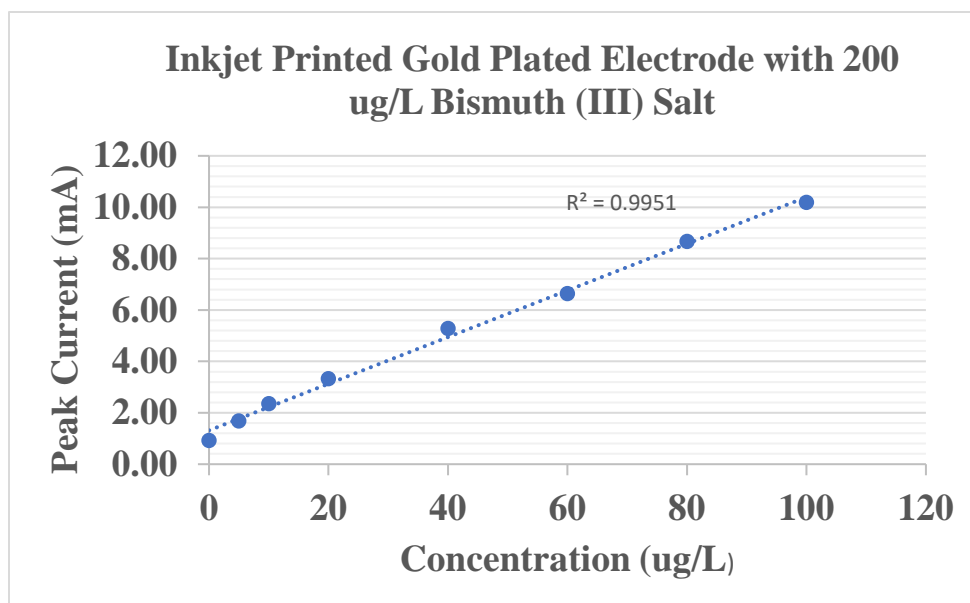


Figure 5.21: Calibration curve for inkjet printed gold plated electrochemical sensor with 200 µg/L bismuth (III) salt in lead (II) contaminated aqueous solution. The data point for each concentration is a mean of three different data collected using three different sensors.

case of in situ Bi (III) functionalization is 14.08 $\mu\text{g/L}$ – USEPA approved lead level is 15 $\mu\text{g/L}$ for drinking water. Finally, Figure 5.21 represents the calibration curve for in situ Bi (III) functionalization.

SECTION 5.4. REUSABILITY

Reusability is an important characteristic for any electrochemical sensor (ECS). This characteristic needs to be assessed, evaluated, and analyzed appropriately. In case of inkjet printed shape memory polymer (SMP) incorporated Au electroplated ECSs, reusability test has been conducted thoroughly. Cleaning cycle is crucial in case of reusing the ECSs. It is mandatory to clean the inkjet printed ECS after every use to get rid of the oxidized layer, improve sensitivity, reproducibility, and get a stable base line. In case of reusing the ECSs, the cleaning cycle also makes sure the electrode gets rid of all the contaminants including the prior experimental sample analyte i.e., lead (II) in this case. Figure 5.22 shows the last cycle of 25 cycles cyclic voltammetry (CV) electrochemical analysis using 0.5 M H_2SO_4 for reusing the inkjet printed ECS for 4 times. It has been observed that for each time (until 4 times) the CV is clear and shows a large potential window for further electrochemical analysis.

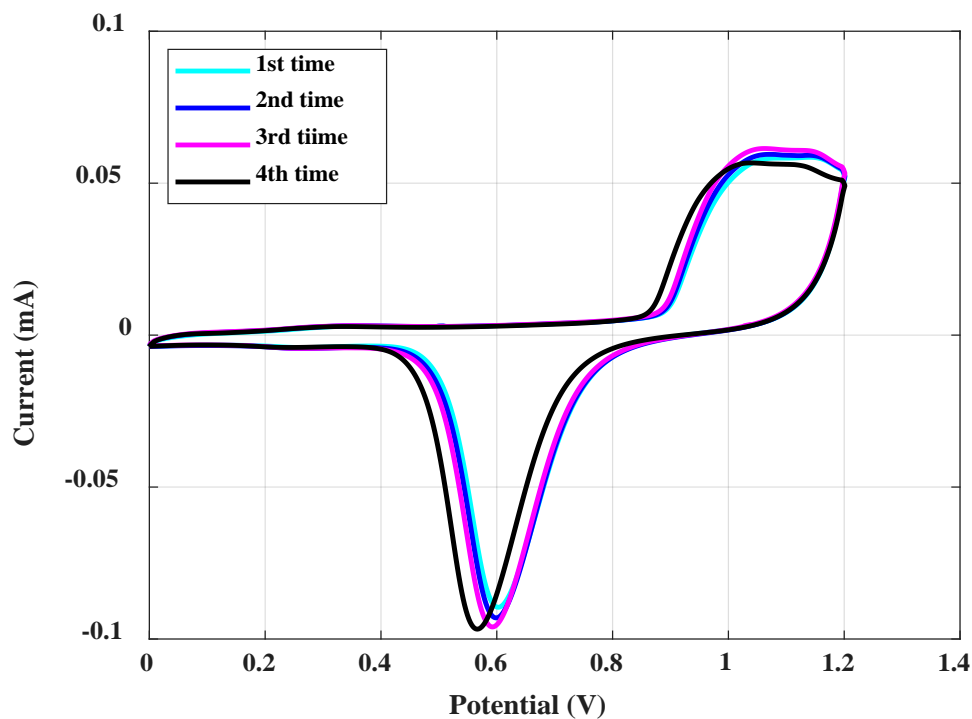


Figure 5.22: Last cycle of 25 cycles of cyclic voltammogram (CV) for 0.5M H₂SO₄ for 4 times before each measurement. Scan rate is 100 mV/s.

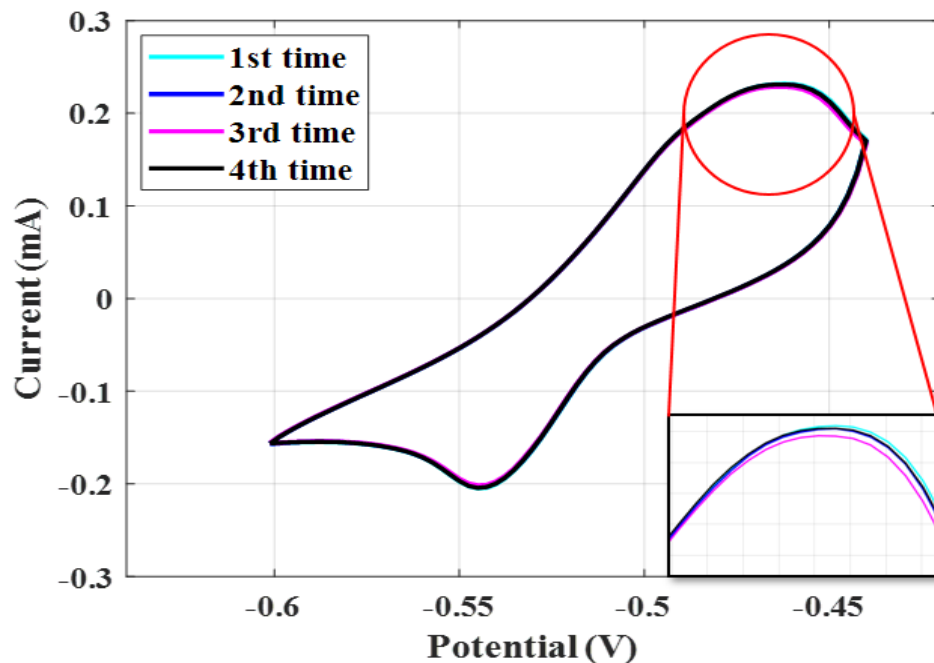


Figure 5.23: Cyclic Voltammetry (CV) of gold (Au) plated electrochemical sensor (ECS) for 5mM lead (II) contaminated 0.1M HCl (optimized DI water) for 4 times at 50 mV/s. The ECS was cleaned with 25 cycles of CV at 100 mV/s using 0.5 M H₂SO₄ prior every use.

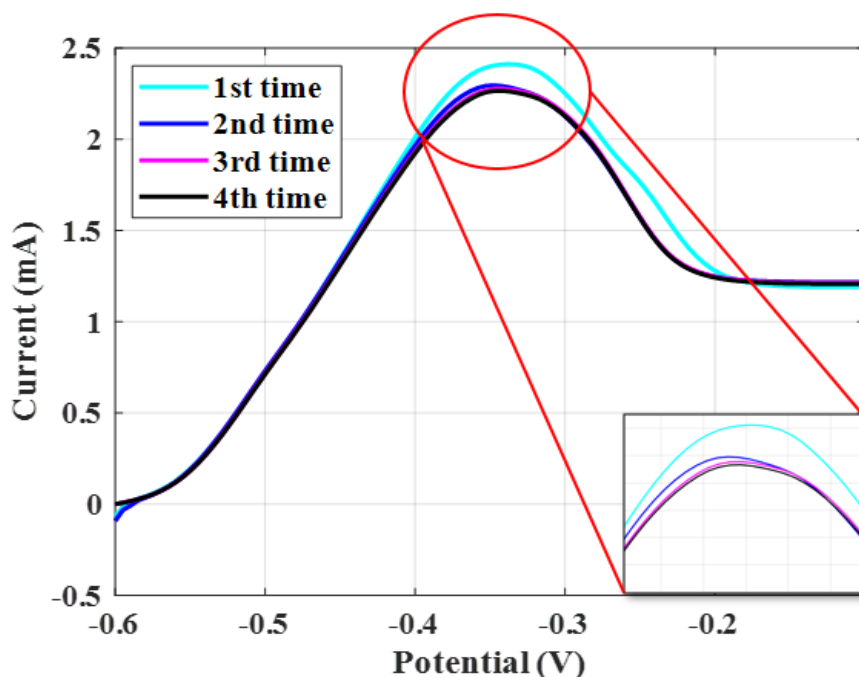


Figure 5.24: Square wave anodic stripping voltammetry (SWASV) of gold (Au) plated electrochemical sensor (ECS) for 5mM lead (II) contaminated 0.1M HCl (optimized DI water) for 4 times - modulation amplitude - 280 mV, frequency - 15 Hz, estimated duration - 4.4 s, and scan rate - 45 mV/s, and deposition time - 5 minutes. The ECS was cleaned with 25 cycles of CV at 100 mV/s using 0.5 M H₂SO₄ prior every use.

Both CV and square wave anodic stripping voltammetry (SWASV) have been conducted for 5 mM lead (II) contaminated optimized DI water to perform reusability test. Figures 5.23 and 5.24 represent CV and SWASV in case of 5 mM lead (II) contaminated 0.1 M HCl. It has been observed that the voltammetry stripping peak in both cases i.e., CV and SWASV are consistent (CV peak currents = $230.63 \mu A \pm 1.45$ and SWASV peak currents = $230.86 \mu A \pm 6.95$). It has also been observed from both electrochemical analysis and mathematical calculation that inkjet printed SMP incorporated Au plated ECSs have acceptable and potential reusability characteristic (up to 4 times). It should be noted that there is a challenge in case of reusing the ECSs for more

than 4 times. It has been observed that the Au plated working electrode breaks after 4th use. There might be several reasons for this occurrence i.e., cleaning with strong (0.5M) H₂SO₄, lots of cleaning cycles, cleaning with electro cleaner during fabrication, or applying high voltage. This phenomenon will be explored in future, and it is assumed that the reusability number will be increased significantly if the reason can be identified and optimized.

SECTION 5.5. SIMULTANEOUS DETECTION OF OTHER HMIS

The selectivity of the inkjet printed gold plated electrochemical sensor has been investigated in case of cadmium (III), copper (II), iron (III), and bismuth (III) ion. It is observed from Figure 5.25 that these heavy metal ions i.e., copper (II) and iron (III) does not have any interference with the lead (II) stripping peak at approximately -480 mV in case of individual sensing phenomenon. However, this experiment does not prove actual selectivity characteristic of the fabricated inkjet printed gold plated ECSs.

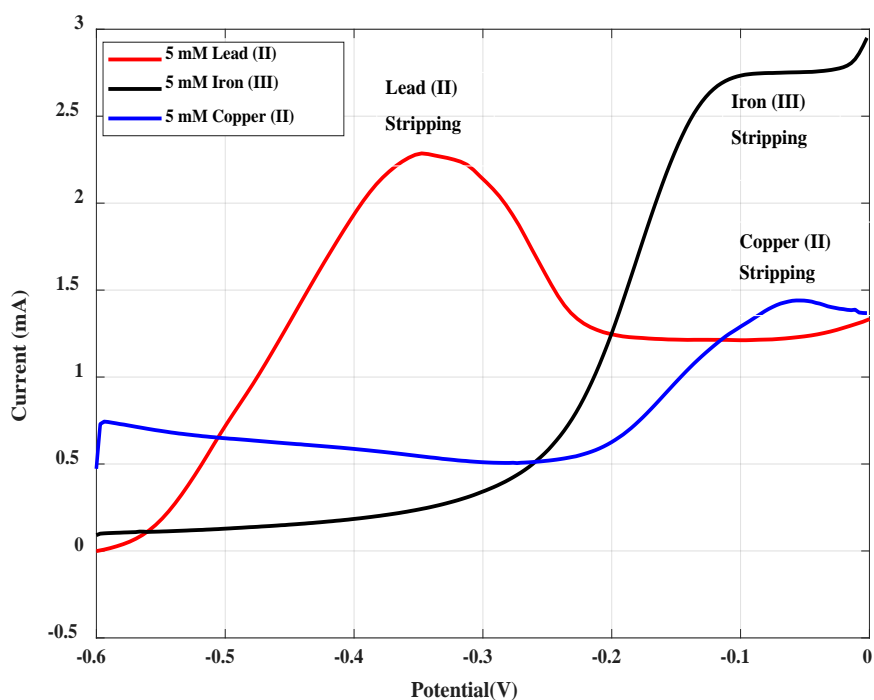


Figure 5.25: Selectivity test for inkjet printed shape memory polymer based gold plated electrochemical sensor in case of lead (II), iron (III), and copper (II) individually.

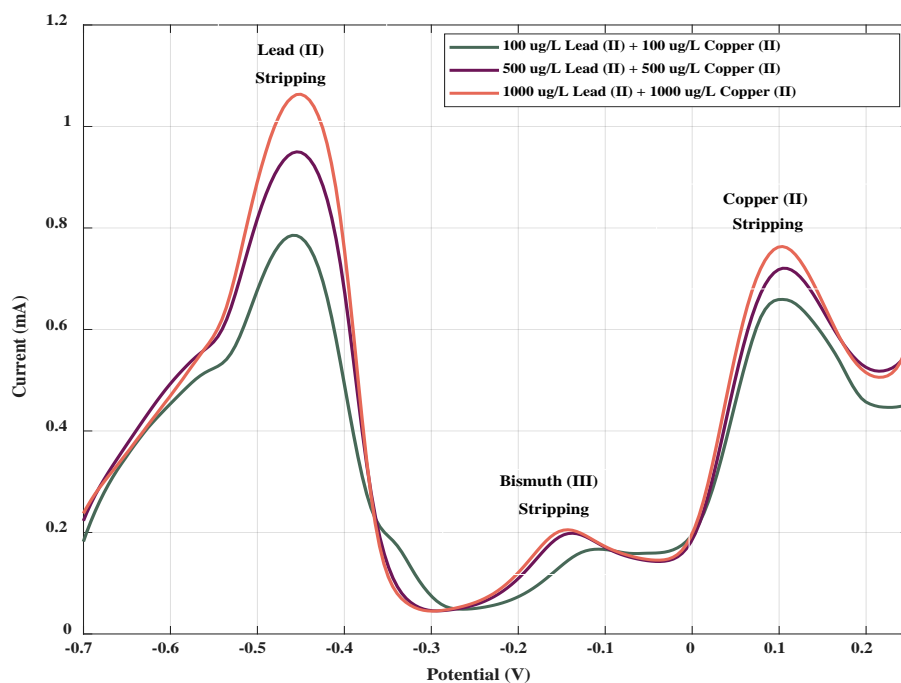


Figure 5.26: Selectivity test for inkjet printed shape memory polymer based gold plated electrochemical sensor in case of simultaneous presence of lead (II), cadmium (II) and copper (II).

Actual selectivity test has been conducted on fabricated inkjet printed ECSs. Three different sample solutions each containing equal amount of lead (II), cadmium (II), and copper (II) have been prepared. Figure 5.26 shows the performance of the fabricated inkjet printed ECSs in case of three different sample solutions i.e., 100 $\mu\text{g/L}$ lead (II), cadmium (II), and copper (II), 500 $\mu\text{g/L}$ lead (II), cadmium (II), and copper (II) and 1000 $\mu\text{g/L}$ lead (II), cadmium (II), and copper (II) respectively. It is observed that cadmium (II) peak is missing in Figure 5.26. This happened due to the presence of copper (II) ion [11]. However, significant peaks of lead (II) and copper (II) ions show promising performance of the fabricated ECSs in case of selectivity for lead (II) sensing in aqueous solution. A miniature bismuth peak is visible due to bismuth coated gold-plated inkjet printed working electrode.

SECTION 5.6. COMPATIBILITY WITH REAL SAMPLE

In order to find the compatibility of the inkjet printed ECSs, it has been utilized for both tap water and river water. Figure 5.27 represents CVs for both blank (only 0.1 M tap water) and 5 mM lead (II) contaminated 0.1 M tap water. Figure 5.28 also shows CVs for both blank (only 0.1 M river water) and 5 mM lead (II) contaminated 0.1 M river water. All the water samples were filtered using filter paper.

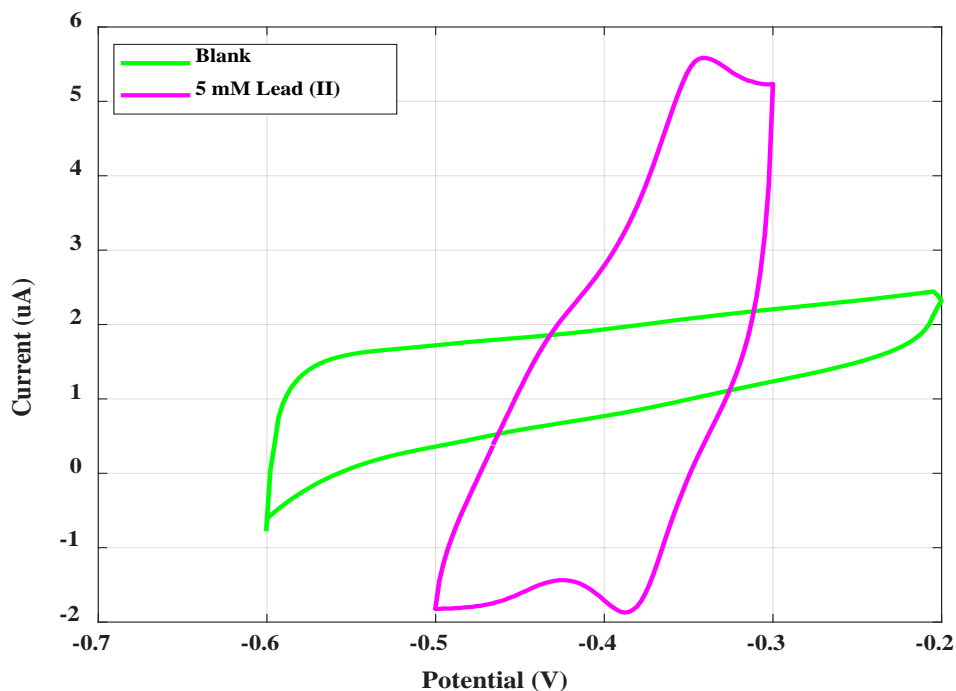


Figure 5.27: Cyclic Voltammetry (CV) of gold (Au) plated electrochemical sensor (ECS) for blank (optimized tap water without lead (II)) – green, 5mM lead (II) (optimized tap water with 5 mM lead (II)) – purple at 100 mV/s.

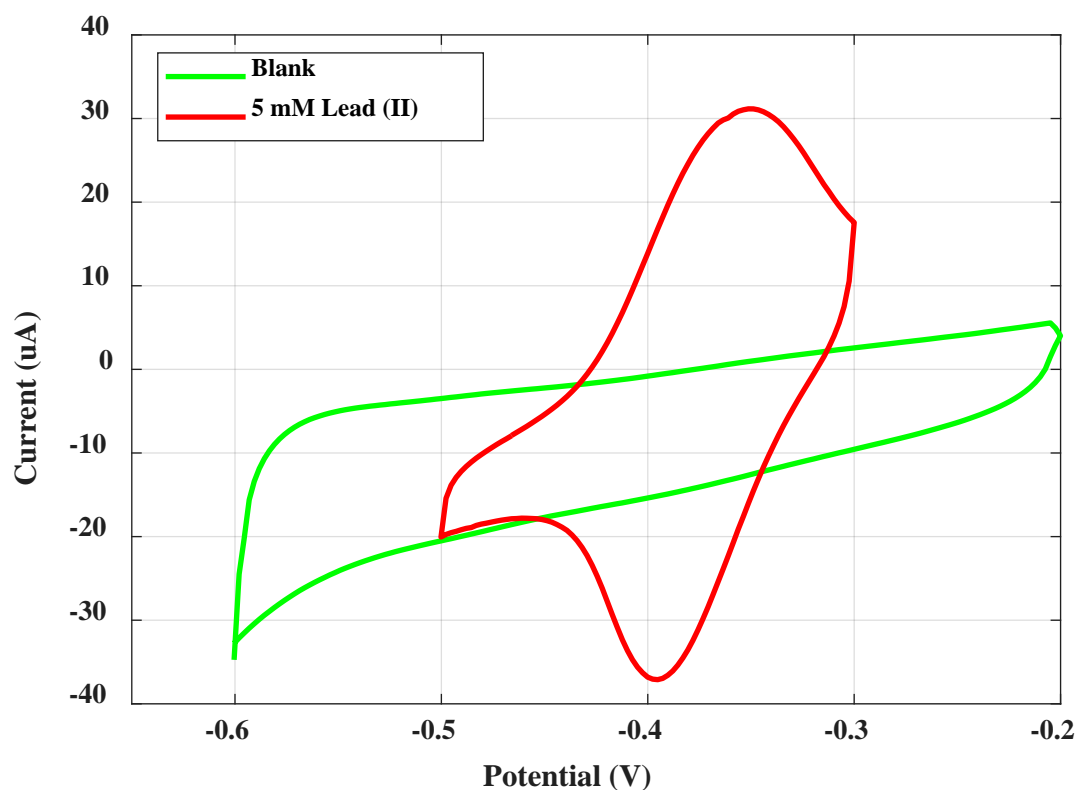


Figure 5.28: Cyclic Voltammetry (CV) of gold (Au) plated electrochemical sensor (ECS) for blank (optimized tap water without lead (II)) – green, 5mM lead (II) (optimized river water with 5 mM lead (II)) – red at 100 mV/s.

SECTION 5.7. UNCERTAINTY ANALYSIS

In this research, “Type A evaluation of standard uncertainty” approach from “Evaluation of Measurement Data – Guide to the expression of uncertainty in measurement” has been utilized to determine the uncertainty in the raw data. The GUM approach has been introduced in Section 2.5 (Chapter 2). The approach allows determining the uncertainty considering conditions for each specific measurement. 15 samples have been considered to collect the raw data of initial dimension, final dimension, reduction factor, resistivity, and oxidation peak from CV electrochemical analysis. The individual initial dimension, final dimension, reduction factor, resistivity, and oxidation peak varied due to fabrication process such as inkjet printing the

electrodes, making small samples, curing and shrinking the electrodes at 180 °C for 3 minutes, and digital reading of the dimension and resistivity. Same solution has been used for characterizing all the 15 electrochemical sensors, so analyte concentration does not have any responsibility for these differences. The experimental variance of the observations estimated the probability distribution of each occurrence (initial dimension, final dimension, reduction factor, resistivity, and oxidation peak). The calculated experimental standard deviation illustrated the dispersion of each observation from their mean. The variance and standard deviation of the mean have been determined by considering the experimental variance and experimental standard deviation out of the total number of observations/occurrences. This variance of mean is defined as Type A variance and the standard deviation of the mean is defined as Type A standard uncertainty. Equations A-4 and A-5 from NIST Technical Note 1297 have also been used to calculate sample mean and standard uncertainty in case of each occurrence for 15 individual observations for 15 different samples/sensors. Both approaches provided very similar standard uncertainty for Type A evaluation.

Systemic errors associated with shrinking/processing temperature (140 ~ 200 °C), room temperature, atmospheric pressure, analyte quantity, processing and electrochemical analyzing response time have been evaluated by varying the above parameters. There were no significant/observable changes while modifying these experimental conditions. Tables 5.1 and 5.2 shows data of Type A and NIST TN 1297 mean and standard deviation of the inkjet printed gold (Au) plated ECSs as well as summary of the uncertainty analysis i.e., the parameters responsible for influencing the variation of the collected factors and the parameters those are neutral in terms of affecting the uniformity of the selected factors – initial dimension, final dimension, reduction factor, resistivity, and oxidation peak.

Table 5.1: Type A and NIST TN 1297 Mean and Standard Deviation Data of Inkjet Printed Gold Plated Electrochemical Sensor.

Number of Sample	Initial Dimension (length×width) (mm)	Final Dimension (length×width) (mm)	Reduction Factor (%)	Resistivity Measurement ($\Omega - \square$)	Measured Peak for Electrochemical Sensing (mA)
1	45.18×28.63	20.11×11.65	55.4×59.3	4.3	1.584
2	44.69×28.44	19.25×11.81	59.6×58.4	4.6	1.572
3	44.62×28.39	18.18×11.79	59.3×58.4	3.9	1.579
4	43.35×27.65	17.86×11.35	58.8×58.9	4.3	1.562
5	44.13×28.90	18.69×12.03	57.6×58.3	4.8	1.581
6	44.12×28.90	19.64×11.60	55.4×59.8	4.2	1.563
7	43.82×28.08	18.25×11.36	58.3×59.5	4.3	1.572
8	44.95×28.23	18.42×11.25	59.0×60.1	4.1	1.564
9	44.69×28.44	19.25×11.81	59.6×58.4	4.2	1.582
10	44.13×28.90	18.69×12.03	57.6×58.3	4.0	1.546
Estimate of Variance	0.0063×0.0219	0.0023×0.0146	0.0235×0.0455	0.0081	0.000066
Experimental Standard Deviation (SD)	0.0793×0.1479	0.0479×0.1208	0.1532×0.2133	0.0900	0.007745
Type A Variance (Experimental Variance of mean)	0.0006×0.0021	0.0002×0.0014	0.0023×0.0045	0.0008	0.000006
Type A Standard Uncertainty (Experimental SD of mean)	0.0244×0.0458	0.0141×0.0374	0.0479×0.0670	0.0282	0.002449
NIST TN 1297 Sample Mean	44.37×28.46	18.83×11.67	58.7×58.9	4.27	1.570
NIST TN 1297 Standard Uncertainty	0.02×0.04	0.01×0.03	0.05× 0.07	0.0285	0.0026

Table 5.2: Summary of Uncertainty Analysis for Inkjet Printed Gold Plated Electrochemical Sensor.

Factor	Standard Uncertainty	Comments
Reduction factor	0.0479×0.0670	This error occurred due to fabrication process such as inkjet printing on the SMP substrate, making small samples, curing and shrinking the samples, and rounding digital reading
Resistivity	0.0282	This occurred in case of changed dimension due to standard error

Measured peak for electrochemical sensing	0.002449	Standard error due to rounding of digital reading
Fabrication/ processing temperature	No Contribution	140 ~ 200 °C
Response time (fabrication)	No contribution	3 ~ 10 minutes
Response time (electrochemical analysis)	No contribution	3 ~ 10 minutes
Analyte amount	No contribution	As long as active electrode surface area is immersed in the analyte, the amount does not influence the calibration

SECTION 5.8. COST ANALYSIS

Cost analysis is an important phenomenon in case of fabricating inkjet printed gold (Au) plated electrochemical sensors (ECSs). The initial significant goal of this dissertation research was to develop fabrication processes those will create an ECS that is cost effective, sensitive, and selective. To ensure cost-effectivity the use of Au nanoparticle conductive ink (3ml costs 855\$ according to Novacentrix – July 10, 2023) has been ignored since the beginning of this research. All the optimization and characterization have been performed considering cost-effectivity. To conduct the cost analysis calculation, the information regarding the fabrication time of each Au plated ECS is extremely important. Table 5.3 indicates the total fabrication time including individual time requirements in each step. It has been observed that an inkjet printed Au plated ECS requires 186 minutes (in total) to complete the fabrication processes. Table 5.4 shows cost per ECS in case of each resources required to fabricate the sensors i.e., shape memory polymer (SMP) film, silver (Ag) nanoparticle conductive ink, 24K brush Au solution, electro cleaner, bleach, and electricity for inkjet printing and shrinking using laboratory oven. It has been observed from Table 5.4 that total cost of each inkjet printed Au plated ECS is approximately a dollar which makes it extremely cost effective compared to other commercially available Au electrodes. It should be noted that one ZP (Zimmer and Peacock) screen printed Au electrode cost $\approx 14.3\$$ - July 10, 2023.

Table 5.3: Time Analysis of Inkjet Printed Gold Plated Electrochemical Sensor.

Fabrication Steps	Required Time (minutes)
Inkjet printing per layer	20
Inkjet printing of total 9 layers	180
Shrinking/curing	3
Electro cleaning	0.5
Gold plating	1
Chlorination	0.5
Final cleaning with DI water	0.5
Drying with compressed air	0.5
Total time	186

Table 5.4: Cost Analysis of Inkjet Printed Gold Plated Electrochemical Sensor.

Name of the item	Cost/Sensor (\$)
Shape memory polymer film	0.0131
Silver nanoparticle conductive ink	0.000006
24K brush gold solution	0.75
Electrocleaner	0.04
Bleach (reusable)	0.01
Electricity-inkjet printing	0.18
Electricity-shrinking/oven	0.006
Electricity-function generator (electro cleaning and gold plating)	0.002
Total cost	1.00

SECTION 5.9. SUMMARY

This chapter contains a bundle of data for inkjet printed ECSs. It started with EESA calculation of the ECSs using Randles-Sevcik quasi reversible equation. The EESA of the fabricated inkjet printed ECS is $7.25 \text{ mm}^2 \pm 0.15 \text{ mm}^2$ (lateral area - 4 mm^2). A mathematical model has been developed utilizing reduction factor and EESA. SEM, EDS, CV, SWASV, LOD, and LOQ have been calculated in case of gold-plated and bismuth coated working electrodes.

Bismuth coated electrodes have been considered for both in-situ and ex-situ fabrication processes. Reusability test has been conducted for 5 times. It has been observed that the fabricated inkjet printed ECS can be reused without any challenge or difficulties until 4 times including 25 cycles of CV with 0.5 M H₂SO₄ – cleaning cycle. Selectivity test has been performed in case of copper (II), iron (III), and cadmium (II). The fabricated ECSs have shown potential performance in case of lead (II) contaminated real water samples i.e., tap water and river water. Finally, uncertainty analysis and cost analysis have also been illustrated in detail in this chapter.

Chapter 6: Conclusion and Future Work

SECTION 6.1. SUMMARY

This PhD dissertation research has developed a simple, miniaturized, sensitive, selective, reproducible, and disposable 3D (inkjet printed – additive manufacturing technology) gold (Au) plated electrochemical sensor (ECS) on shape memory polymer (SMP) for aqueous lead detection. This technology has shown promising output in case of electrochemical sensing (lead (II) detection) due to increased effective electrode surface area. Lateral or mechanical surface area of the inkjet printed Au plated ECS is 4.19 mm^2 – after curing and shrinking. The electrical surface area or effective electrode surface area (EESA) of the same ECS is $22.52 \text{ mm}^2 \pm 5.36$. The electrical or EESA has been calculated using Randles-Sevcik quasi reversible equation. The data represents mean and standard deviation of 15 different ECSs. Based on EESA calculation a mathematical model has been developed to provide conceptual idea regarding the actual – electrical/mechanical and as-printed dimension of the inkjet printed micro electromechanical systems (MEMS) devices on SMP. The design, fabrication processes including printing recipe development for Dimatix Materials Printer (Fujifilm – DMP 2850) in case of both printheads (i.e., legacy – the old one and Samba – newly launched (2021)), optimization and characterization including bismuth (Bi) functionalization, repeatability, reusability, reproducibility, uncertainty analysis, and cost analysis of the novel SMP based IP Au plated ECSs have been investigated, analyzed, developed, and finally optimized in detail. Sensor characterization, optimization, and evaluation have been performed using electrochemical analysis i.e., cyclic voltammetry (CV), square wave anodic stripping voltammetry (SWASV), and electrochemical impedance spectroscopy (EIS). The fabricated ECS consists of Au working electrode (WE), Au counter electrode (CE), and silver chloride (AgCl) reference electrode (RE). Immersion Au plating (24K

brush Au solution) has been applied on IP silver (Ag) electrodes to fabricate Au WE and CE. This Au electroplating technology has made the inkjet printed ECS cost-effective without compromising its performance. It has been observed continuously and consistently that the electrochemical behavior and potential window of the bare Au WE (popular and widely used in electrochemical and biosensing applications) and inkjet printed Au plated WE are similar. Chlorination using sodium hypochlorite solution (only 3%) has been utilized to fabricate AgCl reference electrode. Bi functionalization has been performed in two different ways i.e., ex situ - a full range of CV (-800mV to -200 mV) - has been conducted to Bi coat/deposit the Au electrode with the solution of 400 µg/L Bi salt – BiCl₃ and in situ –CV/SWASV have been performed with lead contaminated aqueous solution diluted with 200 µg/L Bi salt. Scanning electron micrograph (SEM) images and energy dispersive spectroscopy (EDS) have been collected and analyzed for all three types of electrodes i.e., Au electroplated WE, Bi coated WE, and AgCl RE. It has been observed from SEM that the 3D topology – twisted, tangled, and serpentine geometry is present in case of inkjet printed shrunk Au electrodes. The EDSs validated all the developed and optimized fabrication processes by showing significant amount expected material for each electrode i.e., 9.9% Au for Au WE, 7.9% chlorine for AgCl reference electrode, and 33.7% Bi for Bi deposited WE. The limit of detection (LOD) of the fabricated inkjet printed ECSs are 0.64 µg/dL – Bi coated WE, 0.76 µg/dL – Au WE, and 1.4 µg/dL –Au WE with lead contaminated aqueous solution diluted with 200 µg/L Bi salt. The R² – square of the correlation coefficient value in each case are 0.999, 0.992, 0.995 respectively. It should be noted that the USEPA approved lead level in drinking water is 1.5 µg/dL. Fabricated inkjet printed Au plated/Bi coated ECSs showed excellent sensitivity including the potential to measure the reference lead level in drinking water. In case of sensitivity, clean electrodes play a significant role. Optimization of cleaning cycle is extremely

important to get rid of the oxidized layer, improve sensitivity, reproducibility, and get a stable base line. Inkjet printed Au plated/Bi coated ECSs require 25 cycles of CV using 0.5 M H₂SO₄ in order to get rid of any type of contaminant. In addition, some other major characteristics i.e., selectivity, reproducibility, reusability, and application to real samples have also been investigated for the fabricated inkjet printed ECSs. Selectivity test has been conducted in case of other heavy metal ions (HMIs) i.e., iron and copper. The inkjet printed SMP incorporated ECSs shows excellent selectivity. To investigate the potential ECSs reproduction, EIS measurements for the fabricated ECSs ($64.07 \pm 7.19 \Omega$) has also been conducted using phosphate buffer saline (PBS; pH 7.42) - data has been calculated using 10 different measurements collected from 10 different fabricated ECSs. Reusability test demonstrates excellent reusable capability for 4 times. It is also evident that the fabricated inkjet printed Au plated/Bi coated ECSs are compatible with real samples i.e., tap water (El Paso, TX). Finally, the green fabricated – mercury free inkjet printed ECSs have been validated using uncertainty analysis following “Type A evaluation of standard uncertainty” approach from “Evaluation of Measurement Data – Guide to the expression of uncertainty in measurement” for 15 different ECS samples in case of reduction factor (%), resistivity measurement ($\Omega\text{-}\square$), and peak current measurement (mA) – 3 mM of lead contaminated optimized DI water (0.1 M HCl).

SECTION 6.2. CONTRIBUTIONS OF THIS WORK

This PhD dissertation research has contributed directly to three different areas. First, the developed fabrication processes of electrochemical sensor (ECS) are simple, cost-effective, and reproducible. The inkjet printed shape memory polymer (SMP) incorporated gold (Au) plated ECS has been applied for the first time for electrochemical sensing application i.e., heavy metal ions (HMIs) detection. The promising electrochemical performance of the inkjet printed Au plated

electrodes (compared to bare Au electrodes) has opened a window to apply this potential cost-effective sensor for a wide range of electrochemical and biosensing applications.

Second, a mathematical model has been developed to explain the relationship between lateral/mechanical and electrical/effective electrode surface of the micro electromechanical systems (MEMS) i.e., sensors fabricated using inkjet printing additive manufacturing technology on SMP. This model will help to design the sensors based on individual preference/requirement for different electrochemical and biosensing applications.

The third contribution of this dissertation research is that it included the validation of the inkjet printed SMP incorporated Au electroplated ECSs using uncertainty analysis. This is the first instance of including validation of the fabricated inkjet printed ECSs by conducting “Type A evaluation of standard uncertainty” approach from “Evaluation of Measurement Data – Guide to the expression of uncertainty in measurement”. Inclusion of this error analysis helps to develop consistent and standard electrochemical and biosensing devices/sensors.

Section 6.2.1. Publication and Conference Proceeding Contributions

The following manuscript publications in journals and/or conference proceedings related the dissertation research have been produced throughout the time. Two additional journals based on the latest findings are in preparation.

- **Annatoma Arif**, Angela Mendez Contreras, Sheikh Dobir Hossain, and Robert C Roberts, “Inkjet Printed 3D Gold Electrochemical Sensor on Shape Memory Polymer for Lead Detection”, *IEEE Sensors Journal*, vol 23, no. 13, pp 13868 – 13875, 2023.
- **Annatoma Arif**, Ryan Price, and Robert C. Roberts, “Characterization and Fabrication of 3D Inkjet Printed Flexible Copper Electrodes”, *65th Electronic Materials Conference*, Santa Barbara, California, June 28-30, 2023.

- **Annatoma Arif** and Robert C. Roberts, “Flexible Inkjet Printed Gold based Electrochemical Sensor for Aqueous Lead Detection”, *2022 IEEE International Conference on Flexible and Printable Sensors and Systems (FLEPS)*, Vienna, Austria, July 10-13, 2022, pp. 1-3.
- **Annatoma Arif** and Robert C. Roberts, “Characterization of Aqueous Lead Sensing Performance of Bismuth Functionalized 3D Inkjet Printed Electrochemical Electrodes”, *64th Electronic Materials Conference*, Columbus, Ohio, June 29-July1, 2022.
- **Annatoma Arif**, Bertha J. Chavez, Sheikh Dobir Hossain, and Robert C Roberts, “Scaling Effects of Inkjet Microfabricated 3D Gold Electrochemical Sensors for Aqueous Lead Detection”, *Technical Digest, Late News, Solid-State Sensors, Actuators and Microsystems Workshop (Hilton Head 2022)*, Hilton Head, South Carolina, June 5-9, 2022, pp. 1-3.
- **Annatoma Arif**, Angela Mendez Contreras, Sheikh Dobir Hossain, and Robert C Roberts, “Inkjet Printed 3D Gold Electrochemical Sensor on Shape Memory Polymer for Lead Detection”, *IEEE conference on Sensors (Sensors 2021)*, October 31-November 4, 2021.
- **Annatoma Arif**, Angela Mendez Contreras, and Robert C Roberts, “Inkjet Printed 3D Metal Electrodes on Shape Memory Polymer towards Improved Electrochemical Bio-Sensing Performance”, *63rd Electronic Materials Conference*, June 2021.

SECTION 6.3. LIMITATIONS

One limitation of this research can be identified as lack of comparison between data collected utilizing novel inkjet printed gold plated electrochemical sensor and traditional

techniques i.e., electrothermal atomic absorption spectrometry – EAAS, flame atomic absorption spectrometry – FAAS, inductively coupled plasma mass spectrometry – ICPMS, or inductively coupled optical emission spectrometry – ICOES. It is important to compare the newly developed electrochemical sensing system with established traditional techniques to understand the characteristics, behavior, and potential strength of the novel sensing system i.e., inkjet printed gold plated ECSs. Another concern can be pointed out as lack of data collected in case of real contaminated samples. In this research, data has been collected utilizing intentionally contaminated aqueous solution i.e., DI and real samples – tap and river waters. However, it is extremely important to conduct all the experiments and data collection in the laboratory setting with the controlled and known contaminated DI water to develop, characterize, and optimize the sensing system effectively and efficiently. The aim of this research was to take the first step to utilize the inkjet printed Au plated ECSs for heavy metal ion detection and understand its performance thoroughly in a laboratory setting to optimize it completely for further utilization of the inkjet printed Au plated ECSs in case of real lead contaminated drinking water and blood samples.

SECTION 6.4. FUTURE WORK

The immediate future works of this research are comparing the data collected utilizing newly developed inkjet printed Au plated ECSs and traditional technique i.e., ICPMS and apply the fabricated ECSs to determine lead (II) in real contaminated aqueous sample. The broader aspect of this dissertation research is to develop a multi-functional Au plated SMP incorporated inkjet printed electrochemical microchip sensor (green fabricated and mercury free) for HMIs (lead, copper, cadmium, and mercury) detection in aqueous solution i.e., drinking water and blood samples. According to USEPA, the approved lead (II) level in drinking water is $1.5 \mu\text{g}/\text{dL}$.

According to CDC the revised blood lead reference value is $3.5 \mu\text{g}/\text{dL}$ (updated on May 14, 2021). The fabricated inkjet printed Au plated/bismuth (Bi) coated electrochemical sensor (ECS) has showed excellent performance in case of lead detection for further consideration and development. The limit of detection (LOD) for Au plated ECS is $0.76 \mu\text{g}/\text{dL}$ and LOD for Bi coated electrode is $0.64 \mu\text{g}/\text{dL}$. Hence, the future research goal is to apply this potential technology – inkjet printing on SMP to fabricate ECSs and optimize/characterize them to apply for HMIs detection in blood – target concentration is $3.5 \mu\text{g}/\text{dL}$. Therefore, the specific objectives of the future research goals are consistent and reliable ECSs fabrication with increased effective electrode surface area for lead (II) detection in blood with appropriate validation and finalize/develop multi-functional inkjet printed SMP incorporated electrochemical microchip sensor for HMIs detection in drinking water and blood samples.

References

- [1] Centers for Disease Control and prevention, “Childhood lead poisoning prevention,” *National Blood Lead Surveillance Data*,” received and processed by CDC as of April 30, 2019 (accessed on May 6, 2021).
- [2] E.M. Roberts, D. Madrigal, J. Valle, G. King, and, L. Kite, “Assessing child lead poisoning case ascertainment in the US, 1999-2010,” *Official Journal of the Academy of Pediatrics*, vol. 139, 2017.
- [3] D. Stacher, “Screening young children for lead poisoning: guidance for state and local public health officials,” *Center for Disease Control and Prevention: Atlanta, GA, USA*, 1997.
- [4] Center for Disease Control and Prevention, “Blood lead levels in residents of homes with elevated lead in tap water – district of Columbia 2004,” *Center for Disease Control and Prevention: Washington, DC, USA*, vol. 53, pp. 268-270, 2004.
- [5] P.B. Tchounwou, C.G. Yedjou, A.K. Patlolla, and D.J. Sutton, “Heavy Metals Toxicity and the Environment,” *Exp Suppl*, vol. 101, pp. 133-164, 2012.
- [6] United States Environmental Protection Agency, “Ground water and drinking water,” *Basic Information about Lead in Drinking Water*. December 9, 2020 (accessed on May 7, 2021).
- [7] F. Arduini, J.Q. Calvo, A. Amine, G. Palleschi, and D. Moscone, “Bismuth-modified electrodes for lead detection,” *Trends in Analytical Chemistry*, vol. 29, pp. 1295-1304, 2010.
- [8] M.A. Korn, D.S. Nadrade, D.S. Jesus, V.A. Lemos, M.L.S.F. Bandeira, W.N.L. Santos, M.A. Bezerra, F.A.C. Amorin, A.S. Souza, and S.L.C. Ferreira, “Separation and preconcentration procedures for the determination of lead using spectrometric techniques: a review,” *Talanta*, vol. 69, pp. 16-24, 2006

- [9] T.M. Florence, "Anodic stripping voltammetry with a glassy carbon electrode mercury plated," *J. Electroanal. Chem.*, vol. 27, pp. 373-281, 1970.
- [10] J. Wang, J. Lu, S.B. Hocevar, P.A.M. Farias, and B. Ogorevc, "Bismuth coated carbon electrodes for anodic stripping voltammetry," *Analytical Chemistry*, vol. 72, pp. 3218-3222, 2000.
- [11] S. Laschi, I. Palchetti, and M. Mascini, "Gold-based screen-printed sensor for detection of trace lead," *Sensors and Actuators B: Chemical*, vol. 114, no. 1, pp. 460 – 465, 2006.
- [12] N. Serrano, J.M. Diaz-Cruz, C. Arino, and M. Exteban, "Ex situ deposited bismuth film on screen-printed carbon electrode: a disposable device for stripping voltammetry of heavy metal ions," *Electroanalysis*, vol. 22, no. 13, pp. 1460-1467, 2010.
- [13] C. Chen, X. Niu, Y. Chai, H. Zhao, and M. Lan, "Bismuth-based porous screen-printed carbon electrode with enhanced sensitivity for tracing heavy metal detection by stripping voltammetry," *Sensors and Actuators B: Chemical*, vol. 178, pp. 339-342, 2013.
- [14] S.G. Reddy, J.T. Wabeke, B.B. Narakathu, D. Maddipatla, J.S. Arachchilage, S.O. Obare, and M.Z. Atashbar, "A screen printed phenanthroline-based flexible electrochemical sensor for selective detection of toxic heavy metal ions," *IEEE Sensors Journal*, vol 16, pp. 8678-8684, 2016.
- [15] Y. Dai and C.C. Liu, "A simple, cost-effective sensor for detecting lead ions in water using under-potential deposited bismuth sub-layer with differential pulse voltammetry," *MDPI Sensor*, vol. 17, no. 950, 2017.
- [16] L. Yu, P. Zhang, H. Dai, L. Chen, H. Ma, M. Lin, and D. Shen, "An electrochemical sensor based on Co_3O_4 nanosheets for lead ions determination," *The Royal Society of Chemistry*, vol. 7, pp. 39611-39616, 2017.

- [17] W. Kang, X. Pei, C.A. Rusinek, A. Bange, E.N. Haynes, W.R. Heineman, and I. Papautsky, "Determination of lead with a copper-based electrochemical sensor," *Anal. Chem.*, vol. 89, pp. 3345-3352, 2017.
- [18] A. Hatamie, P. Jalilian, E. Rezvani, A. Kakavand, and A. Simchi, "Fast and ultra-sensitive voltammetric detection of lead ions by two-dimensional graphitic carbon nitride (g-C₃N₄) nanolayers as glassy carbon electrode modifier," *Measurement*, vol. 134, pp. 679-687, 2019.
- [19] Y. Fang, B. Cui, J. Huang, and L. Wang, "Ultrasensitive electrochemical sensor for simultaneous determination of cadmium and lead ions based on one-step co-electropolymerization strategy," *Sensor and Actuators B: Chemicals*, vol. 284, pp. 414-420, 2019.
- [20] N.Q. Giao, V.H. Dang, P.T.H. Yen, P.H. Phong, V.T.T. Ha, P.K. Duy, and H. Chung, "Au nanodendrite incorporated graphite pencil lead as a sensitive and simple electrochemical sensor for simultaneous detection of Pb(II), Cu(II) and Hg(II)," *Journal of Applied Electrochemistry*, vol. 49, pp. 839-846, 2019.
- [21] X. Hu, H. Guo, T. Qi, W. Fan, C. Jia, B. Xu, Q. Jin, A. Offenhausser, and J. Zhao, "Miniaturized electrochemical sensor with micropillar array working electrode for trace lead online measurement in tap water," *Journal of Micromechanics and Microengineering*, vol. 29, no. 105005, 2019.
- [22] E. Bernalte, S. Arevalo, J. Perez-Taborda, J. Wenk, P. Estrela, A. Avila, and M.D. Lorenzo, "Rapid and on-site simultaneous electrochemical detection of copper, lead, and mercury in the Amazon river," *Sensors and Actuators B: Chemical*, vol. 307, no. 127620, 2020.

- [23] P. Pathak, J.H. Hwang, R.H.T. Li, K.L. Rodriguez, M.M. Rex, W.H. Lee, H.J. Cho, “Flexible copper biopolymer nanocomposite sensors for trace level lead detection in water,” *Sensors and Actuators B: Chemical*, vol. 344, no. 130263, 2021.
- [24] R.J. Reay, C.W. Storment, A.F. Flannery, S.P. Kounaves, and G.T.A. Kovacs, “Microfabricated electrochemical analysis system for heavy metal detection,” *The 8th International Conference on Solid State Sensors and Actuators*, 1995.
- [25] Zimmer and Peacock, “Pros and cons of screen printed electrodes,” 2020. Available online: <https://www.zimmerpeacocktech.com/2020/11/02/pros-and-cons-of-screen-printed-electrodes/> (accessed on 11 May, 2021).
- [26] <https://www.fda.gov/medical-devices/medical-device-recalls/magellan-diagnostics-recalls-leadcare-ii-leadcare-plus-and-leadcare-ultra-blood-lead-tests-due-risk>.
- [27] Centers for Disease Control and prevention, “Childhood Lead Poisoning Prevention,” <https://www.cdc.gov/nceh/lead/data/blood-lead-reference-value.htm> (accessed on August 06, 2022).
- [28] E.T. Santos; G.D. Silva, S. Miserere, L.T. Kubota, and A. Merkoci, “Simple on-plastic/paper inkjet printed solid-state Ag/AgCl pseudo reference electrode,” *American Chemical Society*, vol. 86, pp. 10531-10534, 2014.
- [29] A. Arif, A.M. Contreras, S.D. Hossain, and R.C. Roberts, “Inkjet printed 3D gold electrochemical sensor on shape memory polymer for lead detection,” *IEEE Conference on Sensors (Sensors 2021)*, October 29-November 4 (Virtual), 2021.
- [30] A. Arif, A.M. Contreras, and R.C. Roberts, “Inkjet printed 3D metal electrodes on shape memory polymer towards improved electrochemical bio sensing performance,” *63rd Electronic Materials Conference*, June 23-25 (Virtual), 2021.

- [31] A. Arif, A. M. Contreras, S. D. Hossain and R. C. Roberts, "Three-Dimensional Inkjet-Printed Electrochemical Sensor on Shape Memory Polymer for Aqueous Lead Detection," in *IEEE Sensors Journal*, vol. 23, no. 13, pp. 13868-13875, 1 July 2023, doi: 10.1109/JSEN.2023.3274643.
- [32] A. Arif and R.C. Roberts, "Flexible inkjet printed gold based electrochemical sensor for aqueous lead detection," *2022 IEEE International Conference on Flexible and Printable Sensors and Systems (FLEPS)*, Vienna, Austria, July 10-13, 2022, pp. 1-3.
- [33] A. Arif, B.J. Chavez, S.D. Hossain, and R.C. Roberts, "Scaling effects of inkjet microfabricated 3D gold electrochemical sensors for aqueous lead detection," *Technical Digest, Late News, Solid-State Sensors, Actuators and Microsystems Workshop (Hilton Head 2022)*, Hilton Head, South Carolina, June 5-9, 2022.
- [34] A. Moya, G. Gabriel, R. Villa, F. Javier del Campo, "Inkjet-printed electrochemical sensors," *Current Opinion in Electrochemistry*, vol. 3, no. 1, pp. 29-39, 2017.
- [35] P. Sundriyal and S. Bhattacharya, "Inkjet-Printed Sensors on Flexible Substrates," In: S. Bhattacharya, A. Agarwal, N. Chanda, A. Pandey, A. Sen, (eds) *Environmental, Chemical and Medical Sensors. Energy, Environment, and Sustainability*. Springer, Singapore, 2018.
- [36] R. E. Sousa, C. M. Costa, S. Lanceros-Méndez, "Advances and future challenges in printed batteries," *ChemSusChem*, vol. 8, 3539, 2015.
- [37] A.M. Gaikwad, A.C. Arias, and D.A. Steingart, "Recent progress on printed flexible batteries: mechanical challenges, printing technologies, and future prospects," *Energy Technology*, vol. 3, pp. 305-328, 2015.
- [38] G.K. Lau and M. Shrestha, "Ink-jet printing of micro-electro-mechanical systems (MEMS)," *Micromachines*, vol. 8, pp. 194, 2017.

- [39] H. Gorter, M.J.J. Coenen, M.W.L. Slaats, M. Ren, W. Lu, C.J. Kuijpers, and W.A. Groen, "Toward inkjet printing of small molecule organic light emitting diodes," *Thin Solid Films*, vol. 532, pp. 11-15, 2013.
- [40] B. Andò, S. Baglio, A. R. Bulsara, V. Marletta, V. Ferrari and M. Ferrari, "A low-cost snap-through-buckling inkjet-printed device for vibrational energy harvesting," *IEEE Sensors Journal*, vol. 15, no. 6, pp. 3209-3220, 2015.
- [41] D. Thuau, K. Kallitsis, F. D. Dos Santos, and G. Hadziioannou, "All inkjet-printed piezoelectric electronic devices: energy generators, sensors and actuators," *J. Mater. Chem. C*, vol. 5, pp. 9963-9966, 2017.
- [42] G. Cummins and M.P.Y. Desmulliez, "Inkjet printing of conductive materials: a review", *Circuit World*, Vol. 38 No. 4, pp. 193-213, 2012.
- [43] Y. Sui and C.A. Zorman, "Review – Inkjet Printing of metal Structures for Electrochemical Sensor Applications," *J. Electrochem. Soc.* vol. 167, pp. 037571, 2020.
- [44] E.W. Miller, A.E. Albers, A. Pralle, E.Y. Isacoff, and C.J. Chang, "Boronate-Based Fluorescent Probes for Imaging Cellular Hydrogen Peroxide," *Journal of the American Chemical Society*, vol. 127, no. 47, pp. 16652-16659, 2005.
- [45] G.C. Jensen, C.E. Krause, G.A. Sotzing, and J. F. Rusling, "Inkjet-printed gold nanoparticle electrochemical arrays on plastic. Application to immunodetection of a cancer biomarker protein," *Phys. Chem. Chem. Phys.*, vol. **13**, pp. 4888-4894, 2011.
- [46] C. Hu, X. Bai, Y. Wang, W. Jin, X. Zhang, and S. Hu, "Inkjet Printing of Nanoporous Gold Electrode Arrays on Cellulose Membranes for High-Sensitive Paper-Like Electrochemical Oxygen Sensors Using Ionic Liquid Electrolytes," *Analytical Chemistry*, vol. 84, no. 8, pp. 3745-3750, 2012.

- [47] A. Maattanen, U. Vanamo, P. Ihalainen, P. Pulkkinen, H. Tenhu, J. Bobacka, and J. Peltonen, "A low-cost paper-based inkjet printed platform for electrochemical analyses," *Sensors and Actuators B: Chemical*, vol. 177, pp. 153-162, 2013.
- [48] C.E. Krause, B.A. Otieno, A. Latus, R.C. Faria, V. Patel, J.S. Gutkind, and J.F. Rusling, "Rapid microfluidic immunoassays of cancer biomarker proteins using disposable inkjet-printed gold nanoparticle arrays," *ChemistryOpen*, vol. 2, pp. 141-145, 2013.
- [49] P. Ihalainen, H. Majumdar, T. Viitala, B. Törngren, T. Närjeoja, A. Määttänen, J. Sarfraz, H. Härmä, M. Yliperttula, R. Österbacka, et al., "Application of paper-supported printed gold electrodes for impedimetric immunosensor development," *Biosensors*, vol. 3, pp. 1-17, 2013.
- [50] P. Ihalainen *et al.*, "An impedimetric study of DNA hybridization on paper-supported inkjet-printed gold electrodes," *Nanotechnology*, vol. 25, no. 9, pp. 094009, 2014.
- [51] Milica Jović, Fernando Cortés-Salazar, Andreas Lesch, Véronique Amstutz, Hongyan Bi, Hubert H. Girault, "Electrochemical detection of free chlorine at inkjet printed silver electrodes," *Journal of Electroanalytical Chemistry*, vol. 756, pp. 171-178, 2015.
- [52] J. Chen, Y. Zhou, D. Wang, F. He, V. M. Rotello, K. R. Carter, J. J. Watkins and S. R. Nugen, "UV-nanoimprint lithography as a tool to develop flexible microfluidic devices for electrochemical detection," *Lab Chip*, vol. 15, pp. 3086-3094, 2015.
- [53] Y. Qin, A. U. Alam, M. M. R. Howlader, N.X. Hu, and M.J. Deen, "Inkjet printing of a highly loaded palladium ink for integrated, low-cost pH sensors. *Adv. Funct. Mater.*, vol. 26, pp. 4923-4933, 2016.
- [54] Z. Xu, Q. Dong, B. Otieno, Y. Liu, I. Williams, D. Cai, Y. Li, Y. Lei, and B. Li, "Real-time in situ sensing of multiple water quality related parameters using micro-electrode array (MEA)

fabricated by inkjet-printing technology (IPT),” *Sensors and Actuators B: Chemical*, vol. 237, pp. 1108-1119, 2016.

- [55] P. Sjöberg, A. Määttä, U. Vanamo, M. Novell, P. Ihalainen, F. J. Andrade, J. Bobacka, and J. Peltonen, “Paper-based potentiometric ion sensors constructed on ink-jet printed gold electrodes,” *Sensors and Actuators B: Chemical*, vol. 224, pp. 325-332, 2016.
- [56] R. Pol, A. Moya, G. Gabriel, D. Gabriel, F. Céspedes, and M. Baeza, “Inkjet-Printed Sulfide-Selective Electrode,” *Analytical Chemistry*, vol. 89, no. 22, pp. 12231-12236, 2017.
- [57] Y. Qin, A.U. Alam, S. Pan, M.M.R. Howlader, R. Ghosh, N.X. Hu, H. Jin, S. Dong, C.H. Chen, M.J. Deen, “Integrated water quality monitoring system with pH, free chlorine, and temperature sensors,” *Sensors and Actuators B: Chemical*, vol. 255, no. 1, pp. 781-790, 2018.
- [58] M. Zea, A. Moya, M. Fritsch, E. Ramon, R. Villa, and G. Gabriel, “Enhanced Performance Stability of Iridium Oxide-Based pH Sensors Fabricated on Rough Inkjet-Printed Platinum” *ACS Applied Materials & Interfaces*, vol. 11, no. 16, pp. 15160-15169, 2019.
- [59] Y. Sui, Y. Dai, C.C. Liu, R.M. Sankaran, C.A. Zorman, “A new class of low-temperature plasma-activated, inorganic salt-based particle-free inks for inkjet printing metals,” *Adv. Mater. Technol.*, vol. 4, no. 8, pp. 1900119, 2019.
- [60] S.D. Amaya, L.K. Lin, R.E. DiNino, C. Ostos, and L.A. Stanciu, “Inkjet printed electrochemical aptasensor for detection of Hg²⁺ in organic solvents,” *Electrochimica Acta*, vol. 316, pp. 33-42, 2019.
- [61] Y. Dai, L.Y. Chiu, Y. Sui, Q. Dai, S. Penumutchu, N. Jain, L. Dai, C. A. Zorman, B. S. Tolbert, R. M. Sankaran, C.C. Liu, “Nanoparticle based simple electrochemical biosensor platform for profiling of protein-nucleic acid interactions,” *Talanta*, vol. 195, pp. 46-54, 2019.

- [62] K. Pokpas, N. Jahed, E. McDonald, P. Bezuidenhout, S. Smith, K. Land, and E. Iwuoha, "graphene-aunp enhanced inkjet-printed silver nanoparticle paper electrodes for the detection of nickel(ii)-dimethylglyoxime [Ni(DMGH₂)] complexes by adsorptive cathodic stripping voltammetry (AdCSV)," *Electroanalysis*, vol. 32, pp. 3017, 2020.
- [63] P.B. Deroco, D.W. Junior, and L.T. Kubota, "Silver inkjet-printed electrode on paper for electrochemical sensing of paraquat," *Chemosensors*, vol. 9, no. 4, pp. 61, 2021.
- [64] M. A. U. Khalid, K. H. Kim, A. R. Chethikkattuveli Salih, K. Hyun, S. H. Park, B. Kang, A. M. Soomro, M. Ali, Y. Jun, D. Huh, H. Cho, and K. H. Choi, "High performance inkjet printed embedded electrochemical sensors for monitoring hypoxia in a gut bilayer microfluidic chip," *Lab Chip*, vol. 22, pp. 1764-1778, 2022.
- [65] M. Li, Y. Zeng, Z. Huang, L. Zhang, Y. Liu, "Vertical graphene-based printed electrochemical biosensor for simultaneous detection of four Alzheimer's disease blood biomarkers," *Biosensors*, vol. 13, no. 8, pp. 758, 2023.
- [66] S. Armenta, S. Garrigues, M.D. LaGuardia, "Green analytical Chemistry," *TrAC Trends in Analytical Chemistry*, vol. 27, no. 6, pp 497-511, 2008.
- [67] Y. Li, H.J. Schluesener, and S. Xu, "Gold Nanoparticle-based Biosensors," *Gold Bulletin*, vol. 43, no. 1, pp 29-41, 2010.
- [68] S. Kim, Y. Jeong, M. Park, Y. Jang, J. Bae, K. Hong, S. Kim, P. Song, J. Yoon, "Development of boron doped diamond electrodes material for heavy metal ion sensor with high sensitivity and durability," *Journal of Materials Research and Technology*, Vol. 23, pp. 1375-1385, 2023, ISSN 2238-7854.

- [69] H. Hou, K.M. Zeinu, S. Gao, B. Liu, J. Yang, and J. Hu, "Recent advances and perspective on design and synthesis of electrode materials for electrochemical sensing of heavy metals," *Energy Environ. Mater.*, vol. 1, pp. 113-131, 2018.
- [70] Z. Lu, J. Zhang, Dai, W. *et al.* "A screen-printed carbon electrode modified with a bismuth film and gold nanoparticles for simultaneous stripping voltammetric determination of Zn(II), Pb(II) and Cu(II)," *Microchim Acta*, vol. 184, pp. 4731-4740, 2017.
- [71] M. Hara, Y. Nagahara, J. Inukai, S. Yoshimoto, and K. Itaya, "In situ STM study of underpotential deposition of bismuth on Au (110) in perchloric acid solution," *Electrochimica Acta*, vol. 51, no. 11, pp. 2327-2332, 2006.
- [72] K. Węgiel, J. Robak, and B. Baś, "Voltammetric determination of iron with catalytic system at a bismuth bulk annular band electrode electrochemically activated," *RSC Adv.*, vol. 7, 22027-22033, 2017.
- [73] G. Kefala, A. Economou, and A. Voulgaropoulos, "A study of Nafion-coated bismuth-film electrodes for the determination of trace metals by anodic stripping voltammetry," *Analyst*, vol. **129**, no. 11, pp. 1082-1090, 2004.
- [74] M.T. Castaneda, B. Perez, M. Pumera, M. del Valle, A. Merkoci, and S. Alegret, "Sensitive stripping voltammetry of heavy metals by using a composite sensor based on a built-in bismuth precursor", *Analyst*, vol. 130, no. 6, pp. 971-976, 2005.
- [75] S. Legeai and O. Vittori, "A Cu/Nafion/Bi electrode for on-site monitoring of trace heavy metals in natural waters using anodic stripping voltammetry: An alternative to mercury-based electrodes," *Analytica Chimica Acta*, vol. 560, no. 1-2, pp. 184-190, 2006.

- [76] G.H. Hwang, W.K. Han, J.S. Park, and S.G. Kang, "An electrochemical sensor based on the reduction of screen-printed bismuth oxide for the determination of trace lead and cadmium," *Sensors and Actuators B: Chemical*, vol. 135, no. 1, pp. 309-316, 2008.
- [77] J. Li, J. Zhang, H. Wei, and E. Wang, "Combining chemical reduction with an electrochemical technique for the simultaneous detection of Cr(VI), Pb(II) and Cd(II)," *Analyst*, vol. 134, no. 2, pp. 273-277, 2009.
- [78] X. Jia, J. Li, and E. Wang, "High-sensitivity determination of lead(ii) and cadmium(ii) based on the CNTs-PSS/Bi composite film electrode," *Electroanalysis*, vol. 22, pp. 1682-1687, 2010.
- [79] Z. Wang, H. Wang, Z. Zhang, and G. Liu, "Electrochemical determination of lead and cadmium in rice by a disposable bismuth/electrochemically reduced graphene/ionic liquid composite modified screen-printed electrode," *Sensors and Actuators B: Chemical*, vol. 199, pp. 7-14, 2014.
- [80] Rutyna and M. Korolczuk, "Determination of lead and cadmium by anodic stripping voltammetry at bismuth film electrodes following double deposition and stripping steps," *Sensors and Actuators B: Chemical*, vol. 204, pp. 136-141, 2014.
- [81] J. Ping, Y. Wang, J. Wu, and Y. Ying, "Development of an electrochemically reduced graphene oxide modified disposable bismuth film electrode and its application for stripping analysis of heavy metals in milk," *Food Chemistry*, vol. 151, pp. 65-71, 2014.
- [82] M.A. Chamjangali, H. Kouhestani, F. Masdarolomoor, and H. Daneshinejad, "A voltammetric sensor based on the glassy carbon electrode modified with multi-walled carbon nanotube/poly(pyrocatechol violet)/bismuth film for determination of cadmium and lead as environmental pollutants," *Sensors and Actuators B: Chemical*, vol. 216, pp. 384-393, 2015.

- [83] C.I. Fort, L.C. Cotet, A. Vulpoi, G.L. Turdean, V. Danciu, L. Baia, and I.C. Popescu, "Bismuth doped carbon xerogel nanocomposite incorporated in chitosan matrix for ultrasensitive voltammetric detection of Pb(II) and Cd(II)," *Sensors and Actuators B: Chemical*, vol. 220, pp. 712-719, 2015.
- [84] S. Lee, S. Bong, J. Ha, M. Kwak, S.K. Park, and Y. Piao, "Electrochemical deposition of bismuth on activated graphene-nafion composite for anodic stripping voltammetric determination of trace heavy metals," *Sensors and Actuators B: Chemical*, vol. 215, pp. 62-69, 2015.
- [85] K.M. Zeinu, *et al.* "A novel hollow sphere bismuth oxide doped mesoporous carbon nanocomposite material derived from sustainable biomass for picomolar electrochemical detection of lead and cadmium," *Journal of Materials Chemistry A*, vol. 4, no. 36, pp. 13967-13979, 2016.
- [86] C. Kokkinos and A. Economou, "Microfabricated chip integrating a bismuth microelectrode array for the determination of trace cobalt (II) by adsorptive cathodic stripping voltammetry," *Sensors and Actuators B: Chemical*, vol. 229, pp. 362-369, 2016.
- [87] S. Lee, S.K. Park, E. Choi, and Y. Piao, "Voltammetric determination of trace heavy metals using an electrochemically deposited graphene/bismuth nanocomposite film-modified glassy carbon electrode," *Journal of Electroanalytical Chemistry*, vol. 766, pp. 120-127, 2016.
- [88] S. Chaiyo, E. Mehmeti, K. Žagar, W. Siangproh, O. Chailapakul, and K. Kalcher, "Electrochemical sensors for the simultaneous determination of zinc, cadmium and lead using a Nafion/ionic liquid/graphene composite modified screen-printed carbon electrode," *Analytica Chimica Acta*, vol. 918, pp. 26-34, 2016.

- [89] X. Xuan and J.Y. Park, "A miniaturized and flexible cadmium and lead ion detection sensor based on micro-patterned reduced graphene oxide/carbon nanotube/bismuth composite electrodes," *Sensors and Actuators B: Chemical*, vol. 255, no. 2, pp. 1220-1227, 2018.
- [90] J.H. Hwang, X. Wang, D. Zhao, M. M. Rex, H. J. Cho, W.H. Lee, "A novel nanoporous bismuth electrode sensor for in situ heavy metal detection," *Electrochimica Acta*, vol. 298, pp. 440-448, 2019.
- [91] Y. He, Z. Wang, L. Ma, L. Zhou, Y. Jiang, and J. Gao, "Synthesis of bismuth nanoparticle-loaded cobalt ferrite for electrochemical detection of heavy metal ions," *RSC Adv.*, vol. 10, no. 46, pp. 27697-27705, 2020.
- [92] C.D. Oliveira, J.V. Maciel, and A. Christ-Ribeiro, *et al.* "A voltammetric approach for the simultaneous determination of Cd and Pb in water applying carbon paste electrode modified with bismuth film," *J Anal Chem*, vol. 77, pp. 369-375, 2022.
- [93] Y. Wang, X. Wu, J. Sun, C. Wang, G. Zhu, L.P. Bai, Z.H. Jiang, and W. Zhang, "Stripping voltammetric determination of cadmium and lead ions based on a bismuth oxide surface-decorated nanoporous bismuth electrode," *Electrochemistry Communications*, vol. 136, pp. 107233-107239, 2022.
- [94] R.C. Roberts, S. Zeng, and N.C. Tien, "Design and fabrication of buckled metal strain gauges using shape memory polymer and inkjet additive microfabrication," *Technical Digest, The 14th IEEE Conference on Sensors*, Busan, Korea, pp. 1665-1668, Nov. 1-4, 2015.
- [95] R.C. Roberts, J. Wu, N.Y. Hau, Y.H. Chang, S.P. Feng, and D.C. Li, "Facile 3D metal electrode fabrication for energy applications via inkjet printing and shape memory polymer," *Journal of Physics: Conference Series*, vol. 557, 2014.

- [96] J. Wu, R. Wang, H. Yu, G. Li, K. Xu, N.C. Tien, R.C. Roberts, and D.C. Li, "Inkjet-printed microelectrodes on PDMS as biosensors for functionalized microfluidic systems," *Lab on a chip*, vol. 15, pp. 690-695, 2015.
- [97] G. Li, R.C. Roberts, and N.C. Tien, "Interlacing method for micro-patterning silver via inkjet printing," *Proc. The 13th International Conference on Sensors (Sensors 2014)*, Valencia, Spain, pp. 1687-1690, November 2-5, 2014.
- [98] J.W. Dickinson, M. Bromley, F.P.L. Andrieux, and C. Boxall, "Fabrication and characterisation of the graphene ring micro electrode (GRiME) with an integrated, concentric Ag/AgCl reference electrode," *Sensors*, vol. 13, no. 3, pp. 3635-3651, 2013.
- [99] A. Arif and R.C. Roberts, "Characterization of aqueous lead sensing performance of bismuth functionalized 3D inkjet printed electrochemical electrodes," *64th Electronic Materials Conference*, Columbus, Ohio, June 29-July1, 2022.
- [100] N.E. Solis-Marcano, M. Morales-Cruz, G. Vega-Hernández, R. Gomez-Moreno, C. Binder, A. Baerga-Ortiz, C. Priest, and C.R. Cabrera, "PCR-assisted impedimetric biosensor for colibactin-encoding *pks* genomic island detection in *E. coli* samples." *Anal Bioanal Chem* 413, 4673–4680, 2021.
- [101] N.E. Solis-Marcano, M. Lopez-Nieves, B. Pinto-Pacheo, and C.R. Cabrera, "Capacitive Biosensing Technique for the Detection of DNA Modification and Hybridization Process Using Tailored Interdigital Microelectrode Arrays," *46th International Conference on Environmental Systems*, 2016.
- [102] X. Adolphe, I. Palchetti, M. Mascini, *et al.* "On the electrochemical flow measurements using carbon-based screen-printed electrodiffusion probes," *J Appl Electrochem*, vol. 35, pp. 599–607, 2005.

- [103] V. Fragkou, Y. Ge, G. Steiner, D. Freeman, N. Bartetzko, A. P. F. Turner, "Determination of real surface area of a screen printed electrode by chronocoulometry," *International Journal of Electrochemical Science*, vol. 7, pp. 6214-6220, 2012.
- [104] S.K. Kim, P.J. Hesketh, C. Li, J.H. Thomas, H.B. Halsall, and W.R. Heineman, "Fabrication of comb interdigitated electrodes array (IDA) for a microbead-based electrochemical assay system," *Biosensors and Bioelectronics*, vol. 20, no. 4, pp. 887-894, 2004.
- [105] H. Peng, C. Soeller, N. Vigar, P. A. Kilmartin, M. B. Cannell, G. A. Bowmaker, R. P. Cooney, J. Travas-Sejdic, "Label-free electrochemical DNA sensor based on functionalised conducting copolymer," *Biosensors and Bioelectronics*, vol. 20, no. 9, pp. 1821-1828, 2005.
- [106] C. Shin, W. Shin, H.G. Hong, "Electrochemical fabrication and electrocatalytic characteristics studies of gold nanopillar array electrode (AuNPE) for development of a novel electrochemical sensor," *Electrochimica Acta*, vol. 53, no. 2, pp. 720-728, 2007.
- [107] X. Kang, Z. Mai, X. Zou, P. Cai, J. Mo, "A sensitive nonenzymatic glucose sensor in alkaline media with a copper nanocluster/multiwall carbon nanotube-modified glassy carbon electrode," *Analytical Biochemistry*, vol. 363, no. 1, pp. 143-150, 2007.
- [108] F. Schröper, D. Brüggemann, Y. Mourzina, B. Wolfrum, A. Offenhäusser, and D. Mayer, "Analyzing the electroactive surface of gold nanopillars by electrochemical methods for electrode miniaturization," *Electrochimica Acta*, volume 53, no. 21, pp. 6265-6272, 2008.
- [109] H. Qiu, L. Xue, G. Ji, G. Zhou, X. Huang, Y. Qu, P. Gao, "Enzyme-modified nanoporous gold-based electrochemical biosensors," *Biosensors and Bioelectronics*, vol. 24, no. 10, pp. 3014-3018, 2009.

- [110] S. Cherevko, C.H. Chung, "Gold nanowire array electrode for non-enzymatic voltammetric and amperometric glucose detection," *Sensors and Actuators B: Chemical*, vol. 142, no. 1, pp. 216-223, 2009.
- [111] M.J. Song, S.W. Hwang, D. Whang, "Non-enzymatic electrochemical CuO nanoflowers sensor for hydrogen peroxide detection," *Talanta*, vol. 80, no. 5, pp. 1648-1652, 2010.
- [112] J. Krejci, Z. Sajdlova, V. Nedela, E. Flodrova, R. Sejnohova, H. Veranova, and R. Plicka, "Effective surface area of electrochemical sensors," *Journal of the Electrochemical Society*, vol. 161, pp. B147-B150, 2014.
- [113] A.G.M. Ferrari, C.W. Foster, P.J. Kelly, D.A.C. Brownson, and C.E. Banks, "Determination of the electrochemical area of screen-printed electrochemical sensing platforms," *Biosensors*, vol. 8, no. 53, 2018.
- [114] G. Jarzabek and Zofia Borkowska, "On the real surface area of smooth solid electrodes," *Electrochimica Acta*, vol. 42, no. 19, pp. 2915-2918, 1997.
- [115] S. Trasatti and O.A. Petrii, "Real surface area measurements in electrochemistry," *Pure and Applied Chemistry*, vol. 63, no. 5, pp. 711-734, 1991.
- [116] T. Grygar *et al.*, "Electrochemical analysis of solids. A review." *Collection of Czechoslovak chemical communications*, vol. 67, no. 2, pp. 163-208, 2002.
- [117] M. Libansky, J. Zima, J. Barek, A. Reznickova, V. Svorick, "Basic electrochemical properties of sputtered gold film electrodes," *Electrochimica Acta*, vol 251, pp. 452-460, 2017.
- [118] J.F. Rusling and M.Y. Brooks, "Analysis of chronocoulometric data and determination of surface concentrations," *Analytical chemistry*, vol. 56, no. 12, pp. 2147-2153, 1984.
- [119] J.E.B. Randles, "A cathode ray polarograph. Part II—The current-voltage curves," *Transactions of the Faraday Society*, vol. 44, pp. 327-338, 1948.

- [120] A. Ševčík, "Oscillographic polarography with periodical triangular voltage," *Collection of Czechoslovak Chemical Communications*, vol. 13, pp. 349-377, 1948.
- [121] R.J. Klingler and J.K. Kochi, "Electron-transfer kinetics from cyclic voltammetry. Quantitative description of electrochemical reversibility," *The Journal of Physical Chemistry*, vol. 85, no. 12, pp. 1731-1741, 1981.
- [122] C.M.A. Brett and O. Brett, "Principles, methods, and applications," *Electrochemistry*, vol. 67, no. 2, pp. 444, 1993.
- [123] A.J. Bard, L.R. Faulkner, and H.S. White, "Electrochemical methods: fundamentals and applications," John Wiley & Sons, 2022.
- [124] D.A. Brownson and C.E. Banks, "The handbook of graphene electrochemistry," vol. 201, *London: Springer*, 2014.
- [125] K. Ngamchuea, S. Eloul, K. Tschulik, *et al.* "Planar diffusion to macro disc electrodes—what electrode size is required for the Cottrell and Randles-Sevcik equations to apply quantitatively?," *J Solid State Electrochem*, vol. 18, pp. 3251-257, 2014.
- [126] R.G. Compton and C.E. Banks, "Understanding voltammetry," *World Scientific*, 2018.
- [127] R. S. Nicholson, "Theory and Application of Cyclic Voltammetry for Measurement of Electrode Reaction Kinetics," *Analytical Chemistry*, vol. 37, no. 11, pp. 1351-1355, 1965.

Appendix

Appendix A: Reduction Factor (%)

Reduction factor (%) has been calculated using the following equation:

$$\text{Reduction factor (\%)} = \frac{A_{\text{initial}} - A_{\text{final}}}{A_{\text{initial}}} \times 100 \quad (\text{A.1})$$

Appendix B: Effective Electrode Surface Area

Effective electrode surface area (EESA) has been calculated using quasi reversible Randles-Sevcik (R-S) equation:

$$I_p(\text{quasi-reversible}) = (2.69 \times 10^5 n^{3/2} AC \sqrt{Dv}) K(\Lambda, \alpha) \quad (\text{B.1})$$

Where, I_p is forward peak (anodic/stripping) current (amps), n is the number of electrons in the electrochemical process ≈ 1 , A is effective electrode surface area (cm^2), C is the concentration (mol/cm^3), D is diffusion coefficient (cm^2/s), and v is scan rate (V/s). The diffusion co-efficient can be estimated from the slope of the plot of I_p vs \sqrt{v} . In the quasi-reversible equation, $K(\Lambda, \alpha)$ is a dimensionless parameter which is defined by calculating Ψ , $\log(\Lambda)$, and $\Delta(\Lambda, \alpha)$ respectively. Ψ is determined from Nicholson plot based on peak to peak separation [127]. In equation 5.5, E_p and $E_{p/2}$ are peak potential and half wave peak potential respectively. Figure B.1 represents $\Delta(\Lambda, \alpha)$ and $K(\Lambda, \alpha)$ with respect to function of $\log(\Lambda)$. Figure B.2 is utilized for determining the value of Ψ based on the peak to peak separation of CV plot.

$$\log(\Lambda) = \log(\Psi \sqrt{\pi}) \quad (\text{B.2})$$

$$\Delta(\Lambda, \alpha) = \frac{E_{p/2} - E_p}{26} \quad (\text{B.3})$$

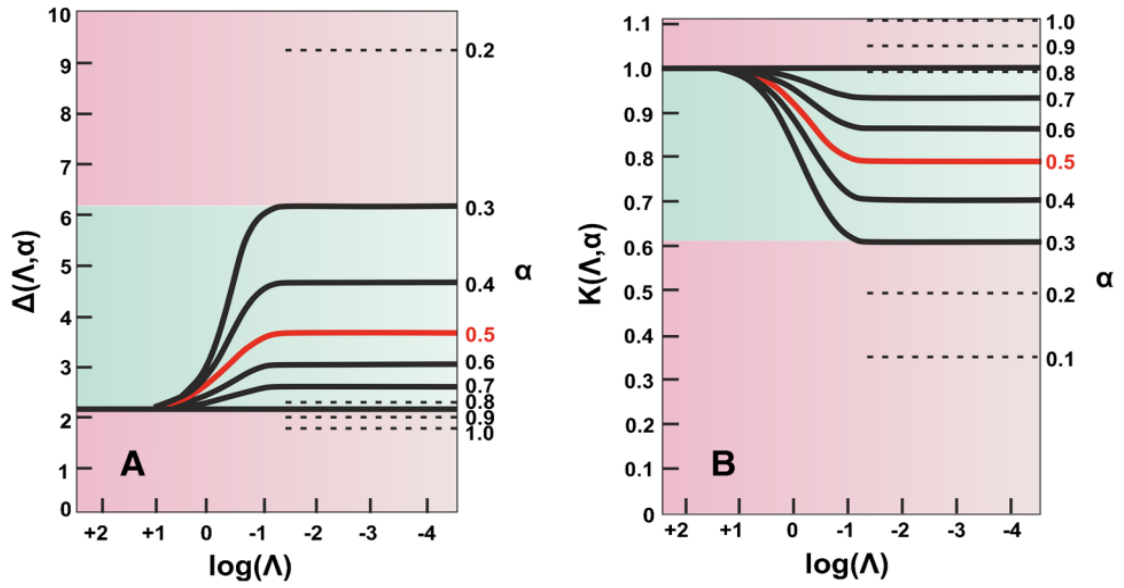


Figure B.1: Plot of (A) $\Delta(\Lambda, \alpha)$ and (B) $K(\Lambda, \alpha)$ with a range of different transfer co-efficient, α - [127, 128].

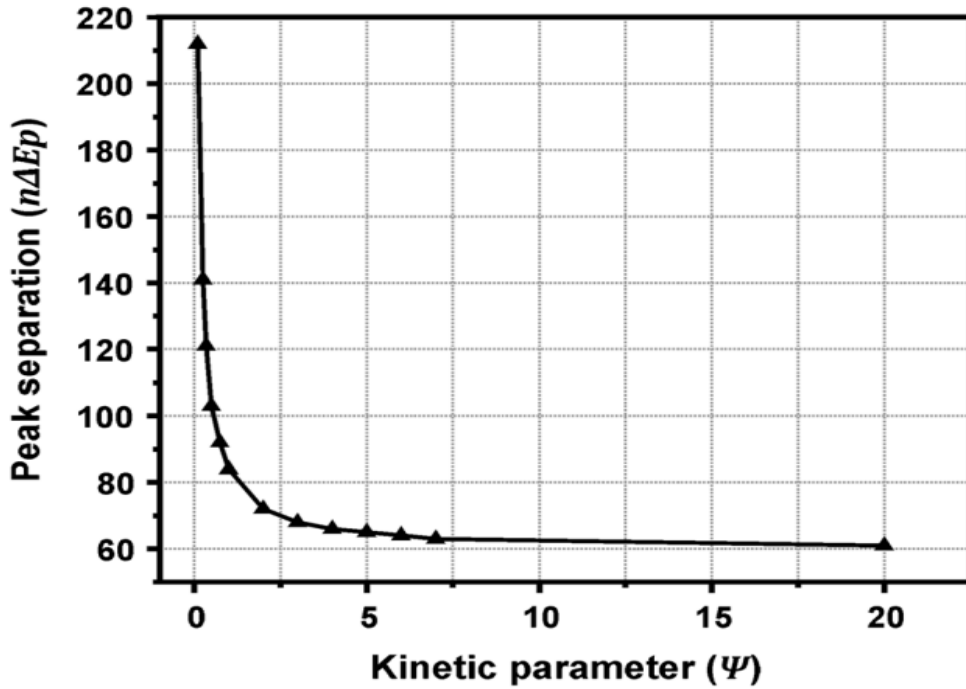


Figure B.2: Peak to peak separation vs. kinetic parameter, Ψ [127, 128].

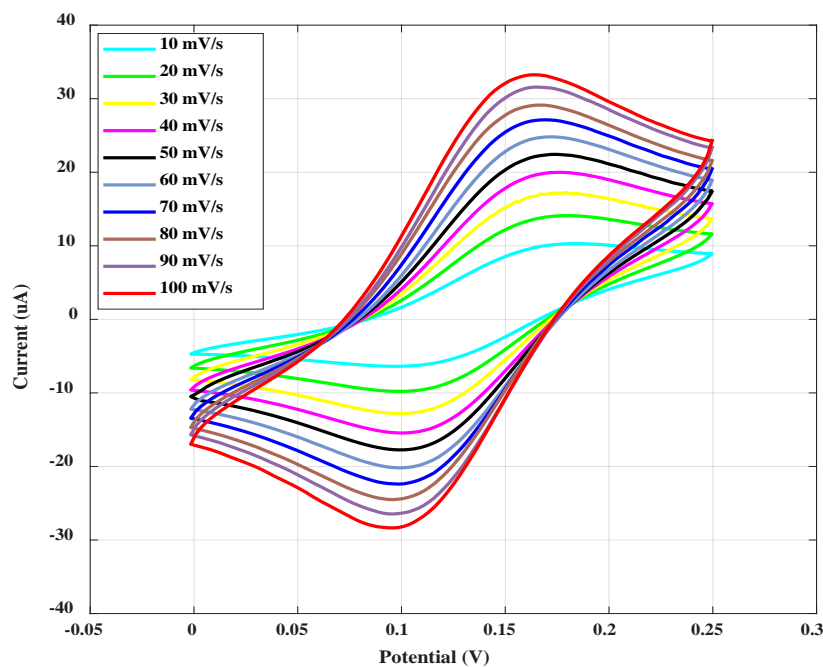


Figure B.3: Cyclic voltammogram (CV) for inkjet printed gold electrochemical sensor (square working electrode surface area) for 3 mM of ferri(III)cyanide/ferro(II)cyanide in 0.1 M KCl (10, 20, 30, 40, 50, 60, 70, 80, 90, and 100 mV/s).

Figure B.3 shows cyclic voltammetry (CV) for 5mM lead (II) contaminated optimized deionized (DI) water in case of 4 different scan rate i.e., 10, 20, 30, and 50 mV/s. The peak to peak separation of the CV plot is 68.37 mV. Based on peak to peak separation, Ψ is ~ 4.25 (from Figure B.2). $\Delta(\Lambda, \alpha)$ becomes 2.10 based on Figure B.3 and equation B.3. So, from Figure B.1 $K(\Lambda, \alpha)$ becomes 1. Hence the quasi reversible R-S equation is:

$$I_p(\text{quasi-reversible}) = (2.69 \times 10^5 n^{3/2} AC \sqrt{Dv}) \quad (\text{B.4})$$

Table B.1 represents peak current (amps) vs. square root of different scan rates. Table B.1 helps to determine D. Figure B.4 shows the peak current (amps) vs. square root of scan rate ($\sqrt{(mV/s)}$) curve. The slope of this curve/straight line equation is defined as diffusion coefficient, D in cm^2/s . For this example, D is $3 \mu\text{cm}^2/\text{s}$. 3 mM ferri(III)cyanide/ferro(II)cyanide has been

utilized to conduct this experiment. So, C would be $3 \mu\text{mol}/\text{cm}^3$. If a peak current at any scan rate is considered, the calculated effective electrode surface area (EESA) or electrical area for this example would be 7.17 mm^2 .

Table B.1: Peak Currents at Different Scan Rates.

Square root of scan rate	Current (μA)
3.162278	1.00E-05
4.472136	1.39E-05
5.477226	1.70E-05
6.324555	1.99E-05
7.071068	2.23E-05
7.745967	2.47E-05
8.3666	2.71E-05
8.944272	2.91E-05
9.486833	3.15E-05
10	3.31E-05

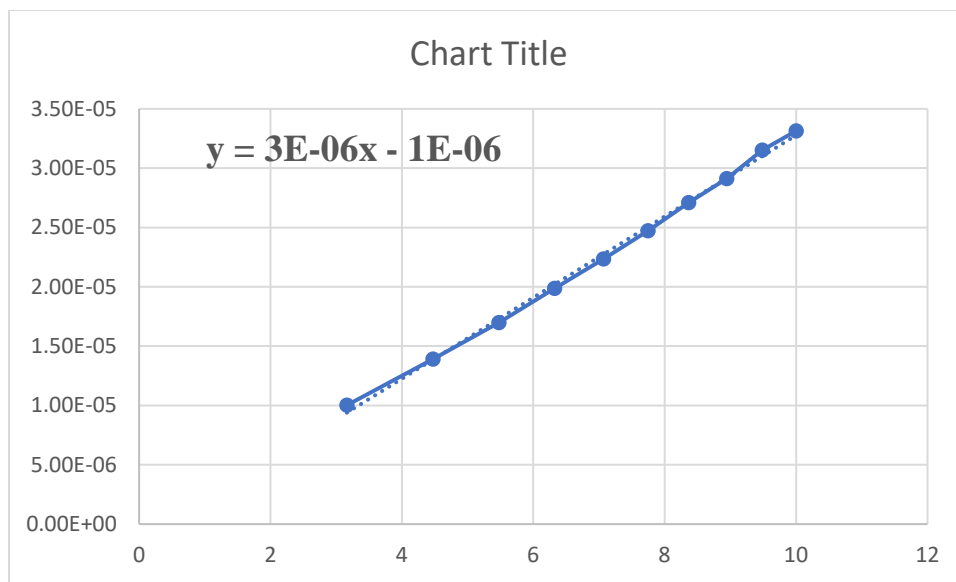


Figure B.4: Peak current vs. square root of scan rate. The slope is defined as diffusion coefficient ($D - \text{cm}^2/\text{s}$).

Appendix C: Limit of Detection and Limit of Quantitation

Limit of detection (LOD) and limit of quantitation (LOQ) are two important parameters to validate any analytical methods. LOD can be defined as the lowest concentration of sample analyte that can be detected continuously and consistently with a stated probability. It is not necessarily quantified as an exact value. It should be noted that LOD is different than sensitivity. Sensitivity can be defined as the ability of an analytical method to identify any small change in the sample analyte. It can be determined by the slope of the calibration curve. On the other hand, LOQ can be defined as the lowest concentration of sample analyte that is an exact value and can be detected with accuracy and precision. LOD and LOQ can be determined in three different ways i.e., visual evaluation, signal to noise ratio, and standard deviation of the electrochemical signal and slope. In this dissertation research, LOD and LOQ have been calculated using standard deviation and slope of the calibration curve. The calibration curve has been developed with the electrochemical response i.e., peak current of square wave anodic stripping voltammetry (SWASV) of lead (II) contaminated optimized deionized (DI) water at different concentrations. The formulae for calculating LOD and LOQ are given below:

$$LOD = 3.3 \frac{\sigma}{S} \quad (C.1)$$

$$LOQ = 10 \frac{\sigma}{S} \quad (C.2)$$

σ is defined as the residual standard deviation of the regression line and S is the slope of the calibration curve.

Table C.1: Peak Currents of Square Wave Anodic Stripping Voltammetry for Different Concentrations of Lead (II) Contaminated Optimized DI Water.

No.	Concentration (ug/L)	Peak Current (uA)
1	0	1.80E+01

2	5	3.60E+01
3	10	6.92E+01
4	20	1.11E+02
5	40	2.09E+02
6	60	2.91E+02
7	80	3.82E+02
8	100	4.90E+02

The regression analysis has been performed using “Data Analysis” tools in Excel. An example of calculating LOD and LOQ is given below. This data/example has been calculated for inkjet printed shape memory polymer (SMP) incorporated bismuth (Bi) functionalized i.e., Bi coated gold-plated electrochemical sensor (ECS). Table C.1 shows stripping peak current of SWASV for different concentrations of lead (II) contaminated optimized DI water. Table C.2 is the summary output of regression analysis/statistics using Excel. This summary contains important information i.e., standard error of intercept, $SE_{intercept}$ which is required to calculate standard deviation of intercept, $SD_{intercept}$. The equation of $SD_{intercept}$ is given below:

$$SD_{intercept} = SE_{intercept} \times \sqrt{\text{No. of observations}} \quad (C.3)$$

Table C.2: Summary Output of Regression Statistics Analyzed using Excel.

<i>Regression Statistics</i>				
Multiple R	0.999490433			
R Square	0.998981127			
Adjusted R Square	0.998811314			
Standard Error	5.978712356			
Observations	8			
ANOVA				
	<i>df</i>	<i>SS</i>	<i>MS</i>	<i>F</i>
Regression	1	210282.72	210282.72	5882.85667
Residual	6	214.470009	35.7450014	
Total	7	210497.19		
	<i>Coefficients</i>	<i>Standard Error</i>	<i>t Stat</i>	<i>P-value</i>

Intercept	17.48779913	3.18881474	5.48410634	0.0015375
X Variable 1	4.650790498	0.06063629	76.6997827	3.3066E-10

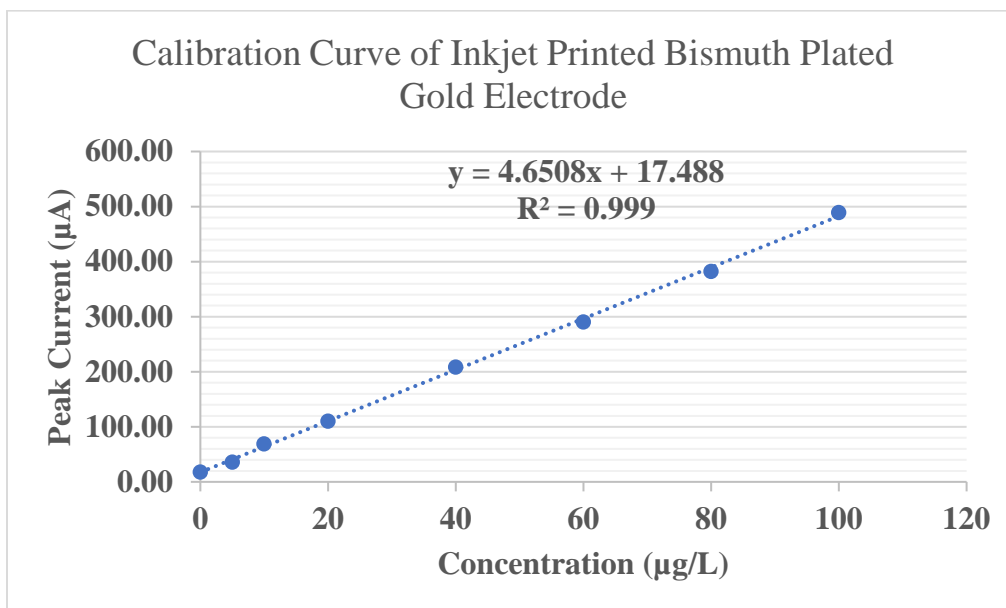


Figure C.1: Calibration curve for bismuth (III) plated inkjet printed gold plated electrochemical sensor. The data point for each concentration is a mean of three different data collected using three different sensors.

Slope, S of the calibration curve is also very important to calculate LOD and LOQ. Figure C.1 represents calibration curve which contains the information of the slope of peak current vs. concentration of lead (II) ions graph. σ from equations C.1 and C.2 is defined as $SD_{intercept}$ and calculated using equation C.3. So, final equations of LOD and LOQ are:

$$LOD = 3.3 \frac{SE_{intercept} \times \sqrt{No. \text{ of observations}}}{S} \quad (C.4)$$

$$LOQ = 10 \frac{SE_{intercept} \times \sqrt{No. \text{ of observations}}}{S} \quad (C.5)$$

In this example, $SE_{intercept}$ is 3.1888, no. of observations is 8, and S is 4.6508. Hence, the calculated LOD and LOQ for the inkjet printed Bi deposited Au electroplated ECS are 6.39 $\mu\text{g/L}$ and 19.39 $\mu\text{g/L}$.

Appendix D: Unit Conversions

- 1 unit = 1000 milliunit
- 1 unit = 1000000 microunit
- 1 unit = 0.001 Kilounit
- 1 ppb = 1 $\mu\text{g/L}$
- 1 $\mu\text{g/L}$ = 0.1 $\mu\text{g/dL}$
- 1 mM/L = 278100 $\mu\text{g/L}$ (molecular mass of lead (II) is 278.10 g/mol)

Vita

Ms. Annatoma Arif completed her Master of Science in Computational Science and Engineering in Fall 2016. Before pursuing her doctoral degree, Ms. Annatoma taught several basic engineering and science courses in two different private universities in Bangladesh from September 2016 to August 2019. Ms. Annatoma was admitted at UTEP in Fall 2019 as a doctoral student. Annatoma's dissertation focuses on development of a novel simple, sensitive, selective, reusable, and disposable electrochemical sensor based on additive manufacturing i.e., inkjet printing technology for lead detection in drinking water and/or blood samples. During her PhD she worked on several other projects i.e., 'Development of a gold based bifunctional electrochemical microchip colorectal cancer sensor – funded by NSF (Award # 2122627)' and 'Inkjet copper film deposition and characterization – funded by DOE-KCNSC (Award # N000427048)'. She also worked as an assistant instructor from Spring 2020 to Spring 2021 to teach/conduct Introduction to Electrical/Computer Engineering (EE 1305/1105) at UTEP.

Annatoma is a skilled researcher with expertise in inkjet printing, 3D printing, additive manufacturing, printed sensor, electrochemical sensor, biosensor, and microsystems. She is committed to making meaningful contributions in related research while she adjusts her academic and professional competencies with exceptional self-management and work habits. In addition to several awards and fellowships, Annatoma received NIST (National Institute of Standards and Technology) Uncertainty Analysis Student Award for her contribution in validating her fabricated inkjet printed electrochemical sensor for lead sensing in aqueous solution during 64th Electronic Materials Conference powered by Materials Research Society and National Science Foundation.

Contact Information: aarif@miners.utep.edu